THE VAPORIZATION AND SUBLIMATION THERMODYNAMICS OF SELECTED LANTHANIDE FLUORIDES

Dissertation for the Degree of Ph. D.

MICHIGAN STATE UNIVERSITY
ROBERT MALCOLM BIEFELD

1974

ABSTRACT

THE VAPORIZATION AND SUBLIMATION THERMODYNAMICS

OF SELECTED LANTHANIDE FLUORIDES

By

Robert Malcolm Biefeld

The vaporization and sublimation reactions for the samarium, thulium and ytterbium fluoride systems have been investigated at high temperatures. Mass loss, X-ray powder diffraction and elemental analyses were used to determine the high temperature reactions in these systems. The ytterbium fluoride system was also examined by mass spectrometry. The appearance potentials and fragmentation patterns for the gaseous ions Yb^+, YbF^+ and YbF_2^+ were determined from the effusates of: (1) a condensed ytterbium fluoride with a composition that varied between $YbF_{2.00}$ to $YbF_{2.40}$, (2) $YbF_{2.40}$ and (3) $YbF_{3.00}$.

Both $SmF_{2.00}$ and $YbF_{2.00}$ decompose when heated to give metal rich vapors and metal deficient residues until residues of the compositions $SmF_{2.40}$ and $YbF_{2.40}$ are reached. Thulium partially reduced TmF_3, but a reduced thulium fluoride was not isolated. Partially reduced TmF_3 decomposes when heated to a metal rich vapor and a TmF_3 enriched residue. The following equilibrium vaporization and sublimation reactions were established:

$$LnF_{2.40}(s,\ell) = (0.60)\ LnF_2(g) + (0.40)\ LnF_3(g), \quad (1)$$

$$LnF_{3.00}(s,\ell) = (0.05)\ LnF_{2.40}(s,\ell) + (0.95)\ LnF_3(g) + (0.03)\ F(g), \quad (2)$$

for Ln = Sm and Yb; and

$$TmF_{3.00}(s,\ell) = TmF_3(g). \quad (3)$$

A target collection Knudsen effusion method was used to obtain equilibrium vapor pressures for these reactions over the temperature

ranges of: 1369-1791 K for $SmF_{2.40}$, 1452-1742 K for $YbF_{2.40}$, 1353-1746 K for $SmF_{3.00}$, 1342-1794 K for $YbF_{3.00}$ and 1348-1809 K for $TmF_{3.00}$.

The following second-law enthalpy and entropy changes with associated standard deviations were derived at the median temperatures: $SmF_{2.40}$, $\Delta H^\circ_{1580} = (90._5 \pm 2._2)$ kcal mol^{-1} and $\Delta S^\circ_{1580} = (37._2 \pm 1._4)$ cal $mol^{-1}K^{-1}$; $YbF_{2.40}$, $\Delta H^\circ_{1597} = (96._9 \pm 1._1)$ kcal mol^{-1} and $\Delta S^\circ_{1597} = (36.8_3 \pm 0.6_7)$ cal $mol^{-1}K^{-1}$; $SmF_{3.00}(s)$, $\Delta H^\circ_{1462} = (95._0 \pm 2._0)$ kcal mol^{-1} and $\Delta S^\circ_{1462} = (42._8 \pm 1._4)$ cal $mol^{-1}K^{-1}$; $SmF_{3.00}(\ell)$, $\Delta H^\circ_{1669} = (83._2 \pm 4._7)$ kcal mol^{-1} and $\Delta S^\circ_{1669} = (34._8 \pm 2._8)$ cal $mol^{-1}K^{-1}$; $YbF_{3.00}$, $\Delta H^\circ_{1568} = (91.1_9 \pm 0.4_1)$ kcal mol^{-1} and $\Delta S^\circ_{1568} = (37.2_8 \pm 0.2_6)$ cal $mol^{-1}K^{-1}$; and $TmF_{3.00}$, $\Delta H^\circ_{1579} = (86.2_4 \pm 0.4_8)$ kcal mol^{-1} and $\Delta S^\circ_{1579} = (34.9_5 \pm 0.3_2)$ cal $mol^{-1}K^{-1}$. Estimated and reported thermodynamic functions were employed to reduce the thermodynamic values to 298 K. The following values with estimated uncertainties were derived by the Σ' method: $SmF_{2.40}(s)$, $\Delta H^\circ_{298} = (100._2 \pm 3._4)$ kcal mol^{-1} and $\Delta S^\circ_{298} = (46._2 \pm 2._8)$ cal $mol^{-1}K^{-1}$; $YbF_{2.40}(s)$, $\Delta H^\circ_{298} = (110._7 \pm 2._3)$ kcal mol^{-1} and $\Delta S^\circ_{298} = (50._8 \pm 2._1)$ cal $mol^{-1}K^{-1}$; $SmF_{3.00}(s)$, $\Delta H^\circ_{298} = (101._7 \pm 2._0)$ kcal mol^{-1} and $\Delta S^\circ_{298} = (52._5 \pm 1._7)$ cal $mol^{-1}K^{-1}$; $YbF_{3.00}(s)$, $\Delta H^\circ_{298} = (111._1 \pm 1._3)$ kcal mol^{-1} and $\Delta S^\circ_{298} = (56._2 \pm 1._3)$ cal $mol^{-1}K^{-1}$; and $TmF_{3.00}(s)$, $\Delta H^\circ_{298} = (108._2 \pm 1._5)$ kcal mol^{-1} and $\Delta S^\circ_{298} = (55._4 \pm 1._3)$ cal $mol^{-1}K^{-1}$. The following ΔH°_{298} values with estimated uncertainties were derived by the third-law procedure: $SmF_{2.40}(s)$, $(104._4 \pm 3._0)$ kcal mol^{-1}; $YbF_{2.40}(s)$, $(109._8 \pm 2._4)$ kcal mol^{-1}; $SmF_{3.00}(s)$, $(101._7 \pm 2._6)$ kcal mol^{-1}; $YbF_{3.00}(s)$, $(107._0 \pm 3._5)$ kcal mol^{-1}; and $TmF_{3.00}(s)$, $(107._5 \pm 2._3)$ kcal mol^{-1}.

The derived thermodynamic values were used with estimated and reported values for the enthalpies of formation and standard entropies S°_{298}, to calculate the enthalpies and entropies for the hypothetical congruent sublimation reactions of $SmF_2(s)$, $SmF_3(s)$, $YbF_2(s)$ and $YbF_3(s)$ at 298 K. Values are as follows: $SmF_2(s)$, $\Delta H^{\circ}_{298} = (99._5 \pm 9._3)$ kcal mol^{-1}, $\Delta S^{\circ}_{298} = (40._9 \pm 6._8)$ cal $mol^{-1}K^{-1}$ and ΔH°_{298}(3rd law) $= (106._5 \pm 9._1)$ kcal mol^{-1}; $SmF_3(s)$, $\Delta H^{\circ}_{298} = (101._2 \pm 2._5)$ kcal mol^{-1}, $\Delta S^{\circ}_{298} = (54._1 \pm 1._9)$ cal mol^{-1} K^{-1} and ΔH°_{298}(3rd law) $= (101._2 \pm 3._2)$ kcal mol^{-1}; $YbF_2(s)$, $\Delta H^{\circ}_{298} = (109._0 \pm 8._4)$ kcal mol^{-1}, $\Delta S^{\circ}_{298} = (46._0 \pm 6._1)$ cal $mol^{-1}K^{-1}$ and ΔH°_{298}(3rd law) $= (11_1 \pm 1_0)$ kcal mol^{-1}; and $YbF_3(s)$, $\Delta H^{\circ}_{298} = (113._3 \pm 1._8)$ kcal mol^{-1}, $\Delta S^{\circ}_{298} = (58._1 \pm 1._4)$ cal $mol^{-1}K^{-1}$ and ΔH°_{298}(3rd law) $= (109._0 \pm 4._1)$ kcal mol^{-1}.

Boiling points and the associated enthalpies of congruent vaporization were derived for $SmF_{2.40}(\ell)$, $SmF_2(\ell)$, $SmF_3(\ell)$, $YbF_{2.40}(\ell)$, $YbF_2(\ell)$, $YbF_3(\ell)$ and $TmF_3(\ell)$.

Calculations with estimated thermodynamic values for $EuF_{3.00}(s)$ indicated that it should sublime in a manner analogous to those of $SmF_{3.00}(s)$ and $YbF_{3.00}(s)$.

The thermodynamic values derived for the hypothetical congruent vaporization and sublimation of the lanthanide fluorides are compared with previously reported values for the alkaline earth difluorides and selected lanthanide fluorides. The differences and similarities are discussed. The trifluoride thermodynamics are similar to those reported by some investigators but not others. The difluoride thermdynamics are similar to those of europium(II) and strontium(II) fluorides.

THE VAPORIZATION AND SUBLIMATION THERMODYNAMICS OF SELECTED LANTHANIDE FLUORIDES

By

Robert Malcolm Biefeld

A DISSERTATION

Submitted to

Michigan State University

in partial fulfillment of the requirements

for the degree of

DOCTOR OF PHILOSOPHY

Department of Chemistry

ACKNOWLEDGEMENTS

It would be impossible to mention all of the people who have contributed to the completion of the research for this dissertation in a short space. However, I wish to thank all of the past and present members of Dr. Harry A. Eick's research group and the faculty and staff of the Chemistry Department at Michigan State University. Special thanks must be given to Dr. A. V. Hariharan for his help with the experimental techniques which were used and to Dr. Harry A. Eick for his helpful suggestions and guidance.

I wish to thank my wife, Dr. Carol G. Biefeld, without whose encouragement, understanding and hours of effort this dissertation might not have been completed.

The financial support of the Chemistry Department at Michigan State University and the U. S. Atomic Energy Commission is acknowledged gratefully.

TABLE OF CONTENTS

Chapter		Page
1.	Introduction	1
2.	Previous Investigations of Lanthanide Fluoride Systems	3
	2.1. Preparation of Lanthanide Fluorides	3
	2.2. Structural Determinations	4
	2.3. Thermochemical Measurements on Lanthanide Halides	7
	2.4. Molecular Geometry and Infrared Spectra of Gaseous Lanthanide Fluorides	11
	2.5. Electronic Structures of the Gaseous Lanthanide Fluorides	13
3.	Theoretical Considerations	15
	3.1. The Phase Rule and Vaporization	15
	3.2. Determination of Vapor Pressure -- The Knudsen Effusion Method	16
	3.3. Temperature Measurement	22
	3.4. Mass Spectrometric Measurements	23
	3.5. X-Ray Fluorescence Analysis	26
	3.6. Thermodynamic Calculations	27
4.	Experimental Materials, Equipment and Procedures	34
	4.1. Materials	34
	4.2. Preparative Procedures and Equipment	35
	4.3. X-Ray Powder Diffraction Analysis	37
	4.4. Metal Analysis	37
	4.5. Mass Spectrometric Procedures	38
	4.6. Target Collection Procedures	38
	4.7. X-Ray Fluorescence Analysis	41
	4.8. Film Thickness Monitor	43
	4.9. Distillation Experiments	44
	4.10. Mass Loss Experiments	44
5.	Results	46
	5.1. Preparations	46
	5.2. Mass Loss Results	49
	5.3. Mass Spectrometric Results	53

TABLE OF CONTENTS (cont'd.)

5.4. Distillation Results 66
5.5. Knudsen Effusion Results 67

6. Discussion 92

6.1. Evaluation of Experimental Procedures 92
6.2. Evaluation of Thermochemical Data and Estimates 94
6.3. Pressure-Composition Diagrams and Stability Relationships 102
6.4. Conclusions and Suggestions for Future Investigations 111

References 113

Appendices 121

LIST OF TABLES

Table		Page
1.	Structural Data of Selected Lanthanide(III) Fluorides	6
2.	Phase Regions Observed in the LnF_2-LnF_3 System for Ln = Eu and Sm	8
3.	X-Ray Fluorescence Spectrometer Conditions	42
4.	Metal Analytical Results for Selected Lanthanide Fluorides	47
5.	X-Ray Diffraction Results for Selected Lanthanide Fluorides	47
6.	Structures of Selected Reduced Lanthanide Fluorides	48
7.	Results of Mass Loss Experiments for Ytterbium Fluoride Samples Confined in Mo	50
8.	Results of Mass Loss Experiments for Samarium and Thulium Fluoride Samples Confined in Mo	52
9.	Appearance Potentials of the Ions Detected in the Ytterbium Fluoride System	62
10.	Fragmentation Patterns for Selected Lanthanide Halides	64
11.	Experimental Conditions for Vaporization Runs in the Ytterbium Fluoride System	68
12.	Results of Linear Least-Squares Analyses of Vaporization Reactions in the Ytterbium Fluoride System	70
13.	Lower Limits of Knudsen Numbers	93
14.	Comparison Between the Sublimation Thermodynamics of Selected Lanthanide(III) Fluorides at 298 K for Incongruent and Congruent Reactions	96
15.	Thermodynamic Values for the Congruent Sublimation of Selected Lanthanide(III) Fluorides	97

LIST OF TABLES (cont'd.)

16. Comparison of Pressures Observed by Various Investigators for Gaseous Lanthanide Fluorides at Median Temperatures 98

17. Thermodynamic Values for the Congruent Sublimation of the Intermediate Fluorides $SmF_{2.40}$ and $YbF_{2.40}$ According to the Reaction $LnF_{2.40}(s) = (0.6)\ LnF_2(g) + (0.4)\ LnF_3(g)$ 100

18. Thermodynamics for the Congruent Sublimation of Selected Metal(II) Fluorides 101

19. Thermodynamic Values for the Congruent Vaporization of Selected Metal Fluorides at their Boiling Points 103

LIST OF FIGURES

Figure		Page
1.	Distillation Assembly	45
2.	Intensity of Yb^+ from YbF_{2+x} ($0.00 \leq x < 0.40$) Confined in Mo *vs.* Time	54
3.	Ionization Efficiency Curve of Yb^+ from YbF_{2+x} ($0.00 \leq x < 0.40$) Confined in Mo	56
4.	Intensity of Yb^+ from YbF_{2+x} ($0.00 \leq x \leq 0.40$) Confined in Mo *vs.* Time	57
5.	Fractional Ion Intensities of Yb^+, YbF^+ and YbF_2^+ from YbF_{2+x} ($0.00 \leq x \leq 0.40$) Confined in Mo *vs.* Time	58
6.	Ionization Efficiency Curves for Yb^+, YbF^+ and YbF_2^+ from YbF_{2+x} ($0.00 \leq x < 0.40$) Confined in Mo	60
7.	Ionization Efficiency Curves for Yb^+, YbF^+ and YbF_2^+ from $YbF_{2.40}$ Confined in Mo	61
8.	Ionization Efficiency Curves for Yb^+, YbF^+ and YbF_2^+ from YbF_3 Confined in Mo	63
9.	Natural Logarithm of the Equilibrium Constant for the Congruent Vaporization of $YbF_{2.40}$ and the Pressure of Yb(g) from YbF_{2+x} ($0.00 \leq x < 0.40$) *vs.* Reciprocal Temperature	71
10.	Rate of Deposition of Yb(g) from YbF_{2+x} ($0.01 \leq x < 0.40$) Confined in Mo *vs.* Time	72
11.	Natural Logarithm of the Equilibrium Partial Pressure of YbF_3(g) from $YbF_3(s,\ell)$ *vs.* Reciprocal Temperature	76
12.	Rate of Deposition for Sm(g) from SmF_{2+x} ($0.00 \leq x < 0.40$) Confined in Mo *vs.* Time	80
13.	Natural Logarithm of the Equilibrium Constant for the Congruent Vaporization of $SmF_{2.40}$ and the Pressures of Sm(g) from SmF_{2+x} ($0.00 \leq x < 0.40$) *vs.* Reciprocal Temperature	81

LIST OF FIGURES (cont'd.)

14. Natural Logarithm of the Equilibrium Partial Pressure of $SmF_3(g)$ from $SmF_3(s,\ell)$ *vs.* Reciprocal Temperature 85

15. Natural Logarithm of the Equilibrium Pressure of $TmF_3(g)$ from $TmF_3(s,\ell)$ *vs.* Reciprocal Temperature 90

16. Qualitative Pressure-Composition Diagram for the Eu-F System 104

17. Qualitative Pressure-Composition Diagram for the Sm-F System 105

18. Qualitative Pressure-Composition Diagram for the Yb-F System 106

19. Qualitative Pressure-Composition Diagram for the Tm-F System 107

LIST OF APPENDICES

Appendix		Page
1.	X-Ray Powder Diffraction Data for the Reduced Lanthanide Fluorides	121
1.1.	X-Ray Powder Diffraction Data for Cubic $YbF_{2.01}$	121
1.2.	X-Ray Powder Diffraction Data for Cubic $YbF_{2.19}$	121
1.3.	X-Ray Powder Diffraction Data for Pseudo-Tetragonal $YbF_{2.29}$	122
1.4.	X-Ray Powder Diffraction Data for Pseudo-Hexagonal $YbF_{2.41}$	123
1.5.	X-Ray Powder Diffraction Data for Cubic $SmF_{2.00}$	124
1.6.	X-Ray Powder Diffraction Data for Pseudo-Hexagonal $SmF_{2.44}$	124
1.7.	X-Ray Powder Diffraction Data for a Reduced Thulium Fluoride	125
2.	Knudsen Effusion Data in Chronological Order	126
2.1.	Data for Yb(g) from YbF_{2+x} ($0.00 \leq x < 0.40$) Confined in Mo	126
2.2.	Data for the Rate of Deposition of Yb(g) *vs.* Time	126
2.3.	Data from $YbF_{2.40}$ Effusion Experiments	127
2.4.	Data from YbF_3 Effusion Experiments	130
2.5.	Data for Sm(g) from SmF_{2+x} ($0.00 \leq x < 0.40$) Confined in Mo	132
2.6.	Data for the Rate of Deposition of Sm(g) *vs.* Time	132
2.7.	Data from $SmF_{2.40}$ Effusion Experiments	133
2.8.	Data from SmF_3 Effusion Experiments	135
2.9.	Data from TmF_3 Effusion Experiments	137
3.	Derived Thermodynamic Functions for Selected Lanthanide Fluorides	139
3.1.	Derived Thermodynamic Functions for $YbF_3(g)$	139
3.2.	Derived Thermodynamic Functions for $YbF_3(s,\ell)$	140

LIST OF APPENDICES (cont'd.)

3.3. Derived Thermodynamic Functions for $YbF_2(g)$ 141

3.4. Derived Thermodynamic Functions for $YbF_2(s,\ell)$ 141

3.5. Derived Thermodynamic Functions for $SmF_3(g)$ 142

3.6. Derived Thermodynamic Functions for $SmF_3(s,\ell)$ 142

3.7. Derived Thermodynamic Functions for $SmF_2(g)$ 143

3.8. Derived Thermodynamic Functions for $SmF_2(s,\ell)$ 143

3.9. Derived Thermodynamic Functions for $TmF_3(g)$ 144

3.10. Derived Thermodynamic Functions for $TmF_3(s,\ell)$ 144

4. Mass Spectrometry Data 145

4.1. Ion Intensity of Yb^+ from $YbF_{2+x}(s)$ Confined in Mo *vs.* Time 145

4.2. Ionization Efficiency Curve Data for Yb^+ from YbF_{2+x} Confined in Mo 146

4.3. Intensity of Yb^+ and Intensity Fractions of Yb^+, YbF^+ and YbF_2^+ from YbF_{2+x} $(0.0 \leq x < 0.4)$ Confined in Mo *vs.* Time 147

4.4. Ionization Efficiency Curve Data for Yb^+, YbF^+ and YbF_2^+ from YbF_{2+x} $(0.0 \leq x < 0.4)$ Confined in Mo 148

4.5. Ionization Efficiency Curve Data for Yb^+, YbF^+ and YbF_2^+ from $YbF_{2.40}$ Confined in Mo 149

4.6. Ionization Efficiency Curve Data for Yb^+, YbF^+ and YbF_2^+ from $YbF_{3.0}(\ell)$ Confined in Mo 150

5. Untreated Data from Knudsen Effusion Experiments in Chronological Order 151

5.1. Target Collection Data for Yb(g) from YbF_{2+x} $(0.00 \leq x < 0.40)$ Confined in Mo 151

5.2. Target Collection Data for $YbF_{2.40}$ Effusion Experiments 152

5.3. Target Collection Data for $YbF_{3.00}$ Effusion Experiments 157

5.4. Target Collection Data for Sm(g) from SmF_{2+x} $(0.00 \leq x < 0.40)$ Confined in Mo 161

5.5. Target Collection Data For $SmF_{2.40}$ Effusion Experiment 1 162

5.6. Target Collection And Deposition Data for $SmF_{2.40}$ Effusion Experiments 163

5.7. Rate Data for $SmF_{2.40}$ Effusion Experiments 165

LIST OF APPENDICES (cont'd.)

5.8. Target Collection Data for $SmF_{3.00}$ Effusion Experiment 1 167

5.9. Target Collection and Deposition Data for $SmF_{3.00}$ Effusion Experiments 168

5.10. Rate Data for $SmF_{3.00}$ Effusion Experiments 170

5.11. Target Collection and Deposition Data for $TmF_{3.00}$ Effusion Experiments 172

5.12. Rate Data for $TmF_{3.00}$ Effusion Experiments 174

5.13. X-Ray Fluorescence Analysis of Standards 176

CHAPTER 1

INTRODUCTION

Chemists and materials scientists are being asked to develop refractory materials for a variety of high temperature applications. New materials will be needed for use in fusion reactors and high temperature batteries, and for high temperature recycling of waste materials. Since lanthanide binary compounds are refractory, some of these chemicals may be of practical importance. To determine if a material may be of use in a particular high temperature application, certain of its properties must be known. The research discussed in this dissertation was undertaken to obtain thermodynamic values for the high temperature sublimation and vaporization reactions of selected refractory lanthanide fluorides. Knudsen effusion, X-ray diffraction and mass spectrometric techniques were used to characterize the high temperature reactions for the phases selected.

The choice of the lanthanide systems investigated in this work was based on the dearth of thermodynamic data on divalent lanthanide binary systems involving elements other than europium. The extension of a few thermochemical measurements across the lanthanide series is a relatively valid practice if the deviations of the "tetrad effect", the lanthanide contraction and the valence states of atomic europium and ytterbium are taken into consideration. However, the prediction of the properties of other divalent lanthanide compounds

from similar properties of europium is less valid. Since the trivalent oxidation state of europium is less stable than the trivalent state of the other lanthanides and since thermochemical trends have not been established experimentally, the prediction of the behavior of the divalent lanthanides, ytterbium, samarium and thulium, from the behavior of divalent europium is, at best, tenuous. In order to establish a trend among the divalent lanthanides, the ytterbium fluoride system was examined extensively, and the samarium and thulium fluoride systems were studied somewhat less extensively.

The vaporization and sublimation reactions and their corresponding thermodynamics were determined for the selected lanthanide fluoride systems. The trends observed among the systems studied for this dissertation are extended to other lanthanide systems when possible. However, the unusual reactions reported in this investigation emphasize the individuality of each lanthanide binary system and the necessity for separate investigations on such systems. The thermodynamic data presented in this dissertation should serve as a contribution to a continuing compilation of fundamental thermodynamic values for, and a better understanding of lanthanide binary systems.

CHAPTER 2

PREVIOUS INVESTIGATIONS OF LANTHANIDE FLUORIDE SYSTEMS

2.1. Preparation of Lanthanide Fluorides

2.1.1. Lanthanide(III) Fluorides

Several recent general reviews of preparatory methods for the lanthanide trihalides are available.[1-3] In addition, these methods have been summarized by Brown[4] and Hariharan.[5] Special precautions against exposure to water and oxygen are necessary for all of the lanthanide trihalides except the trifluorides. Two methods which have been reported to yield very high purity lanthanide trifluoride samples are the direct synthesis from the elements[6] and the high temperature fluorination of the sesquioxide.[7] A more generally applicable method which yields reasonably high purity samples involves dehydration of the hydrated trifluoride.[1,2,5] The hydrated trifluoride is formed by precipitation with concentrated hydrofluoric acid from an acidic aqueous solution. Dehydration is accomplished with anhydrous ammonium fluoride at high temperatures. Heating *in vacuo*, sublimation or distillation serves to purify the product further.[5,8]

2.1.2. Lanthanide(II) Fluorides

Only the difluorides of europium, ytterbium, and samarium have been prepared. Although europium(III) fluoride was reduced successfully to europium(II) fluoride by hydrogen at temperatures above

1573 K[9-11] only partial reduction was achieved for samarium and ytterbium.[9] Other partial reductions have been reported.[12] One method for complete reduction of europium, ytterbium, and samarium trifluorides to the difluorides is the use of the corresponding lanthanide metal in a closed bomb at high temperatures.[11,13,14] A variation of this technique which employs in situ vaporization of the lanthanide metal has also been employed successfully.[15]

2.1.3. Mixed Valence Lanthanide Fluorides

In their attempts to reduce the lanthanides(III) fluorides with hydrogen, Asprey et al.[9] observed an apparent solid solution between LnF_2 and LnF_3 in the form of a cubic structure with variable composition and lattice parameter. Lee et al.[10] and Catalano et al.[11] confirmed the presence of mixed valence compounds by use of both hydrogen and lanthanide metal reduction techniques for the Eu-F system. The direct reduction of the trifluoride with the metal or the technique of mixing the difluoride and the trifluoride and sealing the mixture in a molybdenum or tantalum container has been used to prepare mixed valence fluorides of samarium,[11,13] ytterbium,[14] and europium.[11,14,16]

2.2. Structural Determinations

2.2.1. Lanthanide(III) Fluorides

The lanthanide(III) fluorides of lanthanum to neodymium crystallize with the hexagonal LaF_3 structure.[4] The trifluorides of samarium to lutetium are dimorphic and exhibit the orthorhombic YF_3 structure at lower temperatures, and an hexagonal modification at higher temperatures.[4] The hexagonal high temperature phase has the LaF_3 structure for samarium to holmium while for erbium to lutetium the

exact structure is still uncertain. Recent investigators have redetermined lattice parameters of the structures encountered[7,17,18] and discussed the reasons for the changes in structure.[17] Data for the trifluorides pertinent to this investigation are listed in Table 1.

2.2.2. Lanthanide(II) Fluorides

The structural chemistry of the divalent lanthanide halides is remarkably similar to that of the heavier alkaline earth compounds.[5,19-22] All of the lanthanide(II) fluorides thus far prepared have the cubic calcium fluoride structure. The lattice parameters for the difluorides which have been prepared are as follows: SmF_2, $\underline{a}$ = 0.58710(5) nm; EuF_2, $\underline{a}$ = 0.58423(10) nm; YbF_2, $\underline{a}$ = 0.55991(5) nm.[15]

2.2.3. Mixed Valence Lanthanide Fluorides

The variable lattice parameters of the cubic structures reported for the reduced lanthanide fluorides[9-11] have been explained by nonstoichiometry.[10,11] Catalano et al.[11] have reported two nonstoichiometric regions for samarium and europium fluorides: a cubic region with a range of $LnF_{2.00}$ to $LnF_{2.25}$ and a region of unidentified structure between $LnF_{2.25}$ to $LnF_{2.45}$. They also identified a two phase region, $LnF_{2.45}$ to $LnF_{3.00}$, and were unable to isolate a phase with an F to Ln ratio less than 2.00. Attempts to prepare a LnF_{2-x} phase resulted in a mixture of the metal and the difluoride. The Yb-F system was also examined by Catalano et al.[11,14] with results similar to, but more complex than, those of the Sm- and Eu-F systems. The reaction of thulium(III) fluoride with thulium metal resulted in incomplete reduction. When treated with the respective lanthanide metal, the other lanthanide(III) fluorides exhibited no signs of reduction except for a slight color change for praseodymium(III)

Table 1. Structural Data of Selected Lanthanide(III) Fluorides

Phase	Structural Type	Space Group	Trans Temp(K)[1,2]	Lattice Parameters a(nm)	b(nm)	c(nm)
SmF_3	Orthorhombic YF_3	Pnma	763	0.66715[3]	0.70584	0.44028
	Hexagonal LaF_3	$P\bar{3}c1$	763	0.69536[3]	-------	0.71183
TmF_3	Orthorhombic YF_3	Pnma	1326	0.62779[3]	0.68133	0.44095
	Hexagonal	----	1326	0.703[4]	-----	0.835
YbF_3	Orthorhombic YF_3	Pnma	1259	0.62165[3]	0.67855	0.44314
	Hexagonal	----	1259	0.699[4]	-----	0.832

[1]Temperature above which the hexagonal form becomes stable

[2]Reference 18

[3]Reference 17

[4]Reference 4

and neodymium(III). More complete characterizations of the Eu- and Sm-F systems have been reported by Tanguy et al.[16] and Stezowski and Eick,[13] respectively. In each instance regions of nonstoichiometry were observed for the reduced fluorides. Two new phases were found and described as tetragonal and rhombohedral modifications of the cubic fluorite lattice. These phases were considered to contain interstitial fluoride anions with partial substitution of Ln^{+3} for Ln^{+2}. The composition ranges and the corresponding lattice parameters are listed in Table 2.

2.3. Thermochemical Measurements on Lanthanide Halides

Very few experimental thermodynamic values have been reported for the lanthanide halides. In place of the experimental measurements internally consistent estimates of the thermodynamic properties for the lanthanide halides have been published.[23-26] These estimates have been and will continue to be invaluable in thermodynamic studies. However, comparison of these estimates with recently determined experimental thermodynamic values revealed only marginal agreement.[5,27,28] A continuing effort to add to the existing experimental measurements seems justified.

2.3.1. Calorimetric Investigations

2.3.1.1. Lanthanide(III) Fluorides

The enthalpy increments and related thermodynamic functions have been determined for all of the trifluorides except promethium.[7,18,29,30] Measurements were carried out from 373-1873 K except for EuF_3 (373-1298 K) and include the enthalpies and entropies of transition and melting. The low temperature enthalpy increments from 5 to 300 K have also been determined for CeF_3.[30,31] The enthalpy

Table 2. Phase Regions Observed in the LnF_2-LnF_3 System for Ln = Eu and Sm

x in SmF_x[1]	x in EuF_x[2]	Phase(s)	Lattice Parameters
< 2.00	< 2.00[3]	Ln + LnF_2	-----
2.00 < x < 2.14	-----	homogeneous cubic	0.5867(1) > a > 0.5841(1) nm
-----	2.00 < x < 2.15	"	0.5840(5) > a > 0.5804(5)
2.14 < x < 2.34	-----	cubic + tetragonal	-----
-----	2.15 < x < 2.25	"	-----
2.35	-----	pseudo-tetragonal	a = 0.4106(2), c = 0.5825(3)
-----	2.25	"	a = 0.4085(5), c = 0.5806(5)
2.36 < x < 2.40	-----	tetragonal + rhombohedral	-----
-----	2.25 < x < 2.33	"	-----
2.41 < x < 2.46	-----	rhombohedral	0.7124(2) > a > 0.7096(2) 33.40(2)° > α > 33.23(2)°
-----	2.33 < x < 2.40	"	0.7139(5) > a > 0.7102(5) 33.66(1)° > α > 33.36(1)°
2.46 < x < 3.00	-----	rhombohedral + LnF_3	-----
-----	2.40 < x < 3.00	"	-----

[1]Reference 13

[2]Reference 16

[3]References 11,14

and Gibbs free energy of formation for yttrium(III) fluoride, often considered one of the rare earths, have been measured by fluorine bomb calorimetry [$\Delta H_f^\circ(298\ K) = -(410.7 \pm 0.8)$ and $\Delta G_f^\circ(298\ K) = -(393._6 \pm 1._0)$ kcal mol^{-1}].[32]

2.3.1.2. Lanthanide(II) Fluorides

No data are available for the lanthanide(II) fluorides. The estimative technique of Hariharan,[5] which is to use the values reported for the alkaline earth fluorides, is probably the best alternative.

2.3.1.3. Other Selected Lanthanide Halides

Enthalpy increments have been reported for certain lanthanide(III) chlorides, bromides, and iodides,[33-35] but no experimental data are available for any corresponding lanthanide(II) compounds. The enthalpies of formation of $EuCl_2$[36,37] and $YbCl_2$[38] have been measured.

2.3.2. High Temperature Sublimation and Vaporization Studies

2.3.2.1. Lanthanide(III) Fluorides

Recently there has been a resurging interest in the sublimation and vaporization properties of the lanthanide(III) fluorides. Searcy and coworkers characterized the high temperature behavior of LaF_3, CeF_3 and PrF_3 by a combination of torsion-effusion and torsion-Langmuir techniques.[39-41] By using high temperature mass spectrometric methods, these workers have also demonstrated the existence of $La_2F_6(g)$ and $Ce_2F_6(g)$ and have determined the stabilities and partial pressures of these species in equilibrium with LaF_3 and CeF_3.[42,43] Mass spectrometric studies have been made on the sublimation reactions of all of the lanthanide(III) fluorides except promethium.[44] The bond dissociation energies and stabilities of the gaseous mono- and difluorides of all the lanthanides except promethium were derived

from ionization potentials determined by the electron-impact method.[44] The sublimation thermodynamics and vapor pressures of all the lanthanide(III) fluorides except promethium, samarium, europium and ytterbium were redetermined by simultaneous mass effusion and mass spectrometric measurements.[8,45,46] This latter series of measurements was effected as part of a study on the role of the correlation of entropy and enthalpy in the error analysis for vaporization and sublimation thermodynamics.

2.3.2.2. Lanthanide(II) Fluorides

The vapor pressure and the sublimation and vaporization thermodynamics study on EuF_2 by Petzel and Greis[47] with mass effusion methods is the only determination reported for a lanthanide(II) fluoride.

2.3.2.3. Other Lanthanide Halides

Of particular interest to this dissertation are the thermochemical values reported for the halides of samarium, europium, thulium and ytterbium. The vapor pressures of the halides $SmBr_3$,[48] $SmCl_2$, $EuCl_3$, $TmCl_3$ and $YbCl_3$[49] were measured by the mass effusion method. A boiling point method was used to measure the vapor pressures of $SmCl_2$, $EuCl_2$ and $YbCl_2$.[50] The dissociation pressures of $SmCl_3$, $EuCl_3$ and $YbCl_3$ were determined by the measurement of chlorine pressures with a quartz membrane.[51] The decomposition of $EuBr_3$ to $EuBr_2$ and bromine has also been investigated.[52]

Recently the vaporization and sublimation thermodynamics of europium(II) halides have been studied systematically and correlated by mass spectrometry and Knudsen effusion methods.[5,47,53-55] A close correspondence in the thermochemical properties was reported between the dihalides of europium and the heavier alkaline earths (Ca, Sr

and Ba), especially with those of Sr. Another important observation concerned the constant entropy of congruent sublimation at 298 K for europium(II) halides.[5] From the above observations the thermochemical properties of other lanthanide(II) halides might be expected to correspond to properties of the heavier alkaline earths and the entropy change for the congruent sublimation at 298 K for the dihalides of a particular lanthanide should be constant.

The vaporization and sublimation of $EuCl_2$ and $EuCl_3$ were investigated *via* mass spectrometry by Hastie *et al.*[56]

A target collection technique in conjunction with mass spectrometry was used to study $YbCl_2$.[57] The vaporization thermodynamics of $YbCl_2$ corresponded closely with those of $EuCl_2$ and $SrCl_2$.

None of the other dihalide systems has been investigated.

2.3.3. Galvanic Cell Measurements

The solid electrolyte galvanic cell technique was used to determine the free energies of the displacement reactions for selected metals and their fluorides.[58] The free energies of formation as a function of temperature were reported for YF_3, NdF_3, GdF_3, DyF_3, ErF_3 and LuF_3.

2.4. Molecular Geometry and Infrared Spectra of Gaseous Lanthanide Fluorides

A variety of methods have been used to investigate the molecular geometry of the lanthanide fluorides. These methods include electron diffraction of molecular beams, infrared and Raman spectra of the gaseous fluorides isolated in low temperature, inert gas matrices and electric quadrupole deflection of molecular beams in inhomogeneous electric fields. The information arising from such investigations,

although sometimes contradictory, has been an invaluable aid in estimating the thermodynamic functions of the gaseous lanthanide fluorides.

2.4.1. Lanthanide(III) Fluorides

An unresolved controversy exists over the structures of some gaseous lanthanide(III) fluorides. The trifluorides can assume a planar, D_{3h}, or a non-planar, C_{3v}, structure. Of the fluorides of interest to this dissertation, SmF_3, EuF_3, TmF_3 and YbF_3, only $SmF_3(g)$ has consistently been reported as planar.[59,60] However, SmF_3 was not investigated by Hauge et al.[61] who assigned a non-planar configuration for $EuF_3(g)$ and $YbF_3(g)$ while Wesley and DeKock[60] assigned a planar configuration to these molecules. The results obtained by Kaiser et al.[59] from their electric deflection experimetns were inconclusive for $SmF_3(g)$, $EuF_3(g)$ and $YbF_3(g)$ due to reduction of the samples by the nickel oven. The F-Ln-F angle used by Hauge et al.,[61] 117°, indicates that any distortion from a planar configuration, 120°, for the gaseous lanthanide(III) fluorides is small. The use of Raman measurements resolved the controversy for $PrF_3(g)$, and it is considered planar.[62] However, no other trifluoride was investigated in this manner. The reported reduction of YF_3[63] by tantalum containers cannot be used to explain the spectra observed by Hauge et al.[61] for $EuF_3(g)$ or $YbF_3(g)$ since the spectra did not correspond to those reported for $EuF_2(g)$[64,65] and $YbF_2(g)$.[65] The incorrect choice of configuration for the gaseous trifluorides changes the calculated entropy and free energy function values by R ℓn 2 (R = 1.98717 cal $mol^{-1}K^{-1}$) (cf. Section 3.6.6.3.).

Electron diffraction studies have yielded Ln-F distances for $YF_3(g)$, $LaF_3(g)$ and $NdF_3(g)$.[66]

2.4.2. Lanthanide(II) Fluorides

Both electric deflection[59] and infrared matrix isolation[64,65] experiments are in complete agreement in so far as the structures of $SmF_2(g)$, $EuF_2(g)$ and $YbF_2(g)$ are concerned. The gaseous difluorides have a non-linear structure with a F-Ln-F angle of $(110 \pm 15)^\circ$ for $SmF_2(g)$ and $EuF_2(g)$ and an angle of $(140 \pm 10)^\circ$ for $YbF_2(g)$. Neither electron diffraction nor Raman matrix isolation studies have been carried out on the difluorides.

2.5. Electronic Structures of the Gaseous Lanthanide Fluorides

2.5.1. Lanthanide(III) Fluorides

In the absence of experimental data, an accepted practice for calculating the electronic contribution to the statistical entropy has been to use the data available for the free ion.[60,67,68] Values have been reported for the trivalent lanthanide ions of interest to this dissertation (Sm^{+3}, Eu^{+3}, Tm^{+3} and Yb^{+3}).[69-71]

2.5.2. Lanthanide(II) Fluorides

The same lack of experimental information exists for the gaseous lanthanide(II) fluorides. The ground states of the lanthanide(II) ions are assumed to be those described by Sugar and Reader[72] (i.e., an f^N configuration). The electronic energy levels of the lanthanide(II) ions are taken to be the same as the $(Ln + 1)^{+3}$ levels. For example the reported electronic energy levels for europium(III)[70] were used to estimate the levels for samarium(II).

The scarcity of thermochemical measurements for lanthanide binary compounds requires the use of many estimates in investigations such

as the one reported in this dissertation. Because of this scarcity the thermodynamic values presented herein are deemed to be a small but valuable contribution to the thermodynamic data presently available for the lanthanide halides.

CHAPTER 3

THEORETICAL CONSIDERATIONS

3.1. The Phase Rule and Vaporization

High temperature vaporization and sublimation reactions can be classified broadly as either congruent or incongruent. Congruency requires that the vapor and condensed phases have identical compositions. Conversely, incongruency requires nonidentical compositions for the vapor and condensed phases. The application of the Phase Rule, (3-1), in which for each system F is the number of degrees

$$F = C - P + 2 \qquad (3\text{-}1)$$

of freedom (i.e., the number of parameters that must be specified to establish the state of a system[73]), C the number of independent chemical variables or components and P the number of phases present, further characterizes vaporization reactions at equilibrium. For a congruent reaction in a binary (i.e., two component) system, the number of phases, P, is two (i.e., vapor and solid or liquid). However, the congruency constraint requires that the composition of both of these phases be equal, and the number of independent components, C, is one. Thus, according to the Phase Rule, for a congruent reaction in a binary system only one parameter, e.g. the temperature, needs to be specified to define the pressure of the system (i.e., the system is univariant). For an incongruent reaction in a binary system, the number of independent components, C, is two.

If in addition to the vapor, two condensed phases are present, the state of the system is again defined completely by specifying one parameter. However, if in an incongruent reaction the condensed phase is a solid solution or a solid whose composition can vary within limits, the pressure of the system is not defined completely by fixing the temperature (i.e., the system is bivariant).

The qualitative aspects of vaporization and sublimation reactions in a binary system can be represented in the form of a constant temperature diagram of pressure vs. composition. The composition range of the phases and their vaporization reactions are readily defined from such a diagram. More complete discussions of the Phase Rule, pressure-composition diagrams, and heterogeneous equilibria can be found elsewhere.[73-75]

3.2. Determination of Vapor Pressure -- The Knudsen Effusion Method

3.2.1. The Kinetic Theory of Gases

A variety of methods can be used to determine vapor pressures.[76] The Knudsen effusion method, which was used in the research for this dissertation, is applicable in the pressure range 10^{-10} to 10^{-3} atm.[5] In the Knudsen effusion method the flux of molecules through an orifice in an isothermal cell is determined. Under certain ideal conditions (discussed below) the equilibrium vapor pressure within the container can be calculated from this flux and from the kinetic theory of ideal gases.[77] The appropriate expression for the flux of molecules, dJ, which strike or leave an area, da, in the solid angle, dw, for an ideal gas in equilibrium with its surroundings is given by (3-2).

$$dJ = (\nu\bar{c}/4\pi)\cos\theta \, dw \, da \qquad (3\text{-}2)$$

In (3-2) θ is the angle of the normal to da and the line of direction

defined by dw, ν is the molecular density and $\bar{c}$ is the average molecular thermal speed. Equation (3-2) is called the cosine distribution law. Integration of (3-2) yields the total molecular flux, J, which strikes an area, a,

$$J = a\nu\bar{c}/4. \tag{3-3}$$

Use of (3-3) in combination with the ideal gas law, $pV = NkT$, and $\bar{c} = (8kT/\pi m)^{\frac{1}{2}}$, where k is the Boltzmann constant, T is the absolute temperature, N and m are the number and mass of the molecules, respectively, yields the Hertz-Knudsen equation (3-4),[78,79]

$$p = (w/at)(2\pi kT/m)^{\frac{1}{2}}, \tag{3-4}$$

in which w is the mass of the vapor which strikes an area, a, in a given time, t. If the molecules are allowed to escape through an infinitely thin orifice of area, a, into a vacuum, the above expression remains unchanged provided the rate of molecular escape does not change the equilibrium vapor pressure in the cell.

3.2.2. The Target Collection Technique

One of a variety of methods used to determine the rate at which molecules effuse through an orifice is target collection. In this method a fraction of the effusing gases is collected by condensation on a target located coaxially with and parallel to the orifice. If the orifice and target are circular, and the orifice radius, R_o, is small compared to that of the target radius, R, and to the target to orifice distance, C, application of the cosine distribution law yields an expression, (3-5),[76] for the fraction of the effusate, F,

$$F = R^2/(C^2 + R^2) \tag{3-5}$$

striking the target. Combination of (3-4) and (3-5) and substitution of numerical values for the appropriate constants leads to equation

(3-6). The following values were used: $N = 6.0225 \times 10^{23}$ mol^{-1},

$$p(atm) = (w/44.33\ at)(T/M)^{\frac{1}{2}}(1/F) \qquad (3\text{-}6)$$

$k = 1.3805 \times 10^{-16}$ erg K^{-1}, 1 atm = 1.0133×10^{6} dynes cm^{-2}, and $\pi = 3.1416$. In (3-6) M is the molecular wight of the effusing gas in amu, and the quantities w, a, t, T, M, and F are experimentally determinable. By application of equation (3-6) to a univariant binary system, the equilibrium vapor pressures can, in theory, be determined.

3.2.3. Underlying Assumptions and Limitations of the Knudsen Effusion Method

3.2.3.1. Kinetic Theory of Ideal Gases

Many assumptions are made in the derivation of the equations used in the Knudsen effusion method. The most basic of these is that the vapor species behave as ideal gases. An ideal gas is an isotropic vapor of identical non-interacting point masses with a Maxwellian velocity distribution. Since most gases approach ideality at low pressures,[80] their behavior in the pressure regions measured by the Knudsen method should approximate ideality.[77-80]

3.2.3.2. Experimental Limitations

In the Knudsen effusion method, an attempt is made to approximate ideal conditions so that a physical measurement of the equilibrium vapor pressure of a system can be made. The Knudsen cell must be impervious and inert. Chemical reaction between the cell material and the substance under investigation could alter the activities of the substance and change the corresponding vapor pressures.[80] Ward *et al.* have reported the effect which vapor loss by interactions with the cell wall through collisions can have on the measured vapor

pressures,[81,82] and have demonstrated that these effects can be significant.

Since a real orifice cannot be infinitely thin, the ideal orifice is often approximated with a knife-edged orifice ($L_o/R_o \approx 0$, L_o is the length of the orifice and R_o its radius). However, the orifice will always be of finite thickness and the molecular flux from the cell will be altered. Corrections for this effect have been calculated for various types of orifices[83,84] and are termed Clausing transmission factors because of his original treatment of angular distributions from Knudsen cells.[85,86] Hirth and coworkers[87,88] have extended these calculations to include surface diffusion along the orifice walls and the cell lid. Their calculations involve parameters that are dependent on the cell material and the effusing species. Fortunately, the correction factors for the angular distributions commonly encountered in the target collection method are not significantly different from unity. Ward et al.[81,82,89] have calculated and measured severe deviations from the cosine law at large angles, but observed only minor effects at the small angles used in the target collection technique. They reported a marked effect, independent of the compound involved, for cell geometry. These effects can be minimized by use of a small orifice area as compared to the interior cross sectional area of the cell and by use of a collection technique which employs only small angles. Other reports indicate that only minor deviations from ideal behavior occur for knife-edge orifices or for non-ideal orifices when Clausing transmission factors are used.[90-93]

The Knudsen cell must be maintained at a uniform temperature to insure equilibrium conditions. The complete elimination of a temperature gradient in a cell is very difficult experimentally, and a small but constant temperature gradient of 5 to 10° has been shown to have little effect on the resulting experimental values.[5,94] However, a small variation in the gradient over the temperature range can have a marked effect upon the derived thermodynamic values. The minimization of the effects of temperature gradients has been discussed by Storms.[95]

Additional experimental limitations to the target collection method involve the condensation of the effusing vapor as it strikes the target and the interference from molecular collisions between the effusing vapor and residual gases. Previous investigators[5,96] who employed the same experimental systems that were used for the research done for this dissertation have found no evidence that the lanthanides or the lanthanide halides do not condense when they impinge on a chilled target. If residual pressures are maintained two to three orders of magnitude below those of the effusing vapors, interference from collisions with the residual gases would be limited.

3.2.3.3. Equilibrium in the Knudsen Cell

If a system is at equilibrium the rate of the forward reaction, evaporation, must equal the rate of the reverse reaction, condensation. Introduction of an orifice into the cell dictates that a net loss of vapor occurs and that a steady state situation exists. An expression (3-7) has been derived[97] which relates the measured pressure,

$$p_e = p_m[1 + f(1/\alpha + 1/W_A - 2)] \qquad (3\text{-}7)$$

p_m, to the equilibrium pressure, p_e. In this expression $f = W_a a/A$,

a is the orifice area, A is the sample surface area, W_a and W_A are the Clausing transmission factors for the orifice and the cell body, respectively, and α is the evaporation and/or condensation coefficient. The evaporation coefficient, α_v, is defined as the observed rate of evaporation divided by the equilibrium rate of molecules striking the sample surface. The condensation coefficient, α_c, is defined as the number of molecules which condense divided by the total number of molecules which strike the sample surface. For commonly used Knudsen cells $W_A \approx 0.5$. If $\alpha \approx 1$, $a/A = 0.01$, and $W_a = 1$, then $p_e \approx p_m(1 + 0.01)$. The most common experimental indication of a non-unity vaporization/condensation coefficient is a change in the observed pressure for orifices of different areas. If α differs significantly from unity, a plot of p_m vs. $p_m f$ for orifices of different size should be linear and from this plot one can determine p_e and α. Lack of any observable orifice effect on the measured pressures is a good indication that $p_m \approx p_e$. Paule and Margrave[98] have separated the evaporation and condensation coefficients and derived equation (3-8). However, experimental determination of α_v and α_c cannot be

$$p_e = p_m\alpha_c/\alpha_v[1 + f(1/\alpha_c + 1/W_A - 2)] \qquad (3\text{-}8)$$

effected unequivocally. Recent and more complete discussions of these coefficients and their determination are available.[99,100]

3.2.3.4. Molecular Flow Pressure Limits

Equilibrium pressure determinations from Knudsen effusion experiments are reliable only in the pressure range in which the behavior of the vapor species can be described by the kinetic theory of gases, the molecular flow region. An upper limit for molecular flow has been observed when the mean free path, λ, of the vapor

became small compared to the orifice diameter, $2R_o$.[101] When this condition is approached, collisions occur within the orifice region.[101] Various workers have reported the onset of hydrodynamic flow for Knudsen numbers, $K = \lambda/2R_o$, between 0.05 and 10 for ideal and near-ideal orifices.[39,40,101-105] A lower pressure limit for molecular flow has not been observed experimentally.

3.3. Temperature Measurements

The range of temperatures ($\geq$ 1000 K) encountered in the vaporization reactions for the binary lanthanide compounds are conveniently measured with a disappearing filament optical pyrometer.[106] Temperatures are measured by comparing the intensity of the filament at a given visible wavelength, $\lambda \approx 650$ nm, to the brightness of the radiation from a cavity in the Knudsen cell. The intensity of the filament is varied by changing the current passed through it. This current is then matched by means of a shunt resistance to the e.m.f. of a standard cell and the instrument acts as a zero-current potentiometer. Usually the radiation from the cell cavity is observed through several optical interfaces from outside the vacuum chamber. To correct for optical absorption, the temperature of a constant radiation tungsten strip lamp is determined with the optical interfaces, T_o, and without them, T. Equation (3-9) relates the actual

$$D = (1/T - 1/T_o) \qquad (3\text{-}9)$$

temperature, T, and the observed temperature, T_o, to D which is commonly known as the Wien's Law correction factor.[5,106] This correction factor may be expressed in terms of the wavelength, λ, the emissivity of the cell cavity at that wavelength, ϵ, the transmittance

of the optical elements, τ, and Planck's second radiation constant, $C_2 = 0.438$ cm K by equation (3-10). Over the temperature range of

$$D = (\lambda/C_2)\ell n(\epsilon \cdot \tau) \qquad (3\text{-}10)$$

interest, D is essentially constant for the optical elements used.

Temperatures measured by the optical pyrometers were corrected by intercomparison with another pyrometer that had been calibrated at the National Bureau of Standards to the International Practical Temperature Scale of 1948 (IPTS - 1948). On January 1, 1969, a new scale, IPTS - 1968, became effective. No attempt was made to convert the observed temperatures to the more recent scale; only a very small change $\pm$ (2-5)° would result from such a conversion.[107]

3.4. Mass Spectrometric Measurements

The importance of identifying the molecular species which effuse from the Knudsen cell cannot be overemphasized. Without knowing the molecular composition of the gas in equilibrium with the condensed phase or phases, one cannot be sure that the vaporization reaction postulated is correct. Because of this uncertainty, the equilibrium pressures and the corresponding thermodynamic values will remain in doubt.

A time-of-flight mass spectrometer equipped with a high temperature Knudsen cell inlet was used for this investigation.[110] Ionization of the molecular beam from the Knudsen cell was accomplished by electron bombardment. In a time-of-flight instrument, the ions are accelerated in pulses and separation occurs in a field-free flight region. Mass identification of the ions is based on velocity selection or time-of-flight in this field-free region. The neutral precursors of the ions (i.e., the molecules effusing from the Knudsen cell)

can be identified from the fragmentation patterns (i.e., the masses of the ions observed and their relative intensities at a given ionization energy) and the ions' ionization efficiency curves and appearance potentials.[108,111] Appearance potentials can be determined by a variety of techniques,[112] such as the linear extrapolation procedure of ion intensity vs. electron ionizing energy which was used in this study. This method is known to yield results that are 0.1-0.3 V too high, but use of the known appearance potential for a standard, e.g. Hg, whose ionization efficiency curve is related closely to that of the ions of interest, helps to reduce uncertainties. If two ion formation processes contribute to an observed ion current, the resultant ionization efficiency curve of that ion can exhibit a distinct break.[108] The potential at this distinct break is equal to the appearance potential for the second formation process.[44,108]

The absolute pressure of a molecular precursor, p_i, is related to the intensity, I_i, observed for that ion by equation (3-11).[108]

$$I_i T = p_i \sigma_i \gamma_i A \qquad (3\text{-}11)$$

In (3-11) σ_i is the ionization cross-section for the fragmentation process which produces the ion at a given electron energy, γ_i is the multiplier gain, and A is a function related to the instrumental source configuration, ionizing energy and transmission factors. Calibration of the instrument by use of a substance of known vapor pressure and ionization cross-section (e.g. Ag) during each experiment allows one to determine A for equation (3-11). However, even if the instrument is calibrated in this manner the lack of theoretical or experimental data on ionization cross-sections and instrument sensitivity for most molecules render questionable absolute

pressure data obtained from mass spectrometric investigation of these molecules. Ionization cross-sections can be approximated by the additivity principle from published values for the elements[112] or by the calculations of Mann,[113] but use of these procedures has been questioned extensively (e.g. see 109).

Because of the uncertainties introduced by estimating the quantities in equation (3-11), ion intensities were not used to determine absolute vapor pressures in this dissertation. These uncertainties can be overcome by simultaneous determination of the absolute vapor pressures with an alternate method.[8]

Appearance potentials can also be used to obtain bond dissociation or atomization energies of the effusing molecules.[108,109] If the neutral precursors and their relative contributions to an ion's intensity can be determined, if the fragmentation processes that produce the ion can be identified, and if the appearance potential for each process is determined, the atomization energies for the neutral precursors can be determined from thermochemical cycles. The large uncertainties in the appearance potentials, the kinetic energies of the ions, and the separation and identification of fragmentation processes often render the error limits large and the determination of marginal value.[109] Without extensive calibration procedures, the use of ion intensities and ionization efficiency curves would yield questionable thermochemical values. However, the lack of extensive calibration will not affect the identification of the composition of the gas which effuses from the Knudsen cell.

3.5. X-Ray Fluorescence Analysis

When electromagnetic radiation of sufficient energy interacts with a neutral atom an electron is ejected from an inner atomic orbital. Fluorescent radiation results if an electron from an outer atomic orbital fills the inner vacancy. The energy of the fluorescent radiation is dependent on the energy separation of the inner and outer levels. If these atomic levels are unaffected by chemical bonding, the energy of the fluorescent radiation will be independent of its environment. X-Ray fluorescence spectrometry is the measurement of the energy and intensity of this characteristic fluorescent radiation. Discussions of this method of non-destructive analysis are available (e.g. see 115, 116). Both energy and wavelength dispersive fluorescence methods have been devised. The wavelength dispersive method used in this investigation effects analysis of the fluorescent radiation by diffraction of the beam with a crystal of fixed interplanar d-spacings. The radiation is detected at a given angle, 2θ, with respect to the incident beam. By use of the Bragg equation, (3-12) one can determine the theta, θ, values characteristic

$$n\lambda = 2d \sin\theta \qquad (3\text{-}12)$$

of fluorescent radiation for each element. The intensity of the fluorescent radiation depends upon the characteristic energy chosen, incident tube intensity, and matrix absorption or enhancement effects.

The proper choice of detector depends on the resolution of the analyzing crystal and the energy of the fluorescent radiation. Instrumental factors and matrix effects require calibration for each element before a quantitative anaylsis can be carried out. The optimization procedure used for each instrumental parameter is described

by Neff.[117] His analyses indicate that to discriminate between small differences in concentration, R(I), defined in (3-13), should

$$R(I) = (r_1)^{\frac{1}{2}}/(r_1 - r_o) \qquad (3\text{-}13)$$

be minimized, whereas to extend the detection limits to very low concentration, R(II), defined in (3-14), should be minimized. In

$$R(II) = (r_o)^{\frac{1}{2}}/(r_1 - r_o) \qquad (3\text{-}14)$$

these equations r_o and r_1 are the pulse rates for the background and a standard, respectively.

3.6. Thermodynamic Calculations

3.6.1. The Equilibrium Constant and Standard States

The formalism used to represent the equilibrium constant for the reactions studied in this investigation is represented in equation (3-15), where K is the equilibrium constant, ν_i and ν_j are the

$$K = \pi_i(a_i)^{\nu_i}/\pi_j(a_j)^{\nu_j} \qquad (3\text{-}15)$$

stoichiometric coefficients and a_i and a_j are the activities of the products and reactants, respectively. Throughout this dissertation the activities of all solid or liquid phases are assumed to be unity. Since in a Knudsen effusion experiment the vapors are treated as ideal, all gaseous activities are considered equal to their partial pressures. The standard state for each gas is taken as the ideal gas at one atmosphere. Because the pressures studied are very low, the ideal gas assumption is valid. However, the assumption about the activity of the condensed phases is somewhat arbitrary. The use of Knudsen cells of different materials can help to identify an effect of the cell material on the activities of the condensed phases.[118] Examination of the Knudsen effusion residues by X-ray diffraction can give indications of contamination or changes in the crystal

lattice. In the absence of any experimentally observable interaction between the condensed phase and the Knudsen cell, the condensed phases are assumed to remain in their standard states (i.e., the pure substance).

The equilibrium constant, K, for a chemical reaction at constant temperature, T, is related to the change in free energy, ΔG°_T, by equation (3-16).[119] The symbol Δ is used to represent the sum of

$$\Delta G^\circ_T = - RT\ell n\ K \tag{3-16}$$

an extensive thermodynamic property, X, for the products of a reaction minus the sum for the reactants, i.e.,

$$\Delta X = \sum_i \nu_i X_i - \sum_j \nu_j X_j \tag{3-17}$$

At a given temperature

$$\Delta G^\circ_T = \Delta H^\circ_T - T\Delta S^\circ_T. \tag{3-18}$$

When the identities (3-16) and (3-18) are equated, (3-19) results.

$$- RT\ell n\ K = \Delta H^\circ_T - T\Delta S^\circ_T \tag{3-19}$$

3.6.2. The Slope-Intercept Method

If ΔH° and ΔS° are assumed constant over the experimental temperature range, a plot of $\ell n\ K$ vs. $1/T$ will be linear with slope $-\Delta H^\circ/R$ and intercept $\Delta S^\circ/R$. This method is often referred to as the second-law method.

The resultant values of ΔS° and ΔH° are usually equated, not unambiguously,[120] with the median temperature of the experimental range, T_1. These values for $\Delta H^\circ_{T_1}$ and $\Delta S^\circ_{T_1}$ can then be reduced to a reference temperature, T, by the following equations:

$$\Delta H^\circ_T = \Delta H^\circ_{T_1} + \int_{T_1}^{T} \Delta C_p\, dT; \tag{3-20}$$

$$\Delta S^\circ_T = \Delta S^\circ_{T_1} + \int_{T_1}^{T} (\Delta C_p/T)\, dT. \tag{3-21}$$

Also, corrections must be made for any condensed phase transitions. Throughout this dissertation 298 K is used as the reference temperature.

3.6.3. The Sigma Methods

The Σ- and Σ'-methods use analytical expressions for the heat capactities or thermodynamic functions, respectively, in combination with individual vapor pressure-temperature data points.[80,121] Use of these methods eliminates the assumption that ΔH° and ΔS° do not vary with temperature. Since the thermodynamic functions for the lanthanide trifluorides have been reported,[7,18] the Σ'-method of Cubicciotti[121] is used in this work. The term Σ' is defined as

$$\Sigma' = - R\ell n\ K - \Delta(H^\circ_T - H^\circ_{298})/T + \Delta(S^\circ_T - S^\circ_{298})$$
$$= \Delta H^\circ_{298}/T - \Delta S^\circ_{298}. \qquad (3\text{-}22)$$

A plot of Σ' vs. 1/T is linear with a slope and an intercept that give directly ΔH°_{298} and ΔS°_{298}. The Σ and Σ' methods are more exact than the slope-intercept method only to the extent that the heat capacities or thermodynamic functions are known.

3.6.4. The Third-Law Method

If the absolute entropies, S°_{298}, of the reactants and products are known or can be estimated, another independent method of data reduction is available. The name, third-law method, derives from the use of the absolute entropies. The free energy function,[80]

$$FEF_T = (G^\circ_T - H^\circ_{298})/T = (H^\circ_T - H^\circ_{298})/T - S^\circ_T, \qquad (3\text{-}23)$$

involves the absolute entropy and the enthalpy function for a given phase. For any reaction,

$$\Delta FEF_T = \Delta(G^\circ_T - H^\circ_{298})/T = - R\ell n\ K_T - \Delta H^\circ_{298}/T \qquad (3\text{-}24)$$

Individual values of ΔH°_{298} result from the combination of ΔFEF and

ℓn K at each temperature,

$$\Delta H^{\circ}_{298} = - T(\Delta FEF + R\ell n\ K). \qquad (3\text{-}25)$$

The individual values of ΔH°_{298} derived by the third-law method may be examined to identify temperature or chronological trends. A systematic error in the pressure or temperature determination or in the estimated free energy function change for the reaction may be reflected by a temperature trend.

3.6.5. Comparison of Second- and Third-Law Methods

Comparison of the values for ΔH°_{298} calculated by the two methods is a commonly used check on the experimental measurements and formulation of the vaporization reaction. Large discrepancies in the second- and third-law values can indicate experimental errors, choice of an incorrect reaction, nonequilibrium conditions and/or the use of incorrectly estimated thermodynamic functions. Close agreement of these values is support for the correct assignment of the above parameters. If measured free energy functions are available, disagreement of the second- and third-law methods can be used readily to identify experimental errors. Thorn[122] has discussed the use of second- and third-law values for the identification of systematic and random errors. He recommends that for a more meaningful measure of data consistency than just a comparison of only two calculated enthalpies, comparison be made of the ℓn p vs. 1/T intercept (ΔS°_{I}) for each experiment with the (estimated) absolute entropy change (ΔS°_{T}, third-law). Thorn also describes in the same paper[122] a method of statistically correlating the second-law slopes and intercepts for several experiments, a method that yields information about the probability of the correctness of the derived thermodynamic values.

3.6.6. Estimation of Thermodynamic Functions

3.6.6.1. Solid and Liquid Heat Capacities

Since the heat capacities, C_p°, and the thermodynamic functions for many substances have not been determined, it is often necessary to estimate their values to carry out the data reductions described above. A number of estimative techniques have been developed (e.g. see 5, 80, 123, and 124). Also, estimated values for the lanthanide halides have been reported.[23]

The heat capacities of the solid lanthanide difluorides were estimated at 298 K from the values for the isostructural alkaline earth difluorides by use of the Neumann-Kopp rule,

$$C_p^\circ(MX_2) = C_p^\circ(M'X_2) - C_p^\circ(M') + C_p^\circ(M). \qquad (3\text{-}26)$$

Values for C_p° at the melting point were estimated via Kubaschewski's approximation[123] that close to the transition point, C_p° for a solid is 7 to 7.25 cal K^{-1} g $atom^{-1}$. Similarly, the heat capacity, C_p°, of a liquid was estimated to be the same as that found for the alkaline earth difluorides. These values are close to those estimated[123] for inorganic liquids, $C_p^\circ \approx 8\text{-}8.75$ cal K^{-1} g $atom^{-1}$ [24-26.25 cal K^{-1} mol^{-1} for $MX_2(\ell)$].

3.6.6.2. Standard Entropies for Solids

Latimer's additivity method[125] is used commonly to estimate the standard entropy, S_{298}°, of solid ionic compounds. This method, which takes into account the mass, size, and charge of the ions involved, yields values within 2 to 4 cal K^{-1} mol^{-1} of measured values. Recent revisions of Latimer's numbers[124,126] improve the accuracy to 1 to 2 cal $K^{-1}mol^{-1}$. Of special interest to this dissertation are the

improved values compiled by Westrum.[127] These values allow consideration of the magnetic contribution of the lanthanide ions.

3.6.6.3. Ideal Gas Statistical Calculation of Thermodynamic Functions

If ideal gas behavior is assumed, thermodynamic functions may be calculated from experimental spectroscopic data by the use of statistical mechanics.[5,124,128] The theory involves the formulation of a system partition function, Q, in terms of a molecular partition function, q, for N ideal gas molecules satisfying the condition that the number of available molecular states is much greater than N,

$$Q = q^N/N! . \qquad (3\text{-}27)$$

If it is assumed that the translational, rotational, vibrational and electronic contributions to the molecular partition function are independent, q can be expressed as a product of the independent terms,

$$q(V,T) = q_t(V,T)q_r(T)q_v(T)q_e(T). \qquad (3\text{-}28)$$

These independent partition functions, q_i, can be calculated if spectroscopic data have been determined experimentally or estimated. Also, thermodynamic functions can be derived in terms of these partition functions. The reader is referred elsewhere for the analytical functions and the assumptions used to derive them.[5,124,128]

3.6.7. Error Analysis

A least-squares refinement with associated error analysis was used to derive the second-law enthalpy and entropy values.[129] The accompanying uncertainties are reported as $\pm \sigma$. No attempt has been made to assign to the resultant thermodynamic values uncertainties due to errors in temperature measurements, vapor pressure equipment

constants, Knudsen cell orifice area or X-ray fluorescence analysis. Estimated uncertainties in the thermodynamic functions are included in the thermodynamic values reported at 298 K. An uncertainty in the free energy functions has been estimated, and was included with the standard deviation in the uncertainty of the reported third-law derived enthalpy values. The overall uncertainties in the derived thermochemical values have been based on additivity. The use of additivity is consistent with the representation of the estimated uncertainties as determinate errors rather than indeterminant errors and represents a more liberal uncertainty than the treatment for indeterminate errors.[129,130]

CHAPTER 4

EXPERIMENTAL MATERIALS, EQUIPMENT AND PROCEDURES

4.1. Materials

The following chemicals were used: ytterbium metal (99.9% distilled metal, lot#YbM 3-082D, Research Chemical Co., Phoenix, Ariz.), ytterbium sesquioxide (99.9%, code#1202, LT1114, American Potash and Chemical Corp., W.Chicago, Ill., and 99.99%, lot#YbO 4-008, Research Chemcial Co., Phoenix, Ariz.), samarium metal (99.9%, PSO#2716, lot#Sm-611-M, Michigan Chemical Corp., St. Louis, Mi.), samarium sesquioxide (99.9%, PSO#4056, lot#Sm-102-0, Michigan Chemical Corp., St. Louis, Mi.), thulium metal (99.9%, distilled metal, lot#TmM 3-085D, Research Chemical Co., Phoenix, Ariz., and 99.9%, PSO#6092, lot#Tm-587-M, Michigan Chemical Corp., St. Louis, Mi.), thulium sesquioxide (99.99%, lot#TmO 4-003, Research Chemical Co., Phoenix, Ariz.), hydrofluoric acid (48%, aqueous reagent grade, Matheson, Coleman and Bell, Norwood, Ohio), and reagent grade NH_4F and HNO_3(aq), from various sources.

Materials used included: graphite stock (Becker Brothers Carbon Co., Cicero, Ill.), molybdenum rod and 30% tungsten-molybdenum stock (Kulite Tungsten Corp., Ridgefield, N.J.), platinum (J. Bishop and Co., Malvern, Pa.), copper stock (McMaster Carr Supply Co., Chicago, Ill.), vitreous carbon crucibles (Beckwith Carbon Corp., Van Nuys, Cal.), quartz boats (Thermal Syndicate, Ltd., England), quartz tubing

(Engelhard Industries, Inc., Hillside, N.J.), and seamless tantalum tubing (Fansteel Corp., North Chicago, Ill.).

4.2. Preparative Procedures and Equipment

4.2.1. Preparatory Apparatus

The preparatory apparatus used was similar to that described by Hariharan.[5] The set-up consisted of a 66 cm long by 3 cm inner diameter Vycor reaction tube located in a Lindberg Hevi-Duty tube furnace. The inlet end of the reaction tube was connected by means of a ground glass joint with a vacuum stopcock and rubber tubing to a liquid nitrogen trap, through which the sweep gases, He and H_2, entered the system. A gas-handling manifold with a palladium catalyst and an auxillary inlet line of copper tubing were connected to the liquid nitrogen trap by rubber tubing. The exit side of the reaction tube was connected by means of a ground glass joint to a safety trap. The safety trap was connected by rubber tubing to a gas bubbler. During a typical dehydration reaction (see below) a flow of He and H_2, at rates as estimated from observation of the gas bubbler of 10 to 1, respectively, was maintained over the system.

The temperature of the furnace was controlled by a temperature controller (model TPC-I/3, Weather Measure Corp., Sacramento, Cal.).

4.2.2. Lanthanide(III) Fluorides

Lanthanide(III) fluoride samples were prepared by dehydration of the precipitated trifluoride. The sesquioxide was dissolved in hot concentrated nitric acid. This hot solution was transferred to a polyethylene beaker and while the solution was stirred by use of a teflon rod, a 24% hydrofluoric acid solution was added dropwise until precipitation was complete. The resulting solution was allowed

to digest and cool. A drop or two of the 24% hydrofluoric acid solution was added to the supernatant liquid to test for complete precipitation. The liquid was decanted and the precipitate washed with a 5% hydrofluoric acid solution, water and finally, ethanol. The precipitate was centrifuged in polyethylene test tubes, placed in a platinum boat and dried at 383 K for 10-12 h. The dried precipitate was then mixed intimately with at least a six molar excess of NH_4F and placed in a platinum boat which was heated in the Vycor apparatus described above. The temperature of the Vycor apparatus was increased over a period of 4-6 h to a maximum of 973 K and held at that temperature for 2 h. A subsequent heating under high vacuum (less than 10^{-5} torr) was necessary to remove traces of NH_4F.[8]

4.2.3. Lanthanide(II) and Mixed Valence Fluorides

All reduced lanthanide fluoride specimens were prepared by the method of Stezowski and Eick[13,131] from the metal and the trifluoride. Appropriate amounts of the metal and the trifluoride were sealed into outgassed tantalum thimbles by arc welding in a zirconium-gettered argon atmosphere. The welds were examined for discoloration, indicative of oxidation or reaction between the sample and the thimble, and for faults in the seal. If the weld appeared clean, the sealed thimbles were heated under high vacuum (less than 10^{-5} torr) to 1700-1900 K, held at that temperature for 5-30 min and cooled slowly (2-3 h) to room temperature. If the thimble expanded, a tight weld was indicated. The sample was discarded if the thimble did not expand.

4.2.4. Storage of Samples

All of the lanthanide metals and the prepared fluorides were stored in a controlled atomosphere glove box which has been described

previously,[5,131] or in a vacuum desiccator. The glove box atomosphere was circulated by a permanently sealed bellows pump (model #MB-150, Metal Bellows Corp., Sharon, Mass.). The purification manifolds contained Linde Molecular Sieve pellets to remove moisture and BASF catalytic oxygen remover R 3-11. An open tray of reagent grade phosphorus pentoxide was maintained in the glove box to aid in the removal of water.

4.3. X-Ray Powder Diffraction Analysis

X-Ray powder diffraction photographs were obtained for all samples and experimental residues with a Haegg type Guinier forward-focussing camera (80 mm radius) and Cu $K\alpha_1$ radiation, λ_α = 0.154051 nm,[132] T = (297 ± 5) K. The fine focus X-ray tube was powered by a Picker 809 B generator. Sample preparation, film measurement and Guinier techniques have been discussed extensively elsewhere.[5,131,133,134] In this work, platinum powder served as an internal standard [$\underline{a}$ = 0.39237(3) nm].[135] The X-ray diffraction photographs were used to identify the number and purity of the phases present and for the determination of the lattice parameters of freshly prepared samples, effusion residues and sesquioxide residues from the analytical procedure.

4.4. Metal Analysis

Pyrohydrolysis was used to convert fluoride samples to the sesquioxide for the purpose of metal analysis according to the method of Stezowski and Eick.[13,131] A weighed sample (0.05 to 0.20 g) was placed in a constant-weight platinum boat. This boat, contained in a larger quartz boat, was heated for 3-12 h at 1275 K in a Vycor tube through which water was distilled at a rate of approximately

40 ml/h. The temperature of the sample was then decreased to 1175 K and maintained at that temperature for 3-12 h under a static atmosphere of air to remove adsorbed carbon dioxide.

4.5. Mass Spectrometric Procedures

A Bendix Model 12-107 time-of-flight mass spectrometer equipped with a high temperature Knudsen source inlet[110,136] was used to obtain several spectra in the Yb-F system (cf. Section 3.4.). A Keithley 417 K electrometer was used in lieu of the instrument electrometer to increase the sensitivity. A single cavity Knudsen cell with a conical orifice[136] was heated by radiation and electron bombardment. The instrument was operated in pulse ionization mode with an ionization energy of (45 ± 5) V to obtain spectra over a temperature range of 1075-1825 K. Ion currents derived from the molecular beam were identified by their shutterability. Assignment of masses to ion currents observed in the spectra was accomplished by use of known isotopic distributions and relative time-of-flights as compared with Hg. Ion intensities were taken as the peak height over the recorder's base line. Appearance potentials of the observed ions were obtained as discussed previously (cf. Section 3.4.). Temperatures were measured with a Leeds and Northrup optical pyrometer by sighting directly into the sample cavity. Temperature corrections were made for the optical interfaces and by intercomparison with an NBS calibrated (IPTS - 1948) instrument (cf. Section 3.3.).

4.6. Target Collection Procedures

4.6.1. Target Collection Apparatus

Two different target collection set-ups were employed. An all Vycor apparatus, similar to that described by Ackermann et al.[102]

and Kent,[137] with a demountable pyrex section between the water-cooled heating chamber and the liquid nitrogen-cooled target magazine was used only for some measurements on the Yb-F system. The Vycor system was pumped with a 5 cm mercury diffusion pump. Residual pressures were maintained between 10^{-7}-10^{-5} torr. An all metal system designed by Seiver[133] was used to study all the lanthanide fluoride systems. The metal apparatus was pumped directly with a 10 cm oil diffusion pump and residual pressures varied between 10^{-8}-10^{-6} torr. The targets were contained in a water cooled circular holder rotated by means of a Wilson type O-ring seal.

4.6.2. Target Materials

Two types of targets were used to collect the effusing gases. The copper targets were 2.65 cm in diameter and 0.42 cm thick with a 2.14 x 0.23 cm cylindrical recession on the collection side. The platinum targets were constructed of an aluminum backing of similar dimensions as the copper targets with a 2.10 x 0.005 cm platinum disk inserted into the cylindrical recession. The platinum disk was held in place by an iron wire (5.5 x 0.08 cm) coiled so as to form a spring.

The copper targets were cleaned before each experiment by washing in dilute nitric acid and water and drying in air. The platinum disks were cleaned in concentrated nitric acid and water and oven-dried at 383 K.

4.6.3. Knudsen Effusion Cells

The graphite or molybdenum effusion cells were designed with two cavities and converging conical orifices with an apex angle of $\approx 90°$.[138] Orifice areas were determined before and after each

experiment from photomicrographs (x 80, x 100, and x 200; Bausch and Lomb Dynazoom Metallograph) by measuring the enlarged orifice area with a compensating polar planimeter (Keuffel and Esser Co.). The planimeter was standardized by measuring a known area. The effusion cells were outgassed before use for 2-3 h ($\approx 10^{-6}$ torr) at 1900-2000 K.

4.6.4. Distance Meausrements

The target to Knudsen cell orifice distance was determined by use of either a precision cathetometer (Gaertner Scientific Co., ± 0.005 cm) in the Vycor apparatus or precision vernier calipers (Helias, ± 0.05 cm) in the metal line. The distance varied for each experiment and ranged from ≈ 9-11 cm for the metal line and ≈ 12-13 cm for the Vycor line (see Appendix 5).

4.6.5. Heating

A high frequency induction generator (Thermonic, push-pull type, 250 kHz, 20 kVa) was used to heat the Knudsen cells. Direct coupling of the induction coil with molybdenum cells was used for five of the experiments performed on an intermediate ytterbium fluoride composition. In all of the other experiments the Knudsen cell was heated indirectly by radiation from an inductively heated 30% W-Mo oven. Hariharan[5] has measured the vapor pressure of Ag with this heating arrangement and found the oven to be suitable for use in Knudsen effusion investigations.

4.6.6. Temperature Measurement

Temperatures were measured by use of disappearing filament optical pyrometers (Leeds and Northrup; Micro Optical) by sighting the orifice of the bottom cavity of the Knudsen cells. The

temperatures were corrected as described previously (c.f. Section 3.3.).

In the metal line the absence of a temperature gradient (< 10 K) across the Knudsen cell, in all experiments but one, was confirmed by monitoring the temperature of the top and bottom cavities. In the glass line the apparent surface temperature of the oven was measured at the top and the bottom. If any temperature gradient was present the induction coil was adjusted to compensate for it.

6.6.7. General Target Collection Procedure

The general target collection procedure has been described previously by several investigators (e.g. see 5, 130, 131). Samples of ≈ 0.1-2.0 g were used for each different vaporization experiment. No precautions were necessary to avoid hydrolysis while the sample was transferred to the effusion line. Ten targets were usually collected at both increasing and decreasing temperatures. A minimum of 10 min was allowed for equilibrium to be reached within the Knudsen cell after each temperature change. When temperature drifts of more than ± 10° were observed, the target was not used in the data reduction. Target exposure times were measured with a Lab-chron timer (± 0.01 min). Approximately 4-20 μg of the lanthanide metal was collected on each target for analysis by X-ray fluorescence after the vaporization experiment.

4.7. X-Ray Fluorescence Analysis

A four position Norelco Universal Vacuum spectrograph was used in conjunction with a broad focus tungsten tube powered by a Norelco XRG-5000 X-ray generator. Analysis for the lanthanide metals (Sm, Tm or Yb) was carried out by use of a graphite monochromator

(d = 0.3354 nm; (002) plane) and a NaI (Tl) scintillation counter. The spectrometer instrument settings are presented in Table 3. In this table the discriminator settings E and ΔE refer to the detector pulse height and channel width and were chosen by use of the procedure of Neff[112] to maximize the count rate, equation (3-13), for small differences in concentration (cf. Section 3.5.).

Table 3. X-Ray Fluorescence Spectrometer Conditions

Element	Collector Target	Discriminator Setting		$2\theta(L\alpha_1)$	Counts/μg/min
		E	ΔE		
Sm	Cu	2.25 V	4.75 V	38.3°	2066 ± 258
Tm	Pt	2.00	6.50	29.8	5410 ± 364
Yb	Pt	1.80	5.90	28.8	3828 ± 366

Calibration for each element was achieved by evaporating onto each of ten targets 50 μl of different standard solutions prepared by dissolving weighed amounts of a lanthanide sesquioxide in a volume of dilute nitric acid. Five different amounts in the range of 4-16 μg of lanthanide metal were deposited onto ten targets so that duplicates of each amount were produced. The targets were prepared by depositing and evaporating to dryness 15-20 small droplets to obtain a uniform surface. The target surface exposed to the energizing X-ray beam was defined by a circular 45° beveled insert inside of which the standard was deposited. For the copper and platinum targets the radii of the exposed areas, R, were found to be 0.795(5) and 0.833(5) cm as measured by vernier calipers, respectively. The errors in

the count rates reported in Table 3 are the standard deviations from the means for the ten standard targets.

The normalization method of Hariharan[5] was used in this work to insure precision by counting a control blank and standard before and after every five targets. For additional discussions of the X-ray fluorescence analysis procedures see Hariharan,[5] Work[99] and/or Haschke.[138]

4.8. Film Thickness Monitor

A film thickness monitor (model#219001, Granville-Phillips Co., Boulder, Col.) was utilized to record the rate of deposition of material onto the targets in the metal vaporization apparatus. The instrument uses the change in the frequency of oscillation of a quartz crystal to determine the mass of a coating deposited on its surface. The film thickness changes were recorded during the target collection periods. The rate of deposition indicated by the thin film monitor was found to be directly proportional to the molecular flux from the Knudsen cell as determined by the target collection procedure. The ratio of film thickness to μg of lanthanide metal deposited on a target during a given time period was determined for each target. The mean of these numbers was then used to calculate vapor pressures for temperatures at which the deposition rate was monitored, but no target collected. For a given crystal over a temperature range of 481° the thickness to μg ratio for an intermediate samarium fluoride varied an average of ± 3% with no temperature or chronological trend indicated (see Appendix 5). The lifetime of the crystal varied from one to several effusion experiments and is dependent upon the amount of material deposited on the crystal.

The film thickness monitor was used to expand the number of data points obtained from a single Knudsen effusion experiment.

4.9. Distillation Experiments

Distillation experiments were performed by completely evaporating and condensing SmF_3 and YbF_3. The distillation assembly is depicted in Figure 1. A cylindrical molybdenum apparatus was used for SmF_3 and a graphite apparatus for YbF_3. A temperature gradient was introduced along the edge of the assembly by positioning the induction coil so that the lid extended beyond the top of the coil. The majority of the effusate condensed on the lid.

4.10. Mass Loss Experiments

In the mass loss experiments a sample which contained a predetermined percentage of lanthanide metal was placed in a molybdenum Knudsen cell. The cell was then heated in high vacuum for a given time period. After the effusion experiment the mass loss, percent metal and the X-ray diffraction pattern of the residue were determined. Some samples were vaporized completely (i.e., the Knudsen cell was heated to constant weight) to test for any major sample-cell interaction by mass loss of the Knudsen cell.

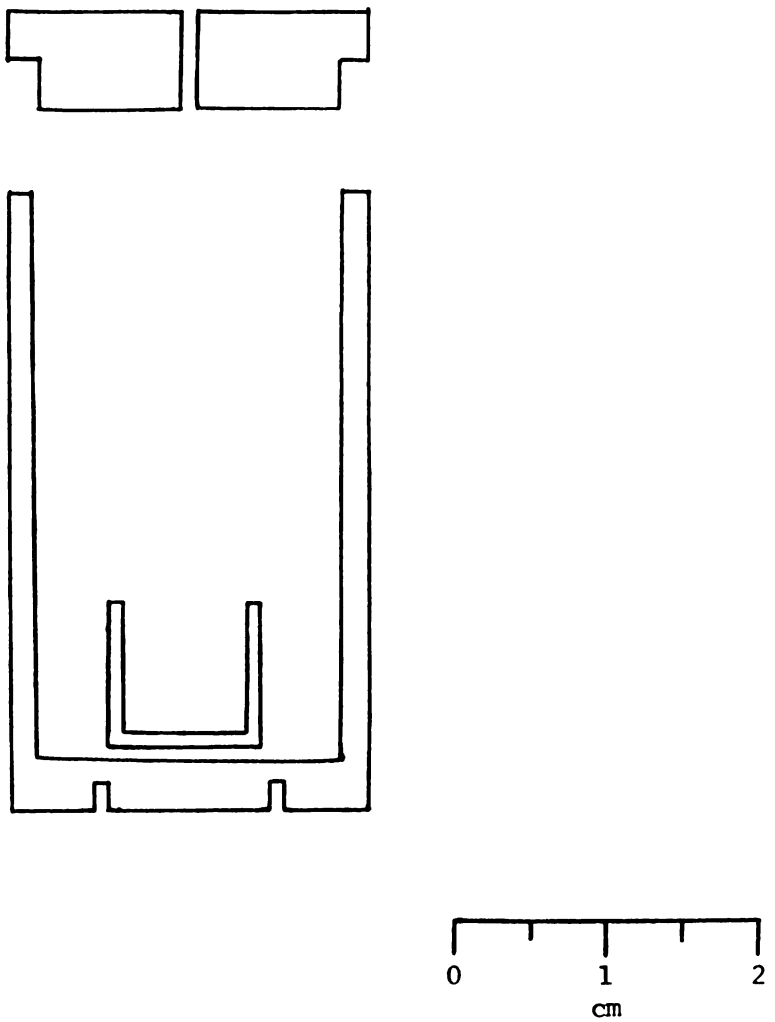

Figure 1. Distillation Assembly

CHAPTER 5

RESULTS

5.1. Preparations

The metal analytical results for the lanthanide(III) fluoride preparations (SmF_3, TmF_3 and YbF_3) are presented in Table 4. The preparative procedure yielded a white powder in each of the three cases. The X-ray powder diffraction results for the trifluorides, presented in Table 5, are in agreement with those previously reported.[4,17,18] Also listed in Table 4 are the metal analytical results for three reduced ytterbium fluorides. Since the metal contents calculated from the molar ratios in which the samples were mixed agreed with the contents determined by analyses for these three separate preparations, analyses were not undertaken for other reduced fluoride preparations. A total of five reduced fluorides were prepared in the ytterbium fluoride system. Their compositions and the symmetry assigned to the observed diffraction patterns are presented in Table 6. Also presented in Table 6 are data on the two reduced fluorides prepared in the samarium fluoride system and the results of the attempted preparation of TmF_2. The relative intensities, d-spacings and assigned Miller indices of the observed reflections are reproduced in Appendix 1.

The tetragonal and hexagonal symmetry assignments for the ytterbium fluoride system are identical to those observed in the

Table 4. Metal Analytical Results for Selected Lanthanide Fluorides

Compound	Calculated	Found[1]
YbF_3	75.2 %	75.2 ± 0.2 %
SmF_3	72.5	72.5 ± 0.2
TmF_3	74.8	74.3 ± 0.3
$YbF_{2.00}$	82.0	81.9 ± 0.4
$YbF_{2.41}$	79.1	78.9 ± 0.5
$YbF_{2.51}$	78.4	78.43 ± 0.01

[1]Errors are standard deviations for analyses

Table 5. X-Ray Diffraction Results for Selected Lanthanide Fluorides

Compound	Structure Type	Space Group	Lattice Parameters[1] a(nm)	b(nm)	c(nm)
YbF_3	Orthorhombic (YF_3)	Pnma	0.6207(8)	0.6788(4)	0.4439(6)
SmF_3	Orthorhombic (YF_3)	Pnma	0.6671(4)	0.7063(7)	0.4402(1)
SmF_3	Hexagonal (LaF_3)	$P\bar{3}c1$	0.698(2)	-----	0.703(5)
TmF_3	Orthorhombic (YF_3)	Pnma	0.6276(7)	0.6812(1)	0.4412(4)

[1]Errors are calculated standard deviations in the least-squares fit

Table 6. Structures of Selected Reduced Lanthanide Fluorides

Compound	Structure(s)	Lattice Parameters a(nm)	b(nm)	c(nm)
$YbF_{2.01}$	Cubic	0.5600(1)	------	------
$YbF_{2.19}$	Cubic	0.5585(1)[2]	------	------
$YbF_{2.29}$	Tetragonal + U[1]	0.3925(2)	------	0.5587(2)
$YbF_{2.41}$	Hexagonal + U[1]	0.3926(4)	------	1.940(2)
$YbF_{2.51}$	Hexagonal + U'[1] + Orthorhombic YbF_3	(same phase as in $YbF_{2.41}$) (see Table 5)		
$YbF_{2.60}$	Hexagonal + U'[1] + Orthorhombic YbF_3	(same phase as in $YbF_{2.41}$) (see Table 5)		
$SmF_{2.00}$	Cubic	0.5872(1)	------	------
$SmF_{2.44}$	Hexagonal	0.4086(1)	------	2.0189(7)
TmF_x	Hexagonal + U"[1] + Orthorhombic TmF_3 + Tetragonal $Tm_3O_4F_6$	0.3953(1) (see Table 5)	------	1.937(1)
		0.5513(2)[3]	-----	0.5355(2)[3]

[1]U, U' and U" = unidentified lines (superstructure)

[2]Vaporization residue

[3]Reference 139

samarium[13,131] and europium[16] fluoride systems. The symmetry changes were explained by distortions of the cubic fluorite lattice. The distortions have been attributed to interstitial anions and cation substitution which results in contraction of the unit cell and an increased density (cf. Section 2.2.3.). Although the distortions of the cubic unit cell cause the tetragonal and hexagonal reflections, the presence of unidentified lines (superstructure) indicates that the actual unit cell is of symmetry lower than the one chosen.

The physical appearances of reduced europium, ytterbium and samarium fluorides have been described previously.[13-16,131] The following color-composition changes were noted during this investigation. Ytterbium fluoride changes from black-green ($YbF_{2.01}$) to green-brown ($YbF_{2.50}$). Samarium fluoride changes from dark purple ($SmF_{2.00}$) to red ($SmF_{2.44}$). The reduced thulium fluoride of unknown composition was tan. Incomplete reduction of TmF_3 was indicated by the presence of reflections assignable to orthorhombic TmF_3 in the X-ray powder diffraction photograph of the partially reduced product (see Appendix 1). A small amount of oxide fluoride contaminant ($Tm_4O_3F_6$) was found in the reduced thulium fluoride preparation. A similar contaminant ($Sm_4O_3F_6$ or $Yb_4O_3F_6$) was also observed in some of the samarium and ytterbium fluoride preparations, but these preparations were discarded.

5.2. Mass Loss Results

The results of a series of mass loss experiments, effected with molybdenum cells and undertaken to determine what changes, if any, would occur in the ytterbium fluoride residues during vaporization are presented in Table 7. Vaporization of reduced ytterbium

Table 7. Results of Mass Loss Experiments for Ytterbium Fluoride Samples Confined in Mo

Before Vaporization		Temperature of Vaporization	After Vaporization		
Composition[1] (F/Yb)	Structure(s)[2]		Mass Loss	Composition[1] (F/Yb)	Structure(s)[2]
2.01	C a = 0.5600(1) nm	1097 K	1 %	2.01	C a = 0.5597(3) nm
"	"	1450	15	2.19	T + C + U a = 0.5585(1)
"	"	1800	27	2.35	H + T + U'
"	"	1800	45	2.39	H + U"
2.29	T + U	1700	31	2.39	H + U"
"	"	1700	45	2.37	H + U"
2.44	H + U"	1673	20	2.37	H + U"
2.51	H + O + U"	1696	37	2.46	H + U"
2.60	H + O + U"	1712	41	2.55	H + O + U"
3.00	O	1560	17	2.96	O + H
"	"	1725	37	2.99	O + H

[1] Average error in composition is ± 0.04

[2] C = cubic, T = tetragonal, H = hexagonal, O = orthorhombic YbF_3, U, U' and U" = unidentified lines (superstructure)

fluorides with compositions in the region YbF_{2+x} ($0.00 \leq x < 0.40$) resulted in a decrease in the percentage of ytterbium in the residue. Vaporization of ytterbium fluoride samples with compositions in the region YbF_{2+x} ($0.40 < x \leq 0.60$) resulted in an increase in the percentage of ytterbium in the residue. No significant change in the composition or X-ray powder diffraction pattern was found for the vaporization of $YbF_{2.40}$. These results indicated that in the region YbF_{2+x} ($0.00 \leq x \leq 0.60$) all compositions, except that of the pseudo-hexagonal phase, $YbF_{2.40}$, undergo incongruent vaporization.

When YbF_3 was vaporized from a molybdenum cell, the percentage of ytterbium metal in the residue increased slightly. The X-ray powder diffraction photographs of these residues indicated the presence of the congruently vaporizing pseudo-hexagonal phase, $YbF_{2.40}$. Results such as these can be explained only by the incongruent vaporization of YbF_3 or by a fluoride-cell interaction. To determine if any fluoride-cell interaction was present, three samples of YbF_3 (0.28, 0.34 and 0.36 g) were vaporized completely at 1800 K. The resulting average mass loss, (100.1 ± 0.3) %, indicated no significant fluoride-cell interaction. Also, three samples of YbF_2 (0.42, 1.58 and 2.25 g) were evaporated completely with an average mass loss of (99.8 ± 0.8) %. The absence of any significant fluoride-cell interaction and the presence of two phases in the residue can be explained only by the incongruent vaporization of YbF_3.

Mass loss experiments were also carried out on the samarium and thulium fluoride systems. The results of these experiments are presented in Table 8. The samarium fluoride system vaporized in the same manner as the ytterbium fluoride system with a congruently

Table 8. Results of Mass Loss Experiments for Samarium and Thulium Fluoride Samples Confined in Mo

Before Vaporization		Temperature of Vaporization	After Vaporization		
Composition[1] (F/Ln)	Structure(s)[2]		Mass Loss	Composition[1] (F/Ln)	Structure(s)[2]
		Ln = Samarium			
2.00	C a = 0.5872(1) nm	1423 K	10 %	2.19	C a = 0.5835(2) nm
"	"	1728	25	2.29	T + H + U
"	"	1485	46	2.36	H
2.44	H	1513	32	----	H
3.00	O	1450	5	2.99	O + H
"	"	1629	13	2.98	O + H
		Ln = Thulium			
2.00	H + O(weak)	1370	25	----	O + H(weak)
3.08	O	1502	12	3.02	O
"	"	1665	24	3.05	O

[1] Average error in composition is ± 0.04

[2] C = Cubic, T = tetragonal, H = hexagonal, O = orthorhombic SmF_3 or TmF_3, U = unidentified lines (super-structure)

vaporizing composition of $SmF_{2.40}$. Total mass loss experiments for the samarium fluoride system, three samples of SmF_3 (0.73, 0.91 and 0.72 g) and two samples of SmF_2 (0.28 and 0.47 g), resulted in mass losses of (99.8 ± 0.2) % for SmF_2 and (99.8 ± 0.3) % for SmF_3 and indicated no fluoride-cell interaction.

The thulium fluoride system exhibited vaporization behavior different from the samarium and ytterbium fluoride systems. Mass loss experiments performed on the reduced thulium fluoride preparations indicated the disappearance of the reduced fluoride phases. The intensities of lines assignable to the orthorhombic trifluoride were stronger in the X-ray diffraction photographs of the residue than in that of the reactant. The TmF_3 samples vaporized congruently with no apparent change in composition or X-ray diffraction pattern. A single total mass loss experiment conducted with a molybdenum cell and 1.0 g TmF_3 resulted in a 99.9 % mass loss.

5.3. Mass Spectrometric Results

The vapors effusing from molybdenum Knudsen cells which contained $YbF_{2.01}$ and $YbF_{3.00}$ were examined by mass spectrometry to determine their molecular structure and their behavior with respect to time and temperature.

Mass spectrometric analysis of the effusate from $YbF_{2.01}$ at temperatures lower than 1477 K indicated only the presence of Yb^+. No other ion had an intensity greater than 1 % of the intensity of Yb^+. When the temperature of the sample was elevated, the Yb^+ intensity increased; but, with time, the Yb^+ intensity decreased and, consequently, was not reproducible with temperature (Figure 2). The ionization efficiency curve for Yb^+, recorded during the initial

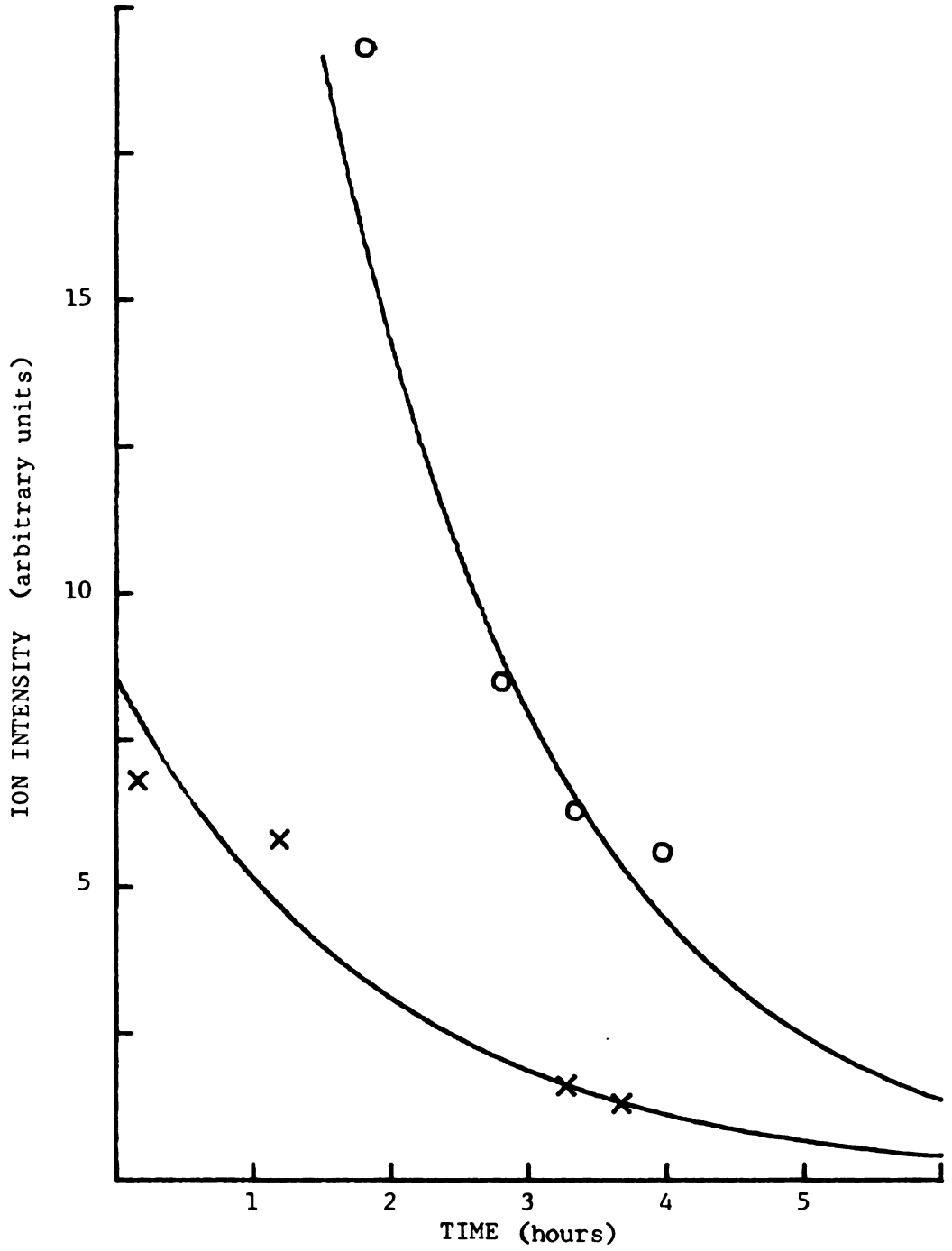

Figure 2. Intensity of Yb^+ from YbF_{2+x} ($0.00 \leq x < 0.40$) Confined in Mo *vs.* Time [O (T = 1396 K); X (T = 1338 K)]

heating period (T = 1335 K), is shown in Figure 3. The appearance potential observed for Yb^+, $(7._7 \pm 1._9)$ V, is not significantly higher than that reported, $(5.9_0 \pm 0.1_0)$[140] and (6.25 ± 0.01)[141] V, for Yb(g). The incongruent vaporization of $YbF_{2.01}$ below 1477 K yields primarily Yb(g), and the pressure of the Yb(g) decreases dramatically as the ytterbium composition of the residue decreases from Yb/F = 0.50, i.e., changes with respect to time. These results, together with the contraction of the cubic lattice (cf. Section 5.2. and Table 7) observed during the initial vaporization of $YbF_{2.01}$, substantiate the incongruent vaporization behavior of this phase. The incongruent vaporization reaction is illustrated in equation (5-1), where $0.01 \leq x \leq 0.19$.

$$YbF_2(s) = (2/2+x)\ YbF_{2+x}(s) + (x/2+x)\ Yb(g) \qquad (5\text{-}1)$$

At temperatures greater than 1477 K ion currents for YbF^+ and YbF_2^+ were observed. Figures 4 and 5 illustrate the behavior of the Yb^+ intensity and the intensity fractions, $[I_{MX_n}{}^+/I_{(total)}]$, of Yb^+, YbF^+ and YbF_2^+ vs. time. Initially the Yb^+ intensity decreased with time while the YbF^+ and YbF_2^+ intensities increased. After 25-30 h had elapsed the intensities became reproducible with both time and temperature. After 33.8 h and 31 % mass loss, the residue was removed from the mass spectrometer and analyzed. The composition, $YbF_{2.39}$, and the X-ray diffraction pattern of the residue indicated the presence of only the pseudo-hexagonal phase. These results also support the conclusion of an initial incongruent vaporization reaction characteristic of solid solution or nonstoichiometry in the composition region YbF_{2+x} $(0.00 \leq x < 0.40)$. The reproducible behavior of the ion intensities of the sample with both time and temperature after

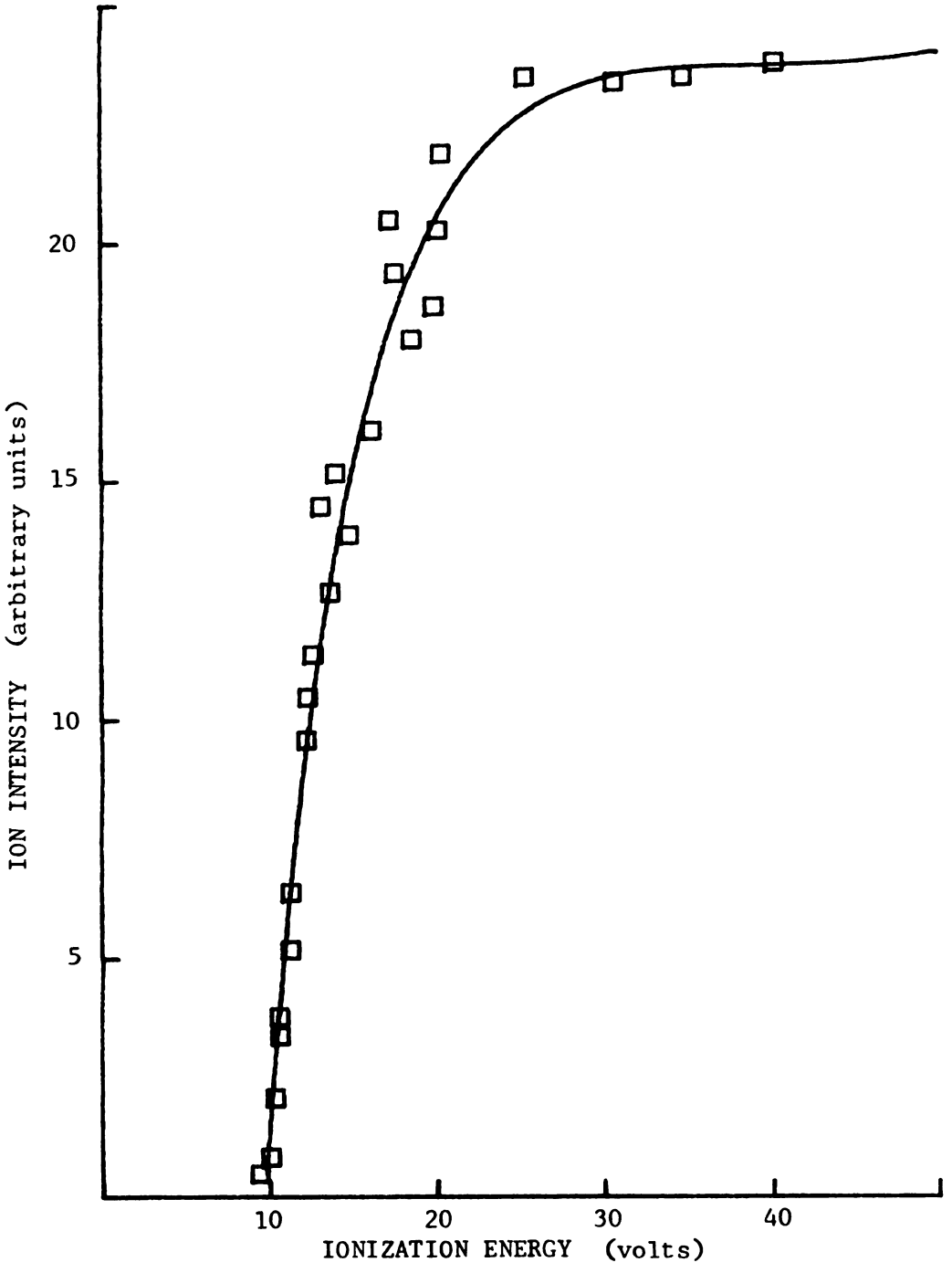

Figure 3. Ionization Efficiency Curve of Yb^+ from YbF_{2+x} ($0.00 \leq x < 0.40$) Confined in Mo (T = 1335 K)

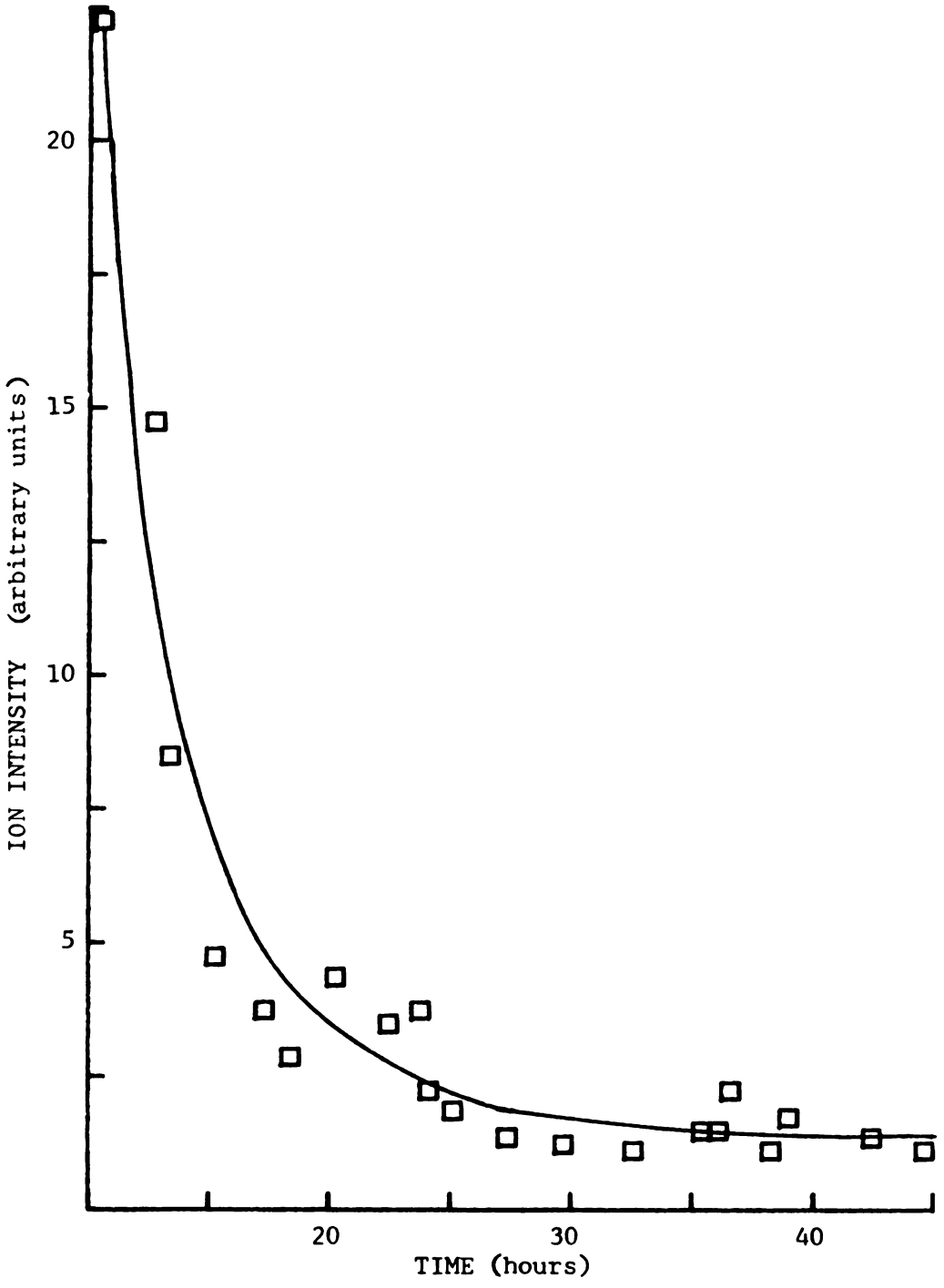

Figure 4. Intensity of Yb^{+} from YbF_{2+x} ($0.00 \leq x \leq 0.40$) Confined in Mo vs Time (T = 1653 K)

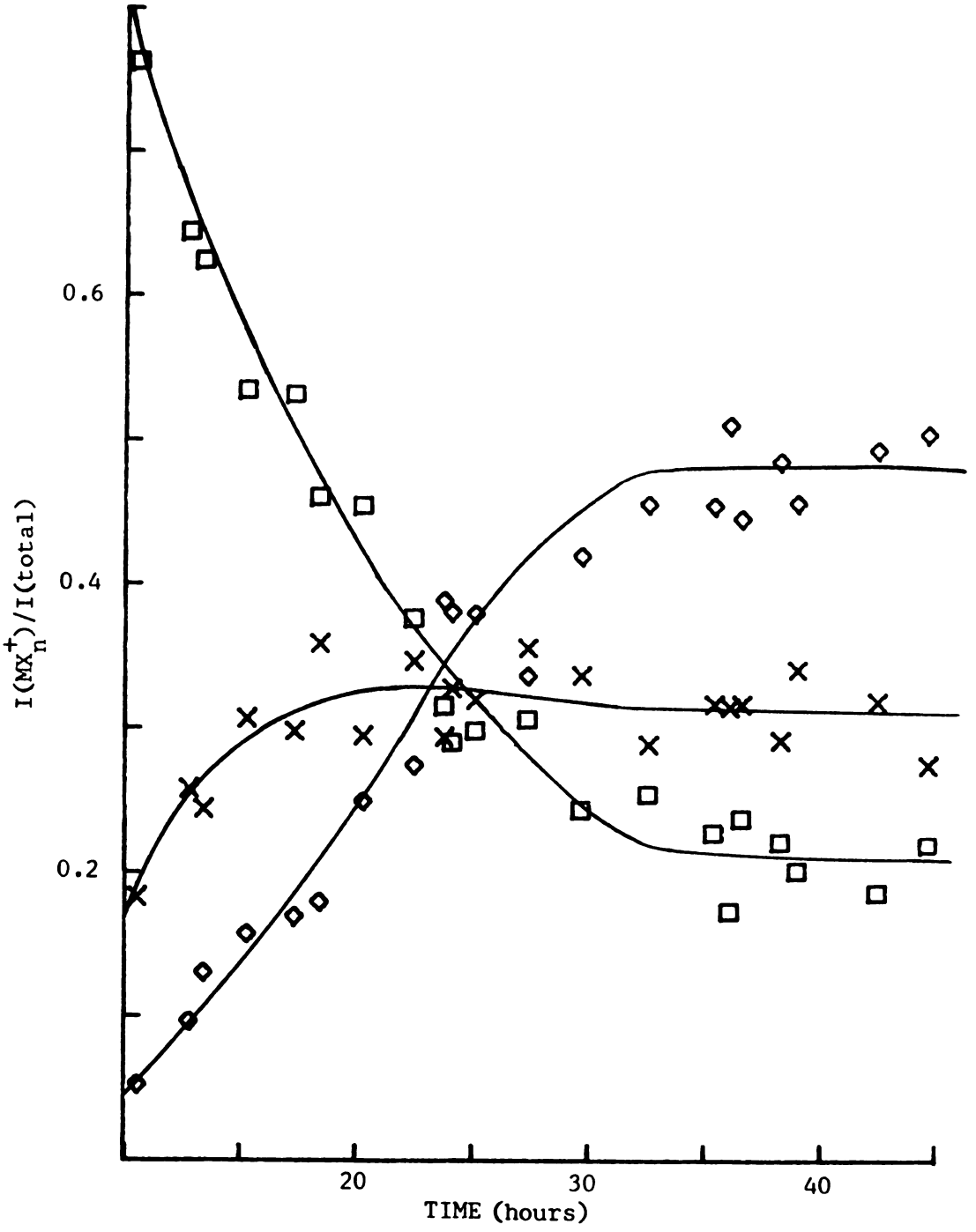

Figure 5. Fractional Ion Intensities of Yb^+(□), YbF^+(X) and YbF_2^+(◇) from YbF_{2+x} ($0.00 \leq x \leq 0.40$) Confined in Mo *vs.* Time (T = 1653 K)

a 31 % mass loss by vaporization reconfirms the congruent vaporization behavior proposed for the pseudo-hexagonal phase, $YbF_{2.40}$.

Ionization efficiency curves, Figures 6 and 7, were obtained from the sample discussed in the preceding paragraph for Yb^+, YbF^+ and YbF_2^+ before 16 h of heating had elapsed (i.e., in the non-reproducible region) and after 42 h, which was in the region of reproducible behavior. The complex shapes of the ionization efficiency curves are similar to those observed by Zmbov and Margrave[44] in their study of reduced lanthanide fluorides. A probable explanation for the shape of the ionization efficiency curves is the presence of two or more molecular precursors. If two species produce the same ion by fragmentation reactions which involve significantly different energies, inflection points can be observed in the ionization efficiency curve for that ion (cf. Section 3.4.). Appearance potentials for a second fragmentation reaction were taken to be the voltages of estimated inflection points[108] (cf. Section 3.4.). These second appearance potentials have an arbitrarily chosen uncertainty of ± 5 V. The first and second appearance potentials observed during the vaporization of compositions in the region YbF_{2+x} ($0.00 \leq x \leq 0.40$) are reported in Table 9.

Examination of the effusate from YbF_3 by mass spectrometry yielded smooth ionization efficiency curves (Figure 8) which are again similar to those reported by Zmbov and Margrave.[44] These smooth curves indicated that $YbF_3(g)$ was the only ytterbium containing precursor detectable. The similarity of the fragmentation pattern observed from YbF_3 (see Table 10) to those reported for other lanthanide trifluorides[43,44] for which stable reduced fluorides are

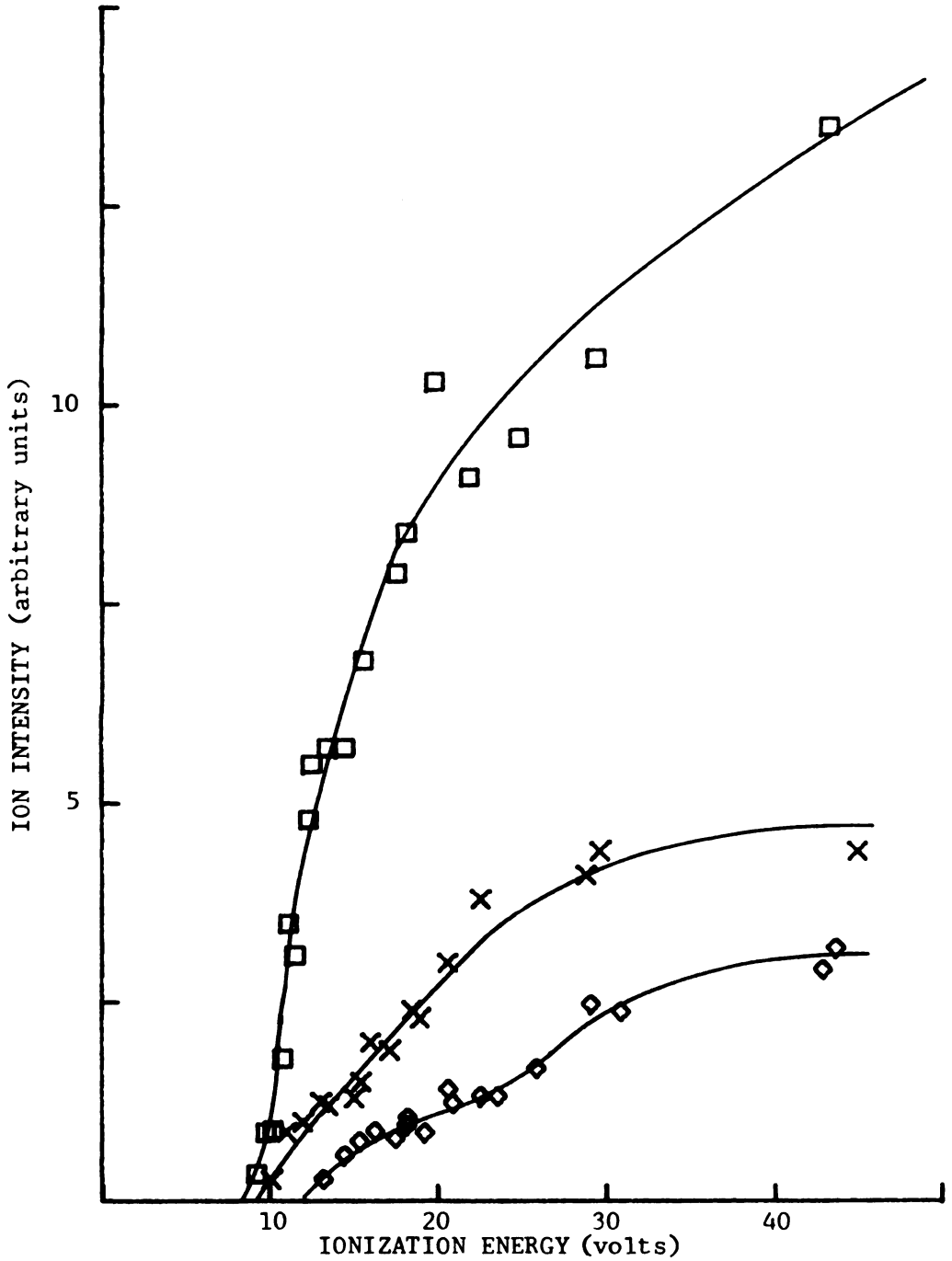

Figure 6. Ionization Efficiency Curves for Yb^+(□), YbF^+(X) and YbF_2^+(◇) from YbF_{2+x} ($0.00 \leq x < 0.40$) Confined in Mo (T = 1667 K)

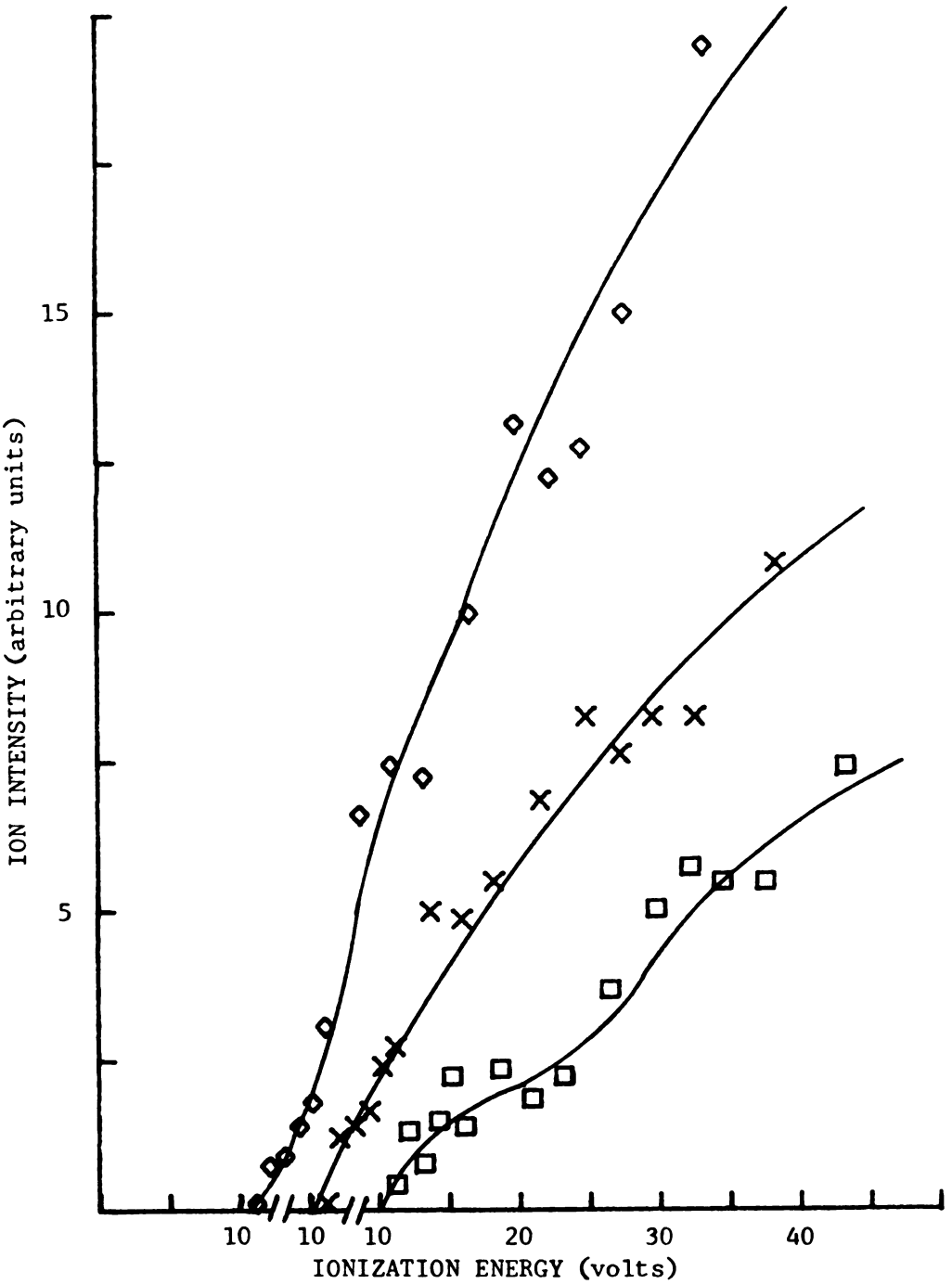

Figure 7. Ionization Efficiency Curves for Yb^+(□), YbF^+(X) and YbF_2^+(◇) from $YbF_{2.40}$ Confined in Mo (T = 1735 K) (displaced abscissa: 0 to 60 V for YbF_2^+, -5 to 55 V for YbF^+, -10 to 50 V for Yb^+)

Table 9. Appearance Potentials of the Ions Detected in the Ytterbium Fluoride System

Condensed Composition[1]	T (K)	Ion	Relative Intensity[2]	1st A.P. (volts)	2nd A.P. (volts)
YbF_2	1335	Yb^+	100	7.7 ± 1.9	------
YbF_{2+x}	1667	Yb^+	100	8.8 ± 2.5	------
"	"	YbF^+	66	8.5 ± 1.7	------
"	"	YbF_2^+	35	11.4 ± 2.2	20 ± 5
$YbF_{2.40}$	1735	Yb^+	26	10.0 ± 5.0	23 ± 5
"	"	YbF^+	56	10.8 ± 2.5	------
"	"	YbF_2^+	100	10.6 ± 2.4	15 ± 5
YbF_3	1673	Yb^+	14	25.3 ± 1.5	------
"	"	YbF^+	8	19.1 ± 1.7	------
"	"	YbF_2^+	100	14.4 ± 1.1	------

[1] $0.00 \leq x < 0.40$

[2] Ionization energy of 45 ± 5 volts

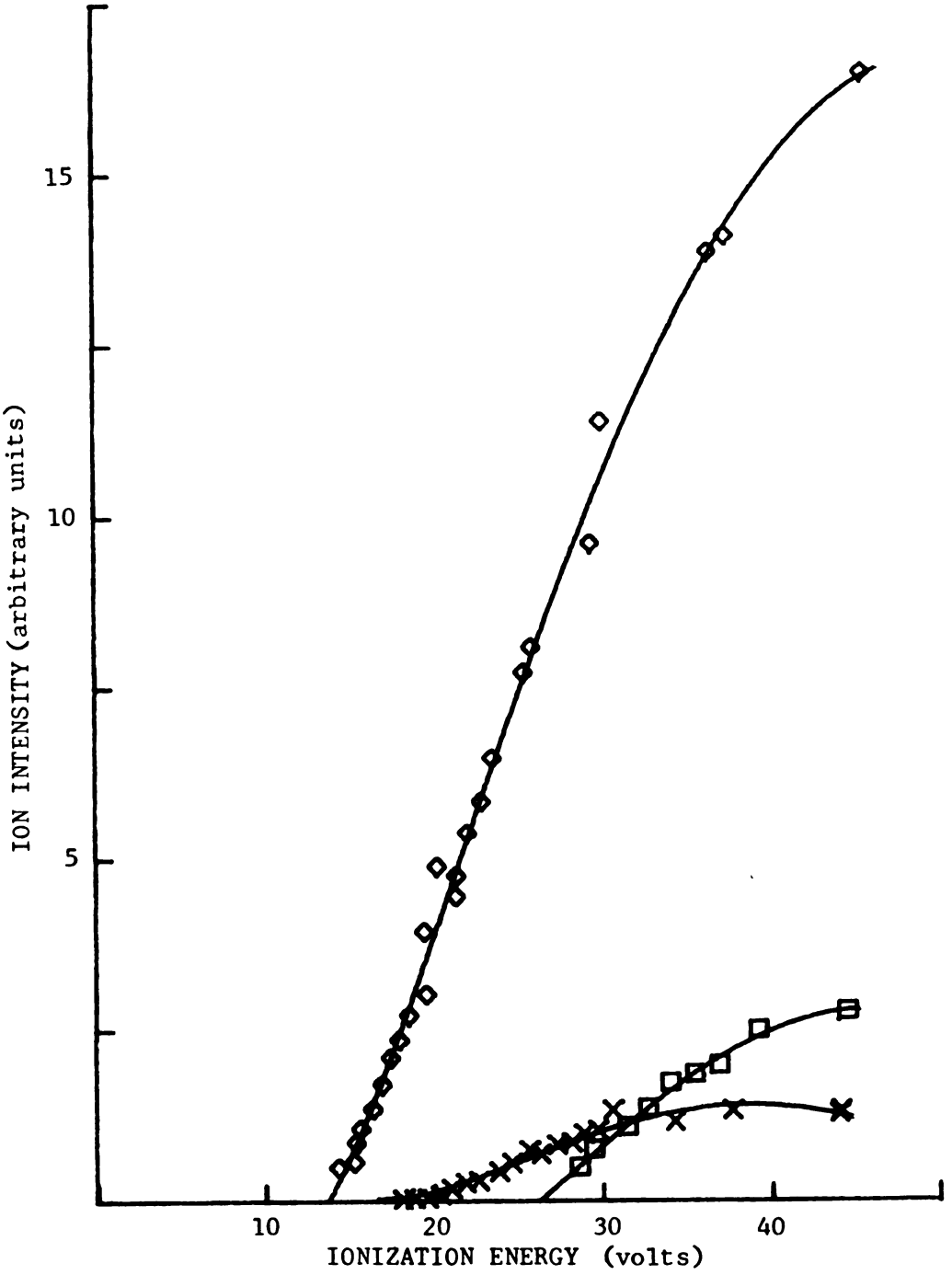

Figure 8. Ionization Efficiency Curves for Yb^+(□), YbF^+(X) and YbF_2^+(◇) from YbF_3 Confined in Mo (T = 1673 K)

Table 10. Fragmentation Patterns for Selected Lanthanide Halides

Halide	Fragmentation Pattern[1]			Ionization Energy
	Ln^+	LnF^+	LnF_2^+	
LuF_3	3	8	100	75 V
LaF_3	11	20	100	70
CeF_3	13	19	100	70
YbF_3	14	8	100	45
EuF_2	33	100	24	30
$EuCl_2$	46	100	12	50
$YbCl_2$	32	100	33	30

[1]References 43, 44, 56, 142

not expected is further support that the effusate consists principally of $YbF_3(g)$. During the mass spectrometric investigation of the effusate from YbF_3, ion current intensities and their relative ratios were reproducible with both time and temperature. The effusate was monitored until 57 mass percent of the sample had been vaporized. The appearance potentials and the fragmentation patterns of the ions observed are listed in Table 9.

Comparison of the second appearance potentials (cf. Table 9) for the ions observed over $YbF_{2.40}$ with those of the ions from the effusate over YbF_3 reveals a striking similarity. From this similarity one can conclude that $YbF_3(g)$ is one of the molecular precursors present in the $YbF_{2.40}$ effusate. The presence of $YbF_2(g)$ over $YbF_{2.40}$ is indicated by the first appearance potential observed for YbF_2^+, $(10._6 \pm 2._4)$ V (cf. Table 9), which is below the appearance potential for YbF_2^+ in the YbF_3 effusate, $(14._4 \pm 1._1)$ V. The observed fragmentation pattern (Table 9) for the ions in the $YbF_{2.40}$ effusate is different from the patterns reported for lanthanide dihalides (Table 10). This difference supports the presence of both $YbF_2(g)$ and $YbF_3(g)$ in the $YbF_{2.40}$ effusate. No evidence is present in the ionization efficiency curves (Figure 7) for a third molecular precursor. Blue et al.[143] report the presence of CaF(g) over $CaF_2(s)$, but the ratio $CaF(g)/CaF_2(g)$ at 1500 K is 10^{-7} and makes the contribution of CaF(g) to the sublimation thermodynamics of $CaF_2(s)$ insignificant.[45] Because of the reported similarities in the thermodynamic values of the alkaline earth and europium dihalides (cf. Section 2.3.) and because of their similar ionic radii, $CaF_2(g)$ was chosen as a model for $YbF_2(g)$. From this model no significant amount of

YbF(g) would be expected in the effusate from $YbF_{2.40}$. From the assumption that no species other than $YbF_2(g)$ and $YbF_3(g)$ are present in significant amounts, the congruent vaporization of $YbF_{2.40}$ can be represented by equation (5-2). The uncertainties in the coefficients

$$YbF_{2.40}(s,\ell) = (0.60)\ YbF_2(g) + (0.40)\ YbF_3(g) \qquad (5\text{-}2)$$

for $YbF_2(g)$ and $YbF_3(g)$ in (5-2) were derived from the uncertainty in the composition of $YbF_{2.40}$ ($\pm$ 0.04) and are both $\pm$ 0.04.

5.4. Distillation Results

The complete distillation of YbF_3 was carried out to determine the coefficients for reaction (5-3). The presence of $YbF_3(g)$ was

$$YbF_{3.00}(s,\ell) = \underline{a}\ YbF_{2.40}(s,\ell) + \underline{b}\ YbF_3(g) + \underline{c}\ F(g) \qquad (5\text{-}3)$$

indicated by the mass spectrometric results (c.f. Section 5.3.). Analysis of the residues from mass loss experiments indicated the presence of two condensed phases, $YbF_{3.00}$ and $YbF_{2.40}$. From the equilibrium constant for reaction (5-4)[144] at the pressures ($\approx 10^{-5}$

$$\tfrac{1}{2}\ F_2(g) = F(g) \qquad (5\text{-}4)$$

atm) and temperatures ($\approx$ 1500 K) investigated, the pressures of $F_2(g)$ can be derived ($\approx 10^{-11}$ atm) and shown to be insignificant.

In the distillation experiment YbF_3 confined in a Mo cell was evaporated completely and the effusate condensed on the lid of the distillation assembly (Figure 1). Since it was not experimentally possible to stop the distillation at the exact moment before the congruent sublimation of $YbF_{2.40}$ commenced, the composition of the condensed effusate represents the combined effusates of YbF_3 and $YbF_{2.40}$. In addition the composition of the condensed effusate is a lower limit since reevaporation of the condensed $YbF_{3.00}$ may have occurred during the experiment. The composition of the condensed

effusate ($YbF_{2.97(4)}$) is related to $YbF_{2.40(4)}$ and $YbF_3(g)$ by equation (5-5). The coefficients a and b are found to be 0.05(6) and 0.95(7),

$$YbF_{2.97} = \underline{a}\ YbF_{2.40} + \underline{b}\ YbF_3(g) \qquad (5\text{-}5)$$

respectively. From these numbers the coefficient for F(g) in equation (5-3) is determined to be (0.03 ± 0.36). Substitution of these coefficients into (5-3) yields

$$YbF_{3.00}(s,\ell) = (0.05)\ YbF_{2.40}(s,\ell) + (0.95)\ YbF_3(g) + (0.03)\ F(g) \qquad (5\text{-}6)$$

for the congruent vaporization of $YbF_{3.00}$.

The distillation of SmF_3 was carried out in a molybdenum assembly, but not enough distillate was collected for quantitative analysis. However, the X-ray powder diffraction photograph indicated the presence of the pseudo-hexagonal phase and SmF_3 was assumed to undergo an incongruent vaporization reaction similar to the one observed for YbF_3 [i.e., (5-6)].

5.5. Knudsen Effusion Results

5.5.1. The Congruent Vaporization of $YbF_{2.40}$

The congruency of reaction (5-2) in combination with the mass spectrometric results requires the mole fraction of $YbF_2(g)$ and $YbF_3(g)$ to be 0.60 and 0.40, respectively. Use of this relationship allows the partial pressures of $YbF_2(g)$ and $YbF_3(g)$ to be calculated from the X-ray fluorescence analysis of the effusate collected on platinum targets. In accordance with previous investigations[57,96] all the effusate which contained a lanthanide metal and impinged on the target was assumed to have condensed. The natural logarithm of the equilibrium constant for reaction (5-2) for 90 pressure-temperature data points from experiments 1 through 10 (Table 11,

Table 11. Experimental Conditions for Vaporization Runs in the Ytterbium Fluoride System

Exp.	% Yb[1]	(F/Yb)[2]	Set-up[4]	Cell	Orifice Area[5]	T Range
1	81.9	2.01	M + O	Mo	7.90×10^{-3} cm^2	1293-1592 K
2	78.4	2.51	"	Mo	1.14	1547-1696
3	78.9	2.44	"	Mo	7.59	1520-1673
4	----	2.4[3]	G + O	C(gr)	5.01	1504-1609
5-7	----	2.4[3]	M	Mo	1.12	1566-1742
8-10	----	2.4[3]	"	Mo	7.28	1452-1640
11-13	75.2	3.00	G + O	Mo	8.33	1342-1620
14,15	"	"	"	Mo	1.11	1511-1794
16	"	"	"	C(gr)	1.10	1521-1667

[1] Average error for all analyses before vaporization = ± 0.3 %

[2] Composition error = ± 0.04

[3] Estimated value

[4] M = metal vacuum line; O = W-Mo oven; G = glass vacuum line

[5] Estimated error = $\pm 0.10 \times 10^{-3}$ cm^2

Appendices 2 and 5) and the five corresponding unweighted linear least-squares equation from Table 12 are presented in Figure 9. The first four data points from experiment 1 (■), also presented in Figure 9, represent pressures for Yb(g) recorded in the composition region YbF_{2+x} ($0.00 \leq x < 0.40$). A change in cell material from molybdenum to graphite had little effect on the equilibrium vapor pressures as evidenced by the results of experiment 4 presented in Figure 9. Also, the change in composition from $YbF_{2.28}$ (experiment 1) to $YbF_{2.49}$ (experiment 2) alters the partial pressures insignificantly. Use of the film thickness monitor during experiment 1 reconfirmed the initial incongruent vaporization behavior of $YbF_{2.00}$. The rate of effusate deposition (vapor pressure) at a constant temperature decreased initially with time (Figure 10), but eventually became reproducible with both time and temperature (Figure 9 and Appendix 2).

From the results of experiments 5 through 10 (performed without the W-Mo oven) the following thermodynamic values are calculated for reaction (5-2) at the median temperature with the errors indicative of the standard deviations of the linear fit: $\Delta H^{\circ}_{1597} = (96._9 \pm 1._1)$ kcal mol^{-1} and $\Delta S^{\circ}_{1597} = (36.8_3 \pm 0.6_7)$ cal $mol^{-1}K^{-1}$.

Thermodynamic functions for $YbF_{2.40}$ were derived at each temperature by combination of those calculated from the enthalpy increments reported for YbF_3[18] (melting point = 1435 K) with the thermodynamic values estimated as described below for YbF_3 and YbF_2 in the ratio 0.40:0.60, respectively (Appendix 3). From the published heat capacities of CaF_2(s), Ca(s) and Yb(s),[25,145,146] the heat capacity, C°_p, of YbF_2(s) at 298 K was estimated as $(17.3_0 \pm 0.2_5)$ cal $mol^{-1}K^{-1}$

Table 12. Results of Linear Least-Squares Analyses of Vaporization Reactions in the Ytterbium Fluoride System

Exp.	Slope	Intercept	Range
	$YbF_{2.40}(s,\ell) = 0.60\ YbF_2(g) + 0.40\ YbF_2(g)$		
	$\ell n\ K$ vs. $10^4/T$		
1	$-4.5_3 \pm 0.1_9$	$17._0 \pm 1._2$	1466-1592 K
2	$-3.8_1 \pm 0.3_3$	$12._7 \pm 2._0$	1572-1728
3	$-4.19_5 \pm 0.08_7$	$14.8_8 \pm 0.5_5$	1520-1673
4	$-4.9_4 \pm 0.1_4$	$19.1_8 \pm 0.8_8$	1504-1609
5-10	$-4.87_4 \pm 0.05_4$	$18.5_3 \pm 0.3_4$	1452-1742
	$YbF_{3.00}(s,\ell) = 0.05\ YbF_{2.40}(s,\ell) + 0.95\ YbF_3(g) + 0.03\ F(g)$		
	$\ell n\ p(YbF_3(g)/atm)$ vs. $10^4/T$		
11-15	$-4.68_2 \pm 0.02_1$	$19.2_9 \pm 0.1_4$	1342-1794
16	$-4.40_0 \pm 0.08_8$	$17.3_7 \pm 0.5_3$	1548-1703

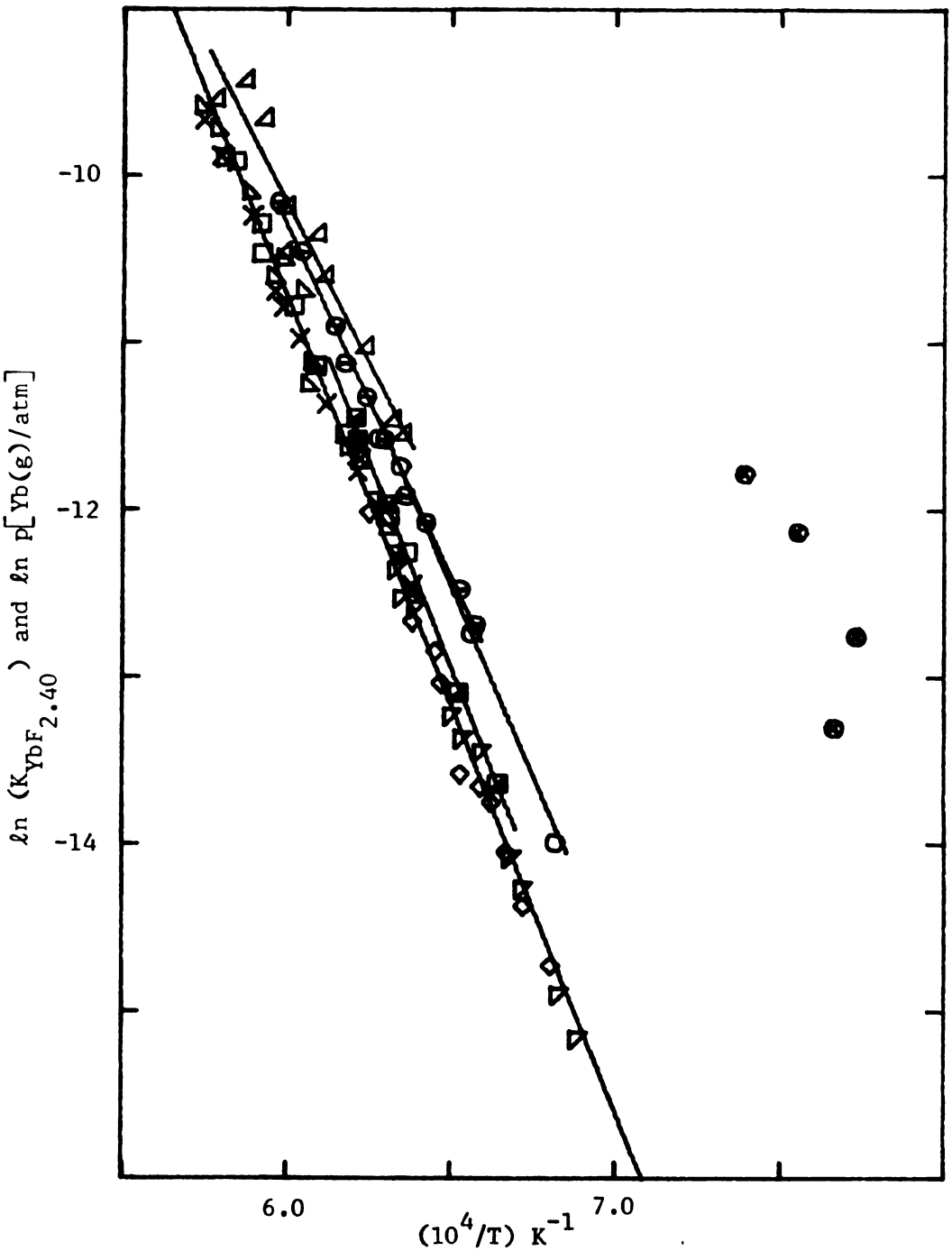

Figure 9. Natural Logarithm of the Equilibrium Constant for the Congruent Vaporization of $YbF_{2.40}$ [Exp. 1(○), 2(◿), 3(⊖), 4(■), 5(□), 6(X), 7(◺), 8(◇), 9(◹) and 10(▽)] and the Pressure of Yb(g) from YbF_{2+x} ($0.00 \leq x < 0.40$) [Exp. 1(⊠)] vs. Reciprocal Temperature

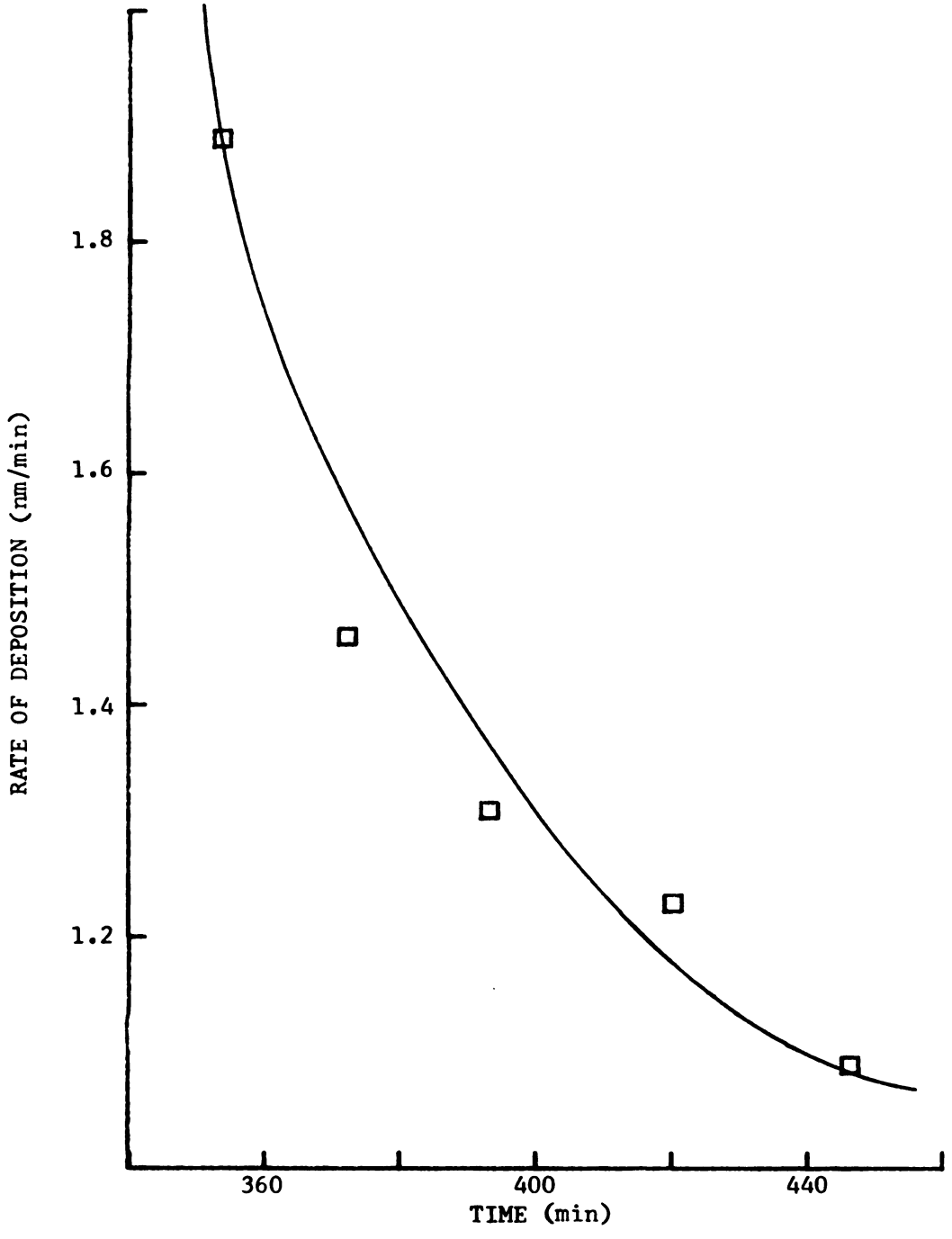

Figure 10. Rate of Deposition of Yb(g) from YbF_{2+x} ($0.01 \leq x < 0.40$) Confined in Mo *vs.* Time (T = 1475 K)

(cf. Section 3.6.6.). The heat capacity of $YbF_2(s)$ at its melting point, 1680 K,[147] was taken as $(21.7_5 \pm 0.2_5)$ cal $mol^{-1}K^{-1}$ [123] (cf. Section 3.6.6.). A linear variation of C_p° with temperature was assumed and equation (5-7) was derived. An enthalpy of fusion of (7.5 ± 0.5)

$$C_p^\circ(YbF_2,s) = \left[(16.4 \pm 0.5) + (3.19 \times 10^{-3})T\right] \text{ cal mol}^{-1}\text{K}^{-1} \quad (5\text{-}7)$$

(298-1680 K)

kcal mol^{-1} for $YbF_2(s)$ and a heat capacity, C_p°, value of (23.9 ± 0.7) cal $mol^{-1}K^{-1}$, assumed constant over the entire liquid range for $YbF_2(\ell)$, were used by analogy with the values reported for $CaF_2(s,\ell)$.[145]

The standard entropies, $S^\circ_{298}(YbF_2,s)$ and $S^\circ_{298}(YbF_3,s)$, were estimated as $(22.5_0 \pm 0.5_0)$ and $(26.5_6 \pm 0.5_0)$ cal $mol^{-1}K^{-1}$, respectively, from the schemes of Westrum[125] and Latimer.[126] The F^- contribution to $S^\circ_{298}(YbF_3,s)$ was derived from the experimental S°_{298} value for $CeF_3(s)$[31] and the estimated contribution for Ce^{+3}.[127] From these values $S^\circ_{298}(YbF_{2.40},s)$ was calculated to be $(24.1_2 \pm 0.5_0)$ cal $mol^{-1}K^{-1}$.

Thermodynamic functions for $YbF_2(g)$ and $YbF_3(g)$ were calculated from measured and estimated molecular constants. A non-linear geometry with a F-Yb-F angle of $(140 \pm 10)^\circ$[65] and a Yb-F distance of 0.210(5) nm, which was estimated to be the same distance as that reported for $CaF_2(g)$,[66] were used for $YbF_2(g)$. A non-planar geometry with a F-Yb-F angle of $(117 \pm 10)^\circ$[61] and a Yb-F distance of 0.203(5) nm, which was estimated by the method of Wesley and DeKock,[60] were used for $YbF_3(g)$. Wave numbers, $\nu_1 = (476 \pm 10)$, $\nu_2 = (114.5 \pm 5.0)$ and $\nu_3 = (462 \pm 10)$ cm^{-1},[65] were used with a ground state statistical weight of one for $YbF_2(g)$. For $YbF_3(g)$ wave numbers, $\nu_1 = (581 \pm 10)$, $\nu_2(E) = (100 \pm 5)$, $\nu_3(E) = (565 \pm 10)$ and $\nu_4 = (144 \pm 5)$ cm^{-1},[61]

were used with a ground state statistical weight of eight. The uncertainty in the entropy and free energy functions which results from uncertainties in the molecular constants and the statistical weight is $\pm 1._3$ cal $mol^{-1}K^{-1}$. Calculated thermodynamic functions are presented in Appendix 3. The pressure-temperature data of experiments 5 through 10 were reduced in accordance with the coefficients of reaction (5-2) and are described in equation (5-8) with appro-

$$\Sigma'(\text{cal mol}^{-1}\text{K}^{-1}) = [(110._7 \pm 1._0) \times 10^3]/T - (50.8_5 \pm 0.6_4) \quad (5\text{-}8)$$

priate standard deviations by the unweighted linear least-squares fit of Σ' vs. 1/T. Combination of the experimental pressures with the free energy functions (third-law procedure) yielded for reaction (5-2) $\Delta H^\circ_{298} = (109.8_3 \pm 0.3_6)$ kcal mol^{-1}.

When uncertainties in the thermodynamic functions are included, the second-law derived values for (5-2) become $\Delta H^\circ_{298} = (110._7 \pm 2._3)$ kcal mol^{-1} and $\Delta S^\circ_{298} = (50._8 \pm 2._1)$ cal $mol^{-1}K^{-1}$; the third-law derived enthalpy with its uncertainty is $\Delta H^\circ_{298} = (109._8 \pm 2._4)$ kcal mol^{-1}.

From $S^\circ_{298}(YbF_2,g)$, $S^\circ_{298}(YbF_3,g)$ and the second-law derived ΔS°_{298} for (5-2), $S^\circ_{298}(YbF_{2.40},s) = (23._8 \pm 3._3)$ cal $mol^{-1}K^{-1}$.

From the derived thermodynamic functions (Appendix 3) and the second-law derived values a boiling point of (2795 ± 5) K was calculated with an enthalpy and entropy of vaporization of $(81._3 \pm 2._3)$ kcal $mol^{-1}K^{-1}$ and $(29._1 \pm 2._1)$ cal $mol^{-1}K^{-1}$, respectively. From the third-law derived value for ΔH°_{298} the boiling point was determined to be (2820 ± 5) K with an associated enthalpy of vaporization of $(80._1 \pm 2._4)$ kcal mol^{-1}.

5.5.2. The Incongruent Vaporization of YbF_3

The natural logarithm of the equilibrium partial pressure of $YbF_3(g)$ for 60 pressure-temperature data points from experiments 11 through 16 (Table 11 and Appendices 2 and 5) and the two corresponding unweighted linear least-squares equations from Table 12 (Mo and graphite cells) are presented in Figure 11. The change of cell material from molybdenum to graphite did not have a significant effect upon the equilibrium partial pressures of $YbF_3(g)$. The stoichiometry of reaction (5-6) requires that the partial pressures of $YbF_3(g)$ and F(g) in the Knudsen cell be related according to (5-9), in which Ln equals Yb. From this equation and the pressure-temperature data from experiments 11 through 15 (Tables 11 and 12), the natural logarithm of the equilibrium constant for (5-6) is represented in (5-10). From (5-10) the following thermodynamic values

$$p_F/[(M_F)^{\frac{1}{2}}(0.03)] = p_{LnF_3}/[(M_{LnF_3})^{\frac{1}{2}}(0.95)] \qquad (5\text{-}9)$$

$$\ell n\ K = -[(45.8_8 \pm 0.2_0) \times 10^3]/T + (18.7_6 \pm 0.1_3) \qquad (5\text{-}10)$$

were calculated for (5-6) at the median temperature: $\Delta H^\circ_{1568} = (91.1_9 \pm 0.4_1)$ kcal mol^{-1} and $\Delta S^\circ_{1568} = (37.2_8 \pm 0.2_6)$ cal $mol^{-1}K^{-1}$. The reported uncertainties are the standard deviations of the linear least-squares equation for $\ell n\ K$ vs. $1/T$. Reduction of the pressure-temperature data of experiments 11 through 15 was carried out in accordance with the coefficients of reaction (5-6) by means of the Σ' method and the derived thermodynamic functions for YbF_2 and YbF_3 (see Appendix 3) and data in the JANAF tables[144] for F(g). The results are described with appropriate standard deviations by the unweighted linear least-squares equation (5-11). From a combination

$$\Sigma'(\text{cal mol}^{-1}\text{K}^{-1}) = [(111.0_5 \pm 0.4_4) \times 10^3]/T - (56.1_7 \pm 0.2_9) \qquad (5\text{-}11)$$

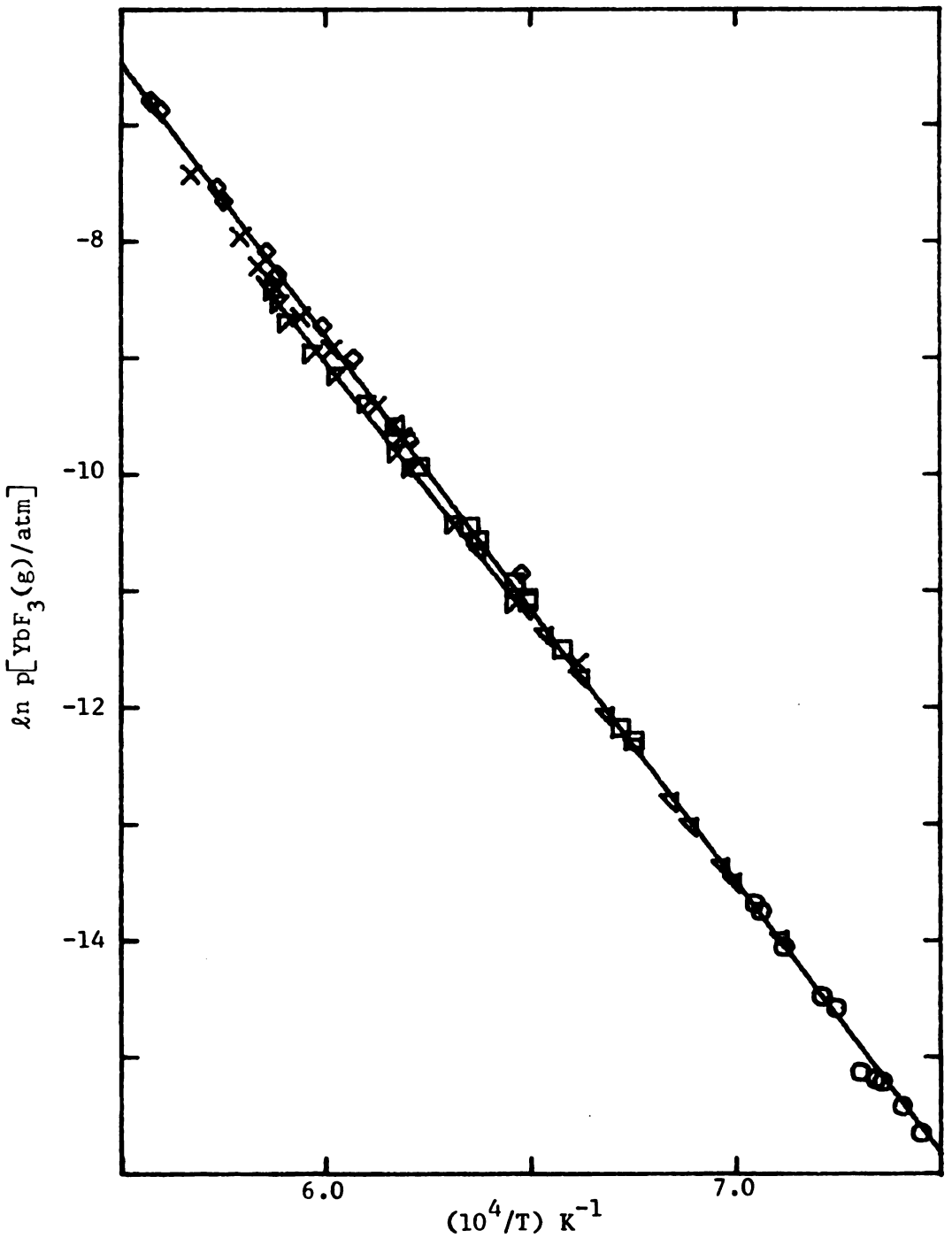

Figure 11. Natural Logarithm of the Equilibrium Partial Pressure of $YbF_3(g)$ from $YbF_3(s,\ell)$ [Exp. 11(□), 12(X), 13(◇), 14(◹), 15(○) and 16(▽)] vs. Reciprocal Temperature

of the calculated equilibrium constant with the derived free energy functions for (5-6), a value for ΔH°_{298} = ($106.9_6 \pm 0.4_2$) kcal mol^{-1} was calculated.

Inclusion of uncertainties in the thermodynamic functions yielded for (5-6) the following values: second-law method, ΔH°_{298} = ($111._1 \pm 1._3$) kcal mol^{-1} and ΔS°_{298} = ($56._2 \pm 1._3$) cal $mol^{-1}K^{-1}$; third-law method, ΔH°_{298} = ($107._0 \pm 3._5$) kcal mol^{-1}.

From $S^\circ_{298}(YbF_3,g)$, $S^\circ_{298}(YbF_{2.40},s)$, $S^\circ_{298}(F,g)$ and the second-law derived ΔS°_{298} for (5-6), $S^\circ_{298}(YbF_3,s)$ = ($23._9 \pm 3._3$) cal $mol^{-1}K^{-1}$.

5.5.3. The Congruent Vaporization of YbF_2 and YbF_3

5.5.3.1. YbF_3

The difference between enthalpies of formation of YbF_3 and $YbF_{2.40}$ {difference calculated as 0.60 x $[\Delta H^\circ_f(YbF_3,s) - \Delta H^\circ_f(YbF_2,s)]$} at 298 K, the enthalpy of formation for F(g) and the second-law derived enthalpy for (5-6) were combined to yield for (5-12) ΔH°_{298} = ($113._3 \pm 1._8$) kcal mol^{-1}. Similar treatments with the second-law derived entropy and the third-law derived enthalpy yielded for (5-12) ΔS°_{298} = ($58._1 \pm 1._4$) cal $mol^{-1}K^{-1}$ and ΔH°_{298} = ($109._0 \pm 4._1$) kcal mol^{-1}, respectively.

$$YbF_3(s) = YbF_3(g) \qquad (5\text{-}12)$$

Combination of $S^\circ_{298}(YbF_3,g)$ and the second-law derived ΔS°_{298} for (5-12) yielded $S^\circ_{298}(YbF_3,s)$ = ($23._8 \pm 3._4$) cal $mol^{-1}K^{-1}$.

From the second-law derived values, the extrapolated boiling point was determined to be (2490 ± 5) K with an enthalpy and entropy of vaporization of ($82._7 \pm 1._8$) kcal mol^{-1} and ($33._2 \pm 1._4$) cal $mol^{-1}K^{-1}$, respectively. From the third-law derived value of ΔH°_{298}, the

extrapolated boiling point was calculated to be (2580 ± 5) K with an associated enthalpy of vaporization of ($77._6 \pm 4._1$) kcal mol^{-1}.

5.5.3.2. $\underline{YbF_2}$

The second-law derived enthalpies for (5-2), (5-12) and (5-13)

$$YbF_{2.40}(s) = (0.60)\ YbF_2(s) + (0.40)\ YbF_3(s) \qquad (5\text{-}13)$$

[ΔH°_{298} for (5-13) estimated as (0 ± 2) kcal mol^{-1}, c.f. Section 5.5.1.] were used to calculate the enthalpy for (5-14), ΔH°_{298} =

$$YbF_2(s) = YbF_2(g) \qquad (5\text{-}14)$$

($109._0 \pm 8._4$) kcal mol^{-1}. Similar use of the second-law derived entropies yielded for (5-14) ΔS°_{298} = ($46._0 \pm 6._1$) cal $mol^{-1}K^{-1}$, while use of the third-law derived enthalpies resulted in ΔH°_{298} = ($11_1 \pm 1_0$) kcal mol^{-1} for (5-14).

Combination of $S^\circ_{298}(YbF_2,s)$ and the second-law derived ΔS°_{298} for (5-14) yielded $S^\circ_{298}(YbF_2,s)$ = ($23._5 \pm 8._1$) cal $mol^{-1}K^{-1}$.

From the second-law derived value for ΔH°_{298} for (5-14) and the derived thermodynamic functions (Appendix 3), the boiling point for YbF_2 was calculated to be (3045 ± 5) K with an associated enthalpy and entropy of vaporization of ($79._6 \pm 8._4$) kcal mol^{-1} and ($26._1 \pm 6._1$) cal $mol^{-1}K^{-1}$, respectively. From the third-law derived value for (5-14), the boiling point was calculated to be (3015 ± 5) K with an associated enthalpy of vaporization of ($8_2 \pm 1_0$) kcal mol^{-1}.

5.5.4. $\underline{\text{The Congruent Vaporization of } SmF_{2.40}}$

The vaporization of $SmF_{2.40}$ was examined by use of the thin film monitor and the target collection techniques. During the initial stages of vaporization the effusate over $SmF_{2.00}$ behaved in a manner identical to that observed for the composition region

YbF_{2+x}, $0.00 \leq x < 0.40$. The rate of deposition (vapor pressure) decreased with time (Figure 12), but eventually became reproducible with both time and temperature (Figures 13 and Appendix 2). Analysis of the residues (Table 8) indicated that the pseudo-hexagonal phase of composition $SmF_{2.40(4)}$ vaporized congruently. The vaporization reaction was considered to be identical to that observed for $YbF_{2.40}$, reaction (5-2), and is

$$SmF_{2.40}(s,\ell) = (0.60)\ SmF_2(g) + (0.40)\ SmF_3(g) \qquad (5\text{-}15)$$

The natural logarithm of the equilibrium constant for (5-15) for 52 pressure-temperature data points from three experiments (Appendices 2 and 5) and the corresponding unweighted linear least-squares equation (5-16) with appropriate standard deviations are presented in

$$\ell n\ K(5\text{-}15) = -\left[(45._6 \pm 1._1) \times 10^3\right]/T + (18.7_3 \pm 0.7_1) \qquad (5\text{-}16)$$

$$(1369\text{-}1791\ K)$$

Figure 13. The first five data points from experiment 1 (▽), also presented in Figure 13, represent Sm(g) pressures measured over the composition region SmF_{2+x} $(0.00 \leq x < 0.40)$ during the incongruent vaporization period. During experiment number three a temperature gradient $(31 \pm 7)°$ was observed between the top and bottom cavities of the Knudsen cell. The temperatures of the top cavity were used and yielded results in agreement with those of the two previous experiments.

Use of the results of these three experiments which were performed in the metal vacuum system with a W-Mo oven yielded for reaction (5-15) at the median temperature the following thermodynamic values with the errors indicative of the standard deviations of the

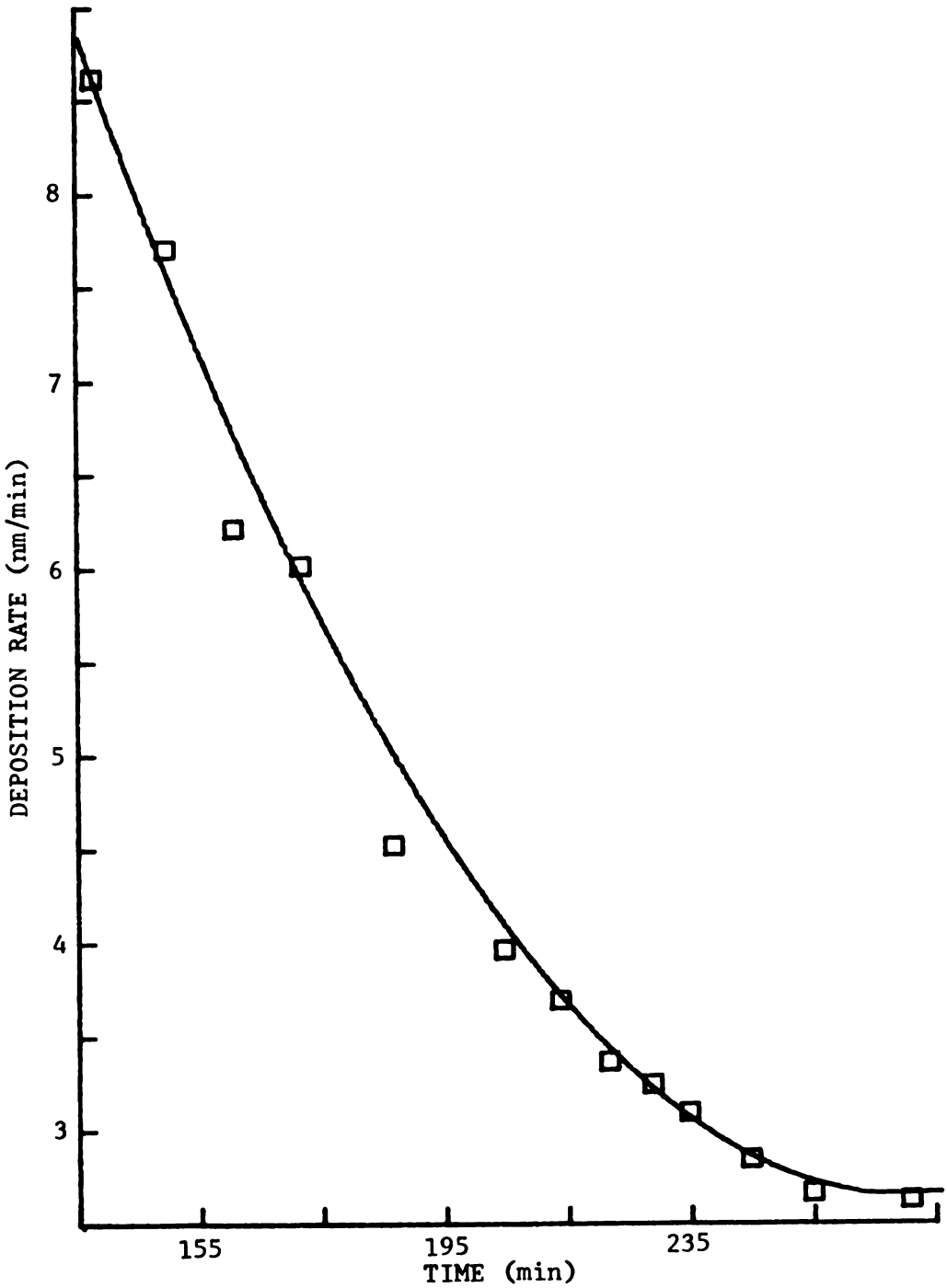

Figure 12. Rate of Deposition for Sm(g) from SmF_{2+x} ($0.00 \leq x < 0.40$) Confined in Mo *vs.* Time (T = 1232 K)

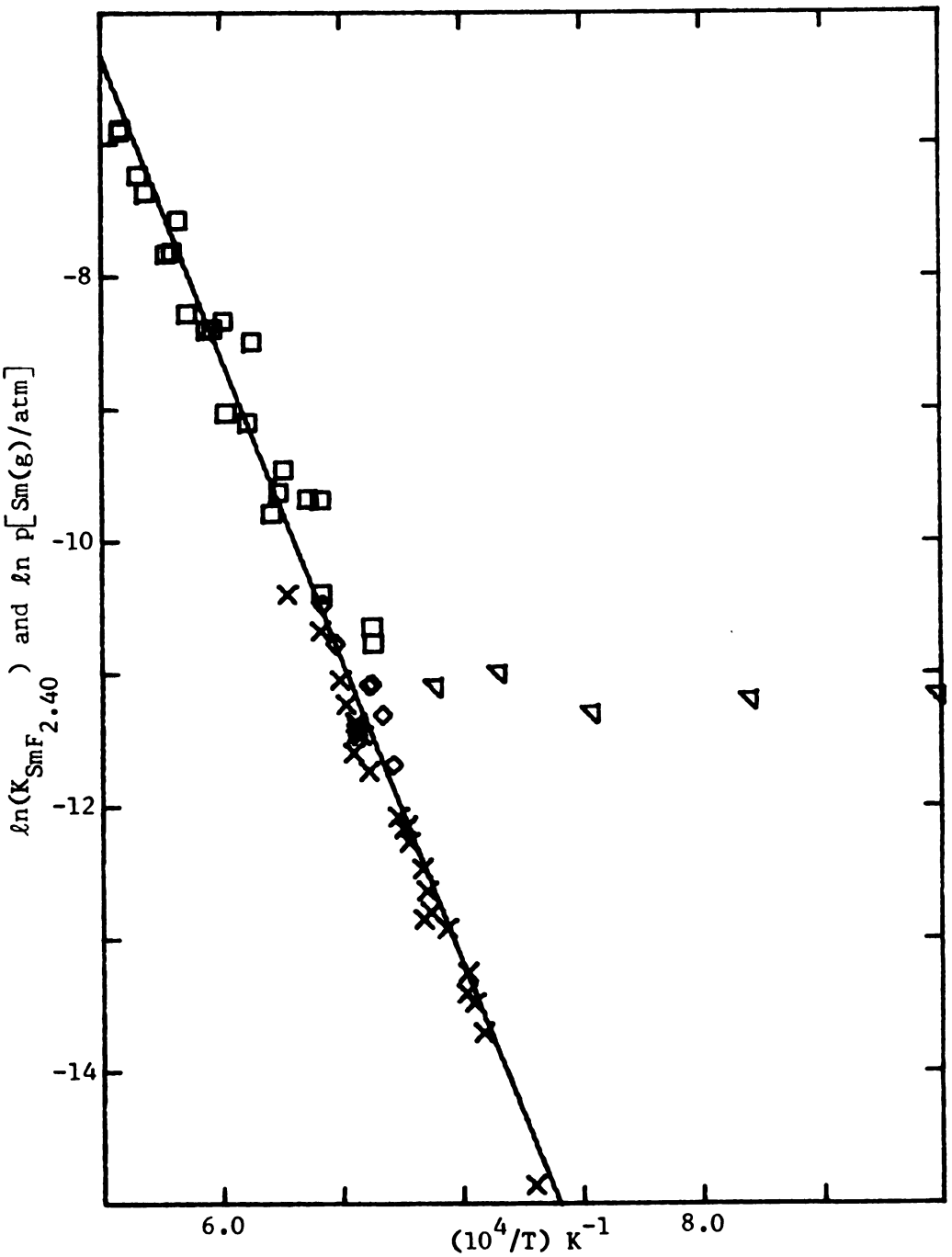

Figure 13. Natural Logarithm of the Equilibrium Constant for the Congruent Vaporization of $SmF_{2.40}$ [Exp. 1(◇), 2(X) and 3(□)] and the Pressure of Sm(g) from SmF_{2+x} ($0.00 \leq x < 0.40$) [Exp. 1(▽)] vs. Reciprocal Temperature

linear fit: $\Delta H^{\circ}_{1580} = (90._5 \pm 2._2)$ kcal mol^{-1} and $\Delta S^{\circ}_{1580} = (37._2 \pm 1._4)$ cal mol^{-1}K^{-1}.

Thermodynamic functions for $SmF_{2.40}$ were derived at each temperature by combination of those calculated from the entahlpy increments reported for SmF_3[18] (melting point = 1573 K) with the thermodynamic values estimated as described below for SmF_3 and SmF_2 in the ratio of 0.40:0.60, respectively (Appendix 3). From the published heat capacities of BaF_2(s), Ba(s), and Sm(s),[25,145,146] the heat capacity, C°_p, of SmF_2(s) at 298 K was estimated as $(14.6_3 \pm 0.2_5)$ cal mol^{-1}K^{-1} (cf. Section 3.6.6.). The heat capacity of SmF_2(s) at its melting point, 1690 K,[147] was taken as $(21.7_5 \pm 0.2_5)$ cal mol^{-1}K^{-1}.[123] By assuming a linear variation of C°_p with temperature, equation (5-17)

$$C^{\circ}_p(SmF_2,s) = (12.7 \pm 0.5) + (6.36 \times 10^{-3})/T \qquad (5\text{-}17)$$

$$(298\text{-}1417\ K)$$

was derived. An enthalpy of fusion of (7.5 ± 0.5) kcal mol^{-1} for SmF_2(s) and a C°_p of (23.9 ± 0.7) cal mol^{-1} K^{-1} assumed constant over the liquid range for $SmF_2(\ell)$ were used by analogy with the values estimated for YbF_2(s,ℓ) (cf. Section 5.5.1.). A C°_p for $BaF_2(\ell)$ was not available.

The standard entropies, $S^{\circ}_{298}(SmF_2,s)$ and $S^{\circ}_{298}(SmF_3,s)$, were estimated as $(27.1_0 \pm 0.5_0)$ and $(27.0_9 \pm 0.5_0)$ cal mol^{-1}K^{-1}, respectively, from the schemes of Westrum[127] and Latimer.[125] The contribution of Sm^{+2} was taken to be the same as that of Eu^{+3} and includes a magnetic contribution of 3.5 cal mol^{-1}K^{-1}. The F^- contribution to $S^{\circ}_{298}(SmF_3,s)$ was taken to be the same as that for the corresponding ytterbium fluorides (cf. Section 5.5.1.). From these values $S^{\circ}_{298}(SmF_{2.40},s)$ was found to be $(27.1_0 \pm 0.5_0)$ cal mol^{-1}K^{-1}.

Thermodynamic functions for $SmF_2(g)$ and $SmF_3(g)$ were calculated from measured and estimated molecular constants. A non-linear geometry with a F-Sm-F angle of $(110 \pm 10)^o$[65] and Sm-F distance of 0.222(5) nm, which was estimated to be the distance reported for $SrF_2(g)$,[66] were used for $SmF_2(g)$. A planar geometry[60] and a Sm-F distance of 0.214(5) nm, which was estimated by the method of Wesley and DeKock,[60] were used for $SmF_3(g)$. For $SmF_2(g)$ wave numbers, $\nu_1 = (456 \pm 10)$, $\nu_2 = (114.5 \pm 5.0)$ and $\nu_3 = (435 \pm 10)$ cm^{-1},[58] were used with the spectroscopic data for isoelectronic Eu^{+3}.[70] Only contributions up to the state $^7F_6$, 4973 cm^{-1} above the ground state, were used to calculate the thermodynamic functions. Since the population of levels higher than $^7F_6$ is small at the temperatures studied, their contributions to the thermodynamic functions were not considered. For $SmF_3(g)$ wave numbers, $\nu_1 = (460 \pm 10)$, $\nu_2 = (123 \pm 10)$, $\nu_3(E) = (508 \pm 10)$ and $\nu_4(E) = (92 \pm 5)$ cm^{-1}, were used with the spectroscopic data for Sm^{+3} [69] up to the $^6H_{13/2}$ (5042 cm^{-1}) energy level. Calculated thermodynamic functions are presented in Appendix 3. The pressure-temperature data of three experiments were reduced in accordance with the coefficients of reaction (5-15) and are described with appropriate standard deviations by the unweighted linear least-squares fit of Σ' vs. 1/T in equation (5-18). Combin-

$$\Sigma'(\text{cal mol}^{-1}\text{K}^{-1}) = [(100._2 \pm 2._1) \times 10^3]/T - (46._2 \pm 1._3) \quad (5\text{-}18)$$

ation of the experimental pressures with the free energy functions (third-law procedure) yielded for (5-15) $\Delta H^o_{298} = (104._4 \pm 1._0)$ kcal mol^{-1}. When uncertainties in the thermodynamic functions are included, the second-law derived values for (5-15) become $\Delta H^o_{298} = (100._2 \pm 3._4)$ kcal mol^{-1} and $\Delta S^o_{298} = (46._2 \pm 2._8)$ cal $mol^{-1}K^{-1}$; the third-law

derived enthalpy with its uncertainty is $\Delta H^{\circ}_{298} = (104._4 \pm 3._0)$ kcal mol^{-1}.

From $S^{\circ}_{298}(SmF_2,g)$, $S^{\circ}_{298}(SmF_3,g)$ and the second-law derived ΔS°_{298} for (5-15), $S^{\circ}_{298}(SmF_{2.40},s) = (29._8 \pm 4._8)$ cal $mol^{-1}K^{-1}$.

From the derived thermodynamic functions (Appendix 3) and the second-law derived values a boiling point for $SmF_{2.40}$ of (2600 ± 5) K was calculated with and enthalpy and entropy of vaporization of $(73._2 \pm 3._4)$ kcal mol^{-1} and $(28._2 \pm 2._8)$ cal $mol^{-1}K^{-1}$, respectively. From the third-law derived value for ΔH°_{298}, the boiling point was determined to be (2510 ± 5) K with an associated enthalpy of vaporization of $(78._4 \pm 3._0)$ kcal mol^{-1}.

5.5.5. The Incongruent Vaporization of SmF_3

The natural logarithm of the equilibrium partial pressure for $SmF_3(g)$ for 49 pressure-temperature data points from three independent experiments performed on $SmF_3(s,\ell)$ are presented in Figure 14 and Appendices 2 and 5. Also presented in Figure 14 are the two unweighted linear least-squares equation (5-19) and (5-20) for 19

$$\ell n\, p[SmF_3(g)/atm] = -[(42._6 \pm 2._4) \times 10^3]/T + (17._0 \pm 1._5) \quad (5\text{-}19)$$

(1592-1746 K)

$$\ell n\, p[SmF_3(g)/atm] = -[(48._8 \pm 1._0) \times 10^3]/T + (22.1_2 \pm 0.7_2) \quad (5\text{-}20)$$

(1353-1571 K)

pressure-temperature data points from $SmF_3(\ell)$ and 30 points from $SmF_3(s)$. The reported errors represent the standard deviation of the linear fits. All three experiments were performed in the metal vacuum system with the W-Mo oven used to heat Mo Knudsen cells. The incongruent vaporization of $SmF_3(s,\ell)$ is represented in accordance with the previously discussed similarity to $YbF_3(s,\ell)$ (cf. Section

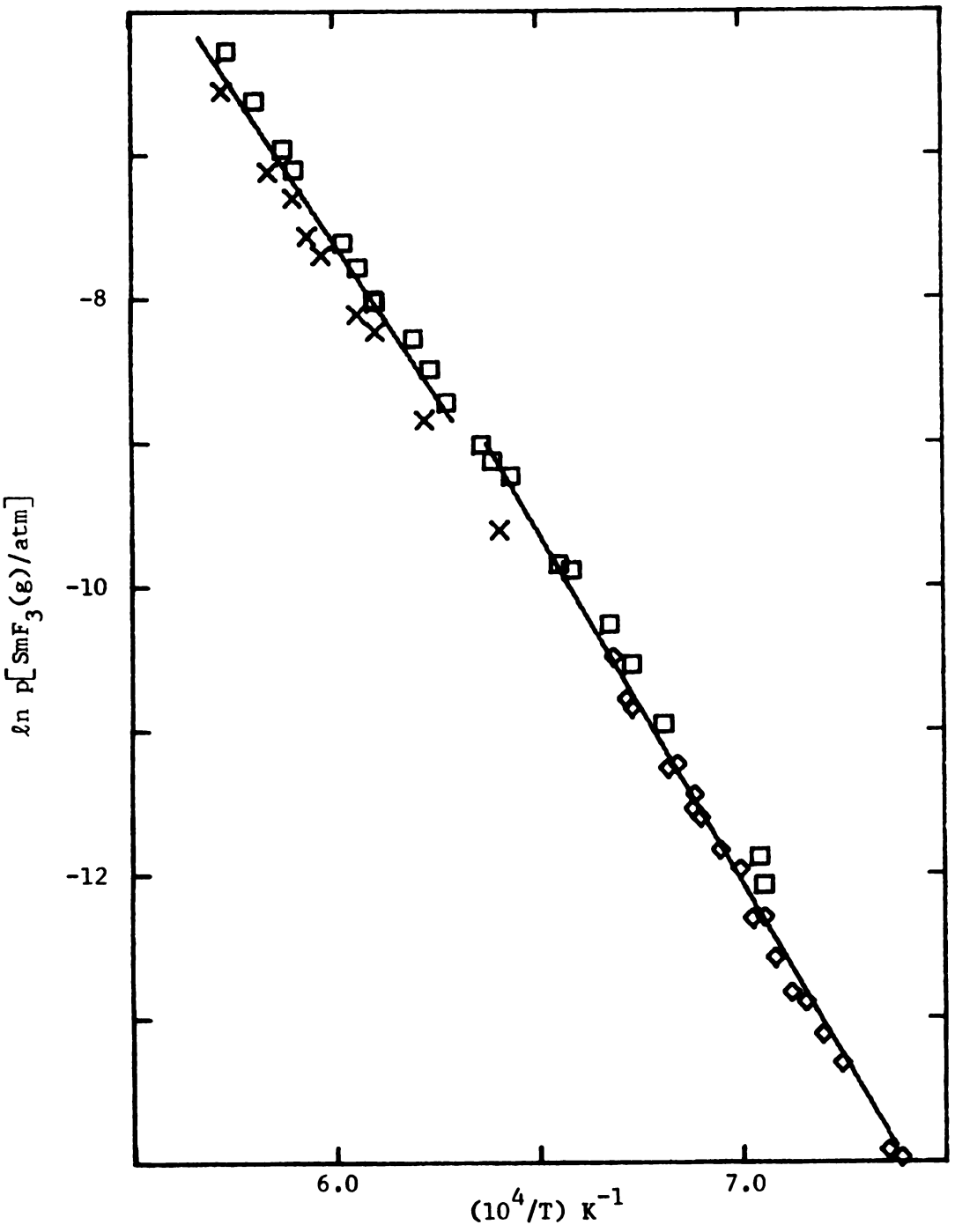

Figure 14. Natural Logarithm of the Equilibrium Partial Pressure of $SmF_3(g)$ from $SmF_3(s,\ell)$ [Exp. 1(X), 2(◇) and 3(□)] vs. Reciprocal Temperature

5.4.) by equation (5-21). The stoichiometry of equation (5-21)

$$SmF_{3.00}(s,\ell) = (0.05)\ SmF_{2.40} + (0.95)\ SmF_3(g) + (0.03)\ F(g) \quad (5\text{-}21)$$

requires the partial pressures of $SmF_3(g)$ and F(g) in the Knudsen cell be related according to equation (5-9) in which Ln equals Sm. The natural logarithms of the equilibrium constants for (5-21) are presented in equations (5-22) and (5-23), respectively, for data

$$\ell n\ K = -\left[(41._9 \pm 2._4) \times 10^3\right]/T + (17._5 \pm 1._4) \quad (5\text{-}22)$$

(1592-1746 K)

$$\ell n\ K = -\left[(47._8 \pm 1._0) \times 10^3\right]/T + (21.5_4 \pm 0.7_1 \quad (5\text{-}23)$$

(1353-1571 K)

above and below the melting point of $SmF_{3.00}(s)$. From (5-22) and (5-23) the following thermodynamic values were calculated for (5-21) at the median temperature: $\Delta H^\circ_{1669} = (83._2 \pm 4._7)$ and $\Delta H^\circ_{1462} = (95._0 \pm 2._0)$ kcal mol^{-1}; $\Delta S^\circ_{1669} = (34._8 \pm 2._8)$ and $\Delta S^\circ_{1462} = (42._8 \pm 1._4)$ cal $mol^{-1}K^{-1}$. The reported uncertainties are the standard deviations of the linear least-squares fits for $\ell n\ K$ vs. 1/T. Reduction of the pressure-temperature data by use of the Σ' method and the derived thermodynamic functions (cf. Section 5.5.4. and Reference 144) yielded (5-24). From a combination of the calculated equilbrium constant

$$\Sigma'(\text{cal mol}^{-1}\text{K}^{-1}) = \left[(101._7 \pm 1._1) \times 10^3\right]/T - (52.4_9 \pm 0.7_1) \quad (5\text{-}24)$$

with the derived free energy functions for (5-21), a value for $\Delta H^\circ_{298} = (101.7_1 \pm 0.5_6)$ kcal mol^{-1} was calculated. When uncertainties in the thermodynamic functions are included, the second-law derived values for (5-21) become $\Delta H^\circ_{298} = (101._7 \pm 2._0)$ kcal mol^{-1} and $\Delta S^\circ_{298} = (52._5 \pm 1._7)$ cal $mol^{-1}K^{-1}$. The third-law derived enthalpy is $(101._7 \pm 2._6)$ kcal mol^{-1}.

From $S^\circ_{298}(SmF_3,g)$, $S^\circ_{298}(SmF_{2.40},s)$, $S^\circ_{298}(F,g)$ and the second-law derived ΔS°_{298} for (5-21), $S^\circ_{298}(SmF_3,s) = (27._1 \pm 3._7)$ cal $mol^{-1}K^{-1}$.

5.5.6. The Congruent Vaporization of SmF_2 and SmF_3

5.5.6.1. SmF_3

The difference in the enthalpies of formation at 298 K for SmF_3 and $SmF_{2.40}$ (difference calculated as in Section 5.5.3.1. for YbF_3 and $YbF_{2.40}$), the enthalpy of formation for F(g) and the second-law derived enthalpy for (5-21) were combined to yield for (5-25) $\Delta H^\circ_{298} = (101._2 \pm 2._5)$ kcal mol^{-1}. Similar treatments with

$$SmF_3(s) = SmF_3(g) \qquad (5\text{-}25)$$

the second-law derived entropy and the third-law derived enthalpy for (5-21) yielded for (5-25) $\Delta S^\circ_{298} = (54._1 \pm 1._9)$ cal $mol^{-1}K^{-1}$ and $\Delta H^\circ_{298} = (101._2 \pm 3._2)$ kcal mol^{-1}, respectively.

Combination of $S^\circ_{298}(SmF_3,g)$ and the second-law derived ΔS°_{298} for (5-25) yielded $S^\circ_{298}(SmF_3,s) = (27._0 \pm 3._9)$ cal $mol^{-1}K^{-1}$. From the second-law derived values the extrapolated boiling point was determined to be (2420 ± 5) K with an associated enthalpy and entropy of vaporization of $(65._5 \pm 2._5)$ kcal mol^{-1} and $(27._1 \pm 1._9)$ cal $mol^{-1}K^{-1}$, respectively. From the third-law derived enthalpy, an extrapolated boiling point was calculated to be (2420 ± 5) K with an associated enthalpy of vaporization of $(65._5 \pm 3._2)$ kcal mol^{-1}.

5.5.6.2. SmF_2

The second-law derived enthalpies for (5-15), (5-25) and (5-26)

$$SmF_{2.40}(s) = (0.60)\ SmF_2(s) + (0.40)\ SmF_3(s) \qquad (5\text{-}26)$$

(estimated as in Section 5.5.3.2. for $YbF_{2.40}$) were used to obtain the enthalpy for (5-27), $\Delta H^\circ_{298} = (99._5 \pm 9._3)$ kcal mol^{-1}. Similar

$$SmF_2(s) = SmF_2(g) \qquad (5\text{-}27)$$

use of the second-law derived entropies yielded for (5-27) ΔS°_{298} = $(40._9 \pm 6._8)$ cal $mol^{-1}K^{-1}$, while use of the third-law derived enthalpies resulted in ΔH°_{298} = $(106._5 \pm 9._1)$ kcal mol^{-1} for (5-27).

Combination of $S^\circ_{298}(SmF_2,g)$ and the second-law derived ΔS°_{298} for (5-27) yielded $S^\circ_{298}(SmF_2,s)$ = $(31._7 \pm 8._8)$ cal $mol^{-1}K^{-1}$.

From the second-law derived value for ΔH°_{298} for (5-27) and the derived thermodynamic functions (see Appendix 3), the extrapolated boiling point for SmF_2 was determined to be (2715 ± 5) K with an associated enthalpy and entropy of vaporization of $(79._1 \pm 9._3)$ kcal mol^{-1} and $(29._2 \pm 6._8)$ cal $mol^{-1}K^{-1}$, respectively. From the third-law derived value for ΔH°_{298} the boiling point was calculated to be (2555 ± 5) K with an associated enthalpy of vaporization of $(87._5 \pm 9._1)$ kcal mol^{-1}.

5.5.7. The Congruent Vaporization of TmF_3

The X-ray diffraction and metal analytical results (Table 8) of the vaporization residues indicated the presence of only one phase, orthorhombic TmF_3. The invariant composition and structure of the condensed phase and the reported mass spectrometric study[44] establish the congruency of the sublimation and vaporization reactions of TmF_3, in accordance with (5-28). Two independent effusion ex-

$$TmF_3(s,\ell) = TmF_3(g) \qquad (5\text{-}28)$$

periments were carried out on TmF_3 confined in Mo cells and heated by the W-Mo oven in the metal vacuum line. The vapor pressures were determined by use of the film thickness monitor and target collection techniques. The natural logarithm of the equilibrium pressure of $TmF_3(g)$ for 49 pressure-temperature data points from two experiments (see Appendices 2 and 5) and the corresponding unweighted linear

least-squares equation, (5-29), with appropriate standard deviations

$$\ell n\ p[TmF_3(g)/atm] = -\left[(43.4_0 \pm 0.2_4) \times 10^3\right]/T + (17.5_9 \pm 0.1_6) \quad (1348\text{-}1809\ K) \qquad (5\text{-}29)$$

are presented in Figure 15. At the median temperature, ΔH°_{1579} = $(86.2_4 \pm 0.4_8)$ kcal mol^{-1} and $\Delta S^\circ_{1579} = (34.9_5 \pm 0.3_2)$ cal $mol^{-1}K^{-1}$. The reported errors represent the standard deviations of the linear fit. Thermodynamic functions (Appendix 3) for TmF_3 (melting point = 1431 K) were derived at each temperature from the enthalpy increments reported by Spedding et al.[18] and the estimated absolute entropy.

The standard entropy, $S^\circ_{298}(TmF_3,s)$ was estimated as $(27.6_2 \pm 0.5_0)$ cal $mol^{-1}K^{-1}$ by the method used previously (cf. Section 5.5.1.).

Thermodynamic functions for $TmF_3(g)$ were calculated from measured and estimated molecular constants. A non-planar geometry[59] and a Tm-F distance of 0.203(5) nm, which was estimated by the method of Wesley and DeKock,[60] were used for $TmF_3(g)$. The observed smooth variation of fundamental vibration frequencies across the lanthanide series[60,61] was used to estimate the wave numbers for $TmF_3(g)$. These wave numbers, $\nu_1 = (580 \pm 10)$, $\nu_2(E) = (129 \pm 10)$, $\nu_3(E) = (561 \pm 10)$ and $\nu_4 = (98 \pm 5)$ cm^{-1}, were used with the spectroscopic data for Tm^{+3}. The lowest electronic energy level[69] was used to calculate the thermodynamic functions (Appendix 3). The pressure-temperature data of two experiments were reduced in accordance with (5-28) and are described with appropriate standard deviations by the unweighted linear least-squares fit of Σ' vs. 1/T in equation (5-30). Combination of the experimental pressures with the derived

$$\Sigma'(\text{cal mol}^{-1}\text{K}^{-1}) = \left[(108.2_4 \pm 0.5_0) \times 10^3\right]/T - (55.3_7 \pm 0.3_2) \qquad (5\text{-}30)$$

free energy functions (third-law procedure) yielded, for (5-28),

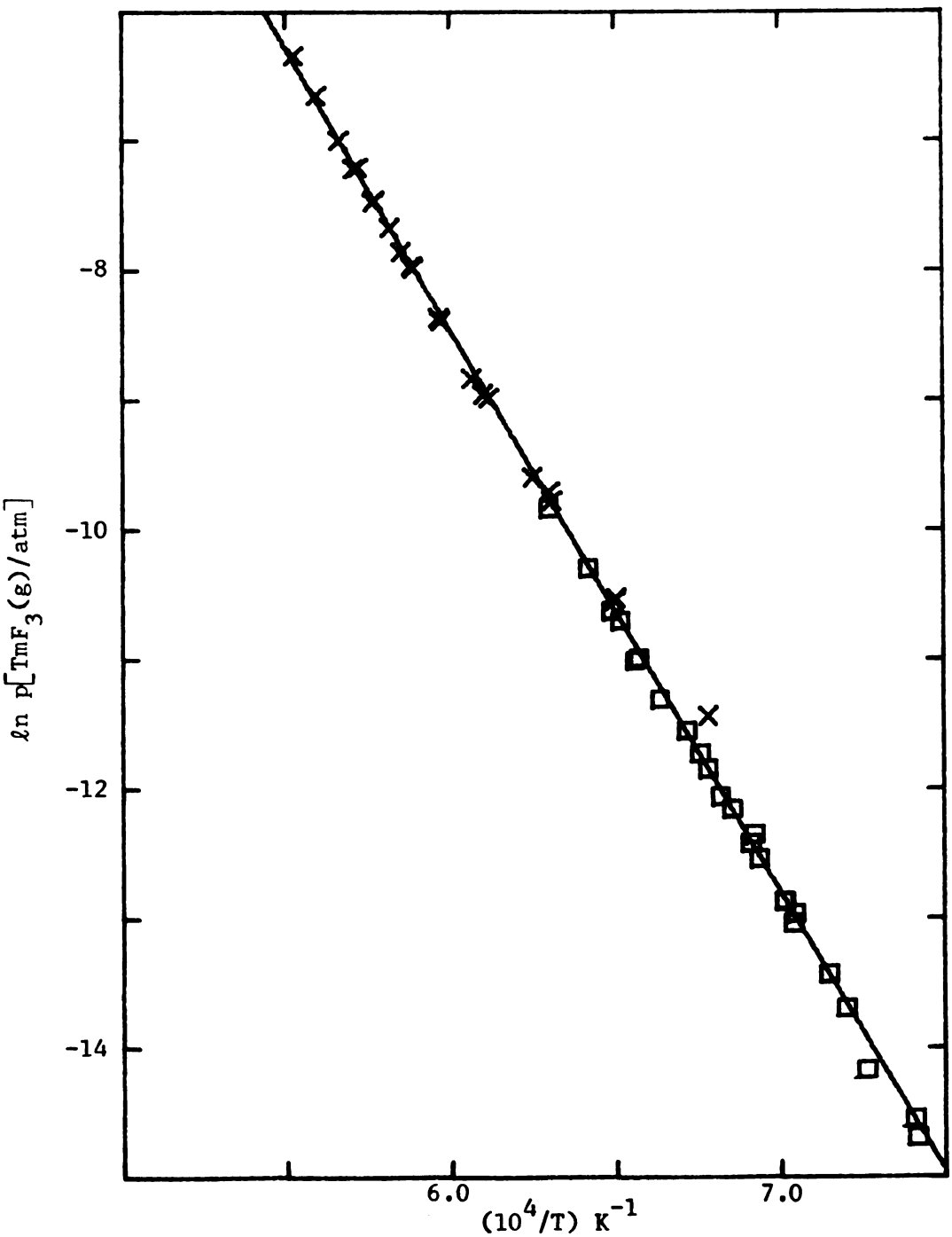

Figure 15. Natural Logarithm of the Equilibrium Pressure of $TmF_3(g)$ from $TmF_3(s,\ell)$ [Exp. 1(□) and 2(X)] vs. Reciprocal Temperature

ΔH°_{298} = ($107.4_9 \pm 0.2_8$) kcal mol^{-1}. When uncertainties in the calculated thermodynamic functions are included, the second-law derived values for (5-28) become ΔH°_{298} = ($108._2 \pm 1._5$) kcal mol^{-1} and ΔS°_{298} = ($55._4 \pm 1._3$) cal $mol^{-1}K^{-1}$. The third-law derived enthalpy with estimated uncertainty is ($107._5 \pm 2._3$) kcal mol^{-1}.

From $S^{\circ}_{298}(TmF_3,g)$ and the second-law derived ΔS°_{298} for (5-28), $S^{\circ}_{298}(TmF_3,s)$ = ($27._1 \pm 3._3$) cal $mol^{-1}K^{-1}$.

An extrapolated boiling point of (2580 ± 5) K was determined from the second-law derived values and the calculated thermodynamic functions (Appendix 3) with an associated enthalpy and entropy of vaporization of ($72._0 \pm 1._5$) kcal mol^{-1} and ($27._9 \pm 1._3$) cal $mol^{-1}K^{-1}$, respectively. From the third-law derived value for ΔH°_{298} for (5-28) the extrapolated boiling point was determined to be (2600 ± 5) K with an associated enthalpy of vaporization of ($71._0 \pm 2._3$) kcal mol^{-1}.

CHAPTER 6

DISCUSSION

6.1. Evaluation of Experimental Procedures

The Knudsen effusion technique is an accepted procedure for the measurement of equilibrium vapor pressures. The attainment of equilibrium within the Knudsen cell was indicated by the invariance of vapor pressures with orifice size and with increasing and decreasing temperatures. The use of near ideal orifices and the target collection technique eliminated the need to consider the effects of cell geometry on the measurements and minimized surface diffusion effects. The third-law derived values (Appendix 2) for all reactions exhibited no temperature or chronological trends. The lowest Knudsen numbers, $\kappa = \lambda/2R_o$, (cf. Section 3.2.4.), where $\lambda = kT/\sqrt{2}\pi p\sigma^2$, are given in Table 13 for each molecule studied. The molecular diameters, σ, are estimated as twice the sum of the lanthanide fluoride distance plus 0.222 nm for the contribution of the fluorines. Lim and Searcy have found that for Knudsen numbers less than 0.2 inconsistent pressures were measured for CeF_3.[40] Values greater than 0.2 gave results consistent with molecular flow. The pressure-temperature data points collected in this work at high temperatures are consistent with those collected at low temperatures, an indication that molecular flow conditions were satisfied throughout the temperature range of the Knudsen effusion experiments.

Table 13. Lower Limits of Knudsen Numbers

Molecule	Diameter (σ)	$\kappa = \lambda/2R_o$
YbF_3	0.628(15) nm	0.34
YbF_2	0.642(15)	3.92
SmF_3	0.650(15)	0.21
SmF_2	0.660(15)	0.21
TmF_3	0.628(15)	0.21

Temperature gradients of more than 10° were encountered in only one experiment ($SmF_{2.40}$, number 3). However, when the temperature of the Knudsen cell sample cavity was measured directly, the vapor pressure results agreed with those determined from an earlier experiment. Use of temperatures from the bottom cavity resulted in calculated pressures much higher than those from two previous experiments. In all other experiments conducted both with and without the W-Mo oven the temperatures of the top and bottom cavities were within 10°. As previously estimated,[5] the error in $\Delta H°$ at 1500 K for a uniform 10° temperature gradient is $\approx$ 1.5 %. The accuracy of the temperature measurements is believed to be $\pm$ 10°, twice the uncertainty quoted in the NBS calibration data for the optical pyrometers used in this investigation.

X-Ray fluorescence analysis of the targets has been demonstrated amply to be a convenient and accurate procedure.[5,99,138] The accuracy is dependent upon the individual calibration procedure and upon how closely it matches the experimetnal situation. Non-uniform deposition of the sample onto a target in the standardization procedure created

an uncertainty of ± 10 %. The accuracy of the vapor pressures determined in the effusion experiments is estimated as ± 15 %, an estimate which takes into account all measurement errors. This uncertainty at a pressure of 1×10^{-5} atm yields a ± 1.2 % error in ℓn p. The most common error in the X-ray fluorescence analysis, caused by non-uniform depth of sample, gives rise to low counting rates. The actual pressures are more likely to be less than the reported ones because of this error.

The appearance potentials and ion currents were not used to obtain thermochemical values because of the associated uncertainties (cf. Section 3.4.), especially when little attempt was made to calibrate the spectrometer. However, the qualitiative use of fragmentation patterns and appearance potentials within the ytterbium fluoride system to define the vapor species present depends only on the relative values of the ion intensities and appearance potentials.

The metal content of the prepared fluorides and the vaporization residues are believed to be known to within the average uncertainty of ± 0.3 %. The compositions of the congruently vaporizing phases, $SmF_{2.40}$ and $YbF_{2.40}$, are the average compositions for two and six analyses, respectively, and are believed to be known to within the average uncertainty of ± 0.04.

6.2. Evaluation of Thermochemical Data and Estimates

The agreement between the various sets of second- and third-law derived values suggests that the chosen reactions are the correct formulations. Choice of one incongruent vaporization reaction which involved $YbF_{2.40}$ yielded third-law derived values that showed a definite temperature trend and indicated that this incongruent

reaction was not the correct formulation. The vaporization reactions for $YbF_3(s,\ell)$ and $SmF_3(s,\ell)$, (5-6) and (5-21), were chosen on the basis of the appearance of the reduced pseudo-hexagonal phase in the X-ray powder diffraction patterns of the residues. If this phase is present because of interaction with the Knudsen cell, the data should be interpreted in terms of the congruent sublimation of $YbF_3(s)$ and $SmF_3(s)$. The values derived by both methods are compared in Table 14. The differences which result in the values because of very slight deviations of the lanthanide(III) fluorides from congruent vaporization are insignificant. Data from previous investigations of lanthanide(III) fluorides effected by Knudsen effusion techniques have been reduced to 298 K with the thermodynamic functions derived in this investigation and are listed in Table 15. The differences between the second- and third-law derived values of other workers[39,40,44,45] and Zmbov and Margrave[37] indicate some possibility for error in Zmbov and Margrave's measurements. The larger differences between second- and third-law derived values reported by Zmbov and Margrave and those determined in the present study (Tables 14 and 15) suggest that the values reported herein are more reliable. The discrepancy between Zmbov and Margrave's values and those presented herein is illustrated further by a comparison of observed pressures (Table 16).

The estimated uncertainties in the thermodynamic functions for the sublimation of the lanthanide(III) fluorides originates primarily with the absolute entropies of the solids and gases involved. The enthalpic functions of all the trifluorides have been determined,[7,18,29] but only for $CeF_3(s)$ is the absolute entropy known.[30,31] The

Table 14. Comparison Between the Sublimation Thermodynamics of Selected Lanthanide(III) Fluorides at 298 K Calculated for Incongruent and Congruent Reactions

Compound	ΔH°_{298} (kcal mol^{-1})[1]	ΔS°_{298} (cal $mol^{-1}K^{-1}$)[1]	ΔH°_{298} (kcal mol^{-1})[2]	ΔS°_{298}(est) (cal $mol^{-1}K^{-1}$)
YbF_3	$(113.3_0 \pm 0.4_6)$	$(58.1_0 \pm 0.3_1)$	$(108.9_9 \pm 0.4_4)$	$(55._3 \pm 2._5)$
YbF_3[3]	$(113.5_4 \pm 0.4_0)$	$(57.9_9 \pm 0.2_6)$	$(109.3_1 \pm 0.4_3)$	$(55._3 \pm 2._5)$
SmF_3	$(101._2 \pm 1._1)$	$(52.4_9 \pm 0.7_1)$	$(101.2_1 \pm 0.5_6)$	$(54._0 \pm 2._5)$
SmF_3[3]	$(103.7_0 \pm 0.9_8)$	$(53.8_3 \pm 0.6_4)$	$(104.0_3 \pm 0.5_1)$	$(54._0 \pm 2._5)$
TmF_3	$(108.2_4 \pm 0.5_0)$	$(55.3_7 \pm 0.3_2)$	$(107.4_9 \pm 0.2_8)$	$(54._9 \pm 2._5)$

[1]Second-law derived values with associated standard deviations

[2]Third-law derived values with associated standard deviations

[3]Derived on the assumption of the congruent vaporization, $LnF_3(s) = LnF_3(g)$

Table 15. Thermodynamic Values for the Congruent Sublimation of Selected Lanthanide(III) Fluorides

Compound[1]	ΔH°_{298} (kcal mol^{-1})[2]	ΔS°_{298} (cal $mol^{-1}K^{-1}$)[2]	ΔH°_{298} (kcal mol^{-1})[3]	ΔS°_{298}(est) (cal $mol^{-1}K^{-1}$)
LaF_3	(98.2)	(46.5 ± 0.7)	(107.8)	($53._6$ ± $2._5$)
LaF_3	(107.8 ± 0.4)	(54.3 ± 0.3)	(106.7)	"
CeF_3	(99.3)	(48 ± 2)	(107.3)	($54._0$ ± $2._5$)
CeF_3	(102.8 ± 0.6)	(53.3 ± 0.4)	(104.0)	"
CeF_3	(106.1 ± 0.4)	(54.0 ± 0.3)	(106.2)	"
SmF_3	(105.7)	(56 ± 2)	(102.3)	($54._0$ ± $2._5$)
TmF_3	(103.4)	(52.4 ± 0.2)	(106.8)	($54._9$ ± $2._5$)
YbF_3	(98.5)	($49._8$ ± $1._0$)	(105.9)	($55._3$ ± $2._5$)

[1]References 39,40,44,45

[2]Second-law derived values with associated standard deviations, when available

[3]Third-law derived values

Table 16. Comparison of Pressures Observed by Various Investigators for Gaseous Lanthanide Fluorides at Median Temperatures

Molecule	- ℓn p	T	p
SmF_3 [1]	11.904	1434 K	6.763×10^{-6} atm
SmF_3 [2]	11.324	1423	1.208×10^{-5}
TmF_3 [1]	14.697	1344	4.124×10^{-7}
TmF_3 [2]	14.577	1344	4.670×10^{-7}
YbF_3 [1]	15.114	1361	2.728×10^{-6}
YbF_3 [2]	13.750	1361	1.069×10^{-6}

[1] Present study
[2] Reference 44

method used in this dissertation to estimate the standard entropies, S°_{298}, of the solids (cf. Section 5.5.1.) involved the known contributions of the cations to the entropies of the various oxides and the measured entropy of $CeF_3(s)$. For the gaseous trifluoride molecules the largest source of uncertainty is the electronic contribution to the entropy. Slight variations in the molecular constants change the absolute entropy only slightly. The excellent agreement between second- and third-law derived values for the hypothetical congruent sublimation of $SmF_3(s)$, and the congruent sublimation of $TmF_3(s)$ supports the use of the electronic energy levels of the corresponding lanthanide ions to calculate the gaseous entropies. The difference between the second- and third-law derived values for the hypothetical congruent sublimation of $YbF_3(s)$ is either the result of the estimated values for the entropies or an error in experimental measurements.

The thermodynamic functions for the difluorides are subject to errors in both the enthalpic functions and the absolute entropies. No measurements of the thermodynamic functions for any of the lanthanide(II) fluorides have been carried out. Close correspondence has been observed between the thermodynamics of vaporization of the europium halides and monochalcogenides and those of the heavier alkaline earths (Ca, Sr, Ba).[5] Use of the thermodynamic functions for an alkaline earth compound is a reasonable means of estimating the thermodynamic functions of the solids. The agreement between the second- and third-law derived values from the congruent sublimations of the intermediate fluorides, $SmF_{2.40}(s)$ and $YbF_{2.40}(s)$ (Table 17) at 298 K indicates the internal consistency of the thermodynamic approximations and is support for their accuracy. The slight disagreement in the values for $SmF_{2.40}(s)$ may be due to the uncertainty in the measurements caused by the temperature gradient in high temperature vaporization experiment three. The thermodynamic values derived for the congruent sublimation of $SmF_2(s)$ and $YbF_2(s)$ are compared in Table 18 with values reported for the alkaline earths and europium(II) fluorides. The observed differences in the second- and third-law derived values for SmF_2 and YbF_2 may be ascribed to the uncertainties introduced by thermodynamic calculations with estimated thermal functions. The observed temperature gradient might play a role in the values for SmF_2, but all of the values are within the quoted uncertainties which arise from the estimates. The values in Table 18 support the predicted[5] correspondence of the sublimation thermodynamics of the lanthanide(II) fluorides to those of the alkaline earth fluorides.

Table 17. Thermodynamic Values for the Congruent Sublimation of the Intermediate Fluorides $SmF_{2.40}$ and $YbF_{2.40}$ According to the Reaction $LnF_{2.40}(s) = (0.6)\ LnF_2(g) + (0.4)\ LnF_3(g)$

Solid	ΔH°_{298} (kcal mol^{-1})[1]	ΔS°_{298} (cal $mol^{-1}K^{-1}$)[1]	ΔH°_{298} (kcal mol^{-1})[2]	ΔS°_{298}(est) (cal $mol^{-1}K^{-1}$)
$YbF_{2.40}$	$(110._7 \pm 1._0)$	$(50.8_5 \pm 0.6_4)$	$(109.8_3 \pm 0.3_6)$	$(51._1 \pm 2._5)$
$SmF_{2.40}$	$(100._2 \pm 2._1)$	$(46._2 \pm 1._3)$	$(104._4 \pm 1._0)$	$(48._9 \pm 2._5)$

[1]Second-law derived values with associated standard deviations

[2]Third-law derived values with associated standard deviations

Table 18. Thermodynamics for the Congruent Sublimation of Selected Metal(II) Fluorides

Metal[1]	ΔH°_{298} (kcal mol^{-1})[2]	ΔS°_{298} (cal $mol^{-1}K^{-1}$)[2]	ΔH°_{298} (kcal mol^{-1})[3]	ΔS°_{298}(est) (cal $mol^{-1}K^{-1}$)
Ca	$(103.2_6 \pm 0.2_3)$	$(48.3_0 \pm 0.1_5)$	(101.5_3)	$(47._1 \pm 2._5)$
Ca	(102.5)	(48.1)	(101.0)	$(47._1 \pm 2._5)$
Sr	(100)	(46.4)	-------	-----
Ba	(90)	(45.8)	-------	-----
Eu	$(100.8_4 \pm 0.9_2)$	$(48.9_2 \pm 0.6_0)$	(98.3)	$(47._3 \pm 2._0)$
Sm	$(99._5 \pm 9._3)$	$(40._9 \pm 6._8)$	$(106._5 \pm 9._1)$	$(45._5 \pm 2._5)$
Yb	$(109._0 \pm 8._4)$	$(46._0 \pm 6._1)$	$(11_1 \pm 1_0)$	$(47._0 \pm 2._5)$

[1]References 5, 17, 45 and 105

[2]Second-law derived values with associated uncertainties

[3]Third-law derived values with associated uncertainties

Brewer's estimates[24] of the boiling point, ΔH_v^o and ΔS_v^o are reported in Table 19 along with the values derived in this work. The experimental and estimated values agree reasonably well for SmF_2 and SmF_3, but differ markedly for YbF_2, YbF_3 and TmF_3. This difference indicates that the values estimated for the heavier lanthanides are in error.

6.3. Pressure-Composition Diagrams and Stability Relationships

Figures 16 to 19 are qualitative pressure-composition diagrams of the lanthanide fluoride systems (Eu, Sm, Yb and Tm). The vaporization behavior of the phases in the Eu-F system (Figure 16) has been extrapolated from those observed in the Sm- and Yb-F systems and the reported behavior of $EuF_2(s,\ell)$. The vapor pressures of $EuF_3(g)$ are those reported by Zmbov and Margrave.[44] The decomposition of $EuF_3(s)$ has been depicted because of the behavior observed for $YbF_3(s)$ and $SmF_3(s)$. The enthalpies at 298 K for reaction (6-1) calculated

$$LnF_3(s) = LnF_2(s) + F(g) \qquad (6\text{-}1)$$

from Brewer's estimates[23] and the JANAF Tables[144] are $(13_4 \pm 1_4)$, $(11_0 \pm 1_4)$ and $(11_5 \pm 1_4)$ kcal mol^{-1} for Ln = Sm, Eu and Yb, respectively. These enthalpies indicate that the decomposition of $EuF_3(s)$ is more energetically favored than that for either $YbF_3(s)$ or $SmF_3(s)$. Thus, EuF_3 is likely to vaporize in a manner analogous to the vaporization mode of SmF_3 and YbF_3 (cf. Section 5.5.2. and 5.5.5.). This vaporization mode is reflected in their pressure-composition diagrams (Figures 16 to 18). Figure 16 illustrates the reported congruent sublimation of $EuF_2(s)$ and the postulated incongruent vaporization of all other Eu-F compounds. Figures 17 and 18 depict the behavior found for $YbF_2(s)$ and $SmF_2(s)$. The vaporization behavior

Table 19. Thermodynamic Values for the Congruent Vaporization of Selected Metal Fluorides at Their Boiling Points

Fluoride	T_b (K)	ΔH^o_v (kcal mol^{-1})	ΔS^o_v (cal $mol^{-1}K^{-1}$)
SmF_2 [1]	(2715 ±5)	($79._1 \pm 9._3$)	($29._2 \pm 6._8$)
SmF_2 [2]	(2555 ± 5)	($87._5 \pm 9._1$)	($34._2 \pm 3._6$)
SmF_2 [3]	(2700)	(78)	(29)
SmF_3 [1]	(2420 ± 5)	($65._5 \pm 2._5$)	($27._1 \pm 1._9$)
SmF_3 [2]	(2420 ± 5)	($65._5 \pm 3._2$)	($27._1 \pm 1._3$)
SmF_3 [3]	(2600)	(62)	(24)
YbF_2 [1]	(3045 ± 5)	($79._6 \pm 8._4$)	($26._1 \pm 6._1$)
YbF_2 [2]	(3015 ± 5)	($8_2 \pm 1_0$)	($27._2 \pm 3._3$)
YbF_2 [3]	(2650)	(75)	(28)
YbF_3 [1]	(2490 ± 5)	($82._7 \pm 1._8$)	($33._2 \pm 1._4$)
YbF_3 [2]	(2580 ± 5)	($77._6 \pm 4._1$)	($30._1 \pm 1._6$)
YbF_3 [3]	(2500)	(60)	(24)
TmF_3 [1]	(2580 ± 5)	($72._0 \pm 1._5$)	($27._9 \pm 1._3$
TmF_3 [2]	(2600 ± 5)	($71._0 \pm 2._3$)	($27.3_1 \pm 0.8_8$)
TmF_3 [3]	(2500)	(60)	(24)

[1] Second-law derived values with estimated uncertainties

[2] Third-law derived values with estimated uncertainties

[3] Brewer's estimates; reference 23

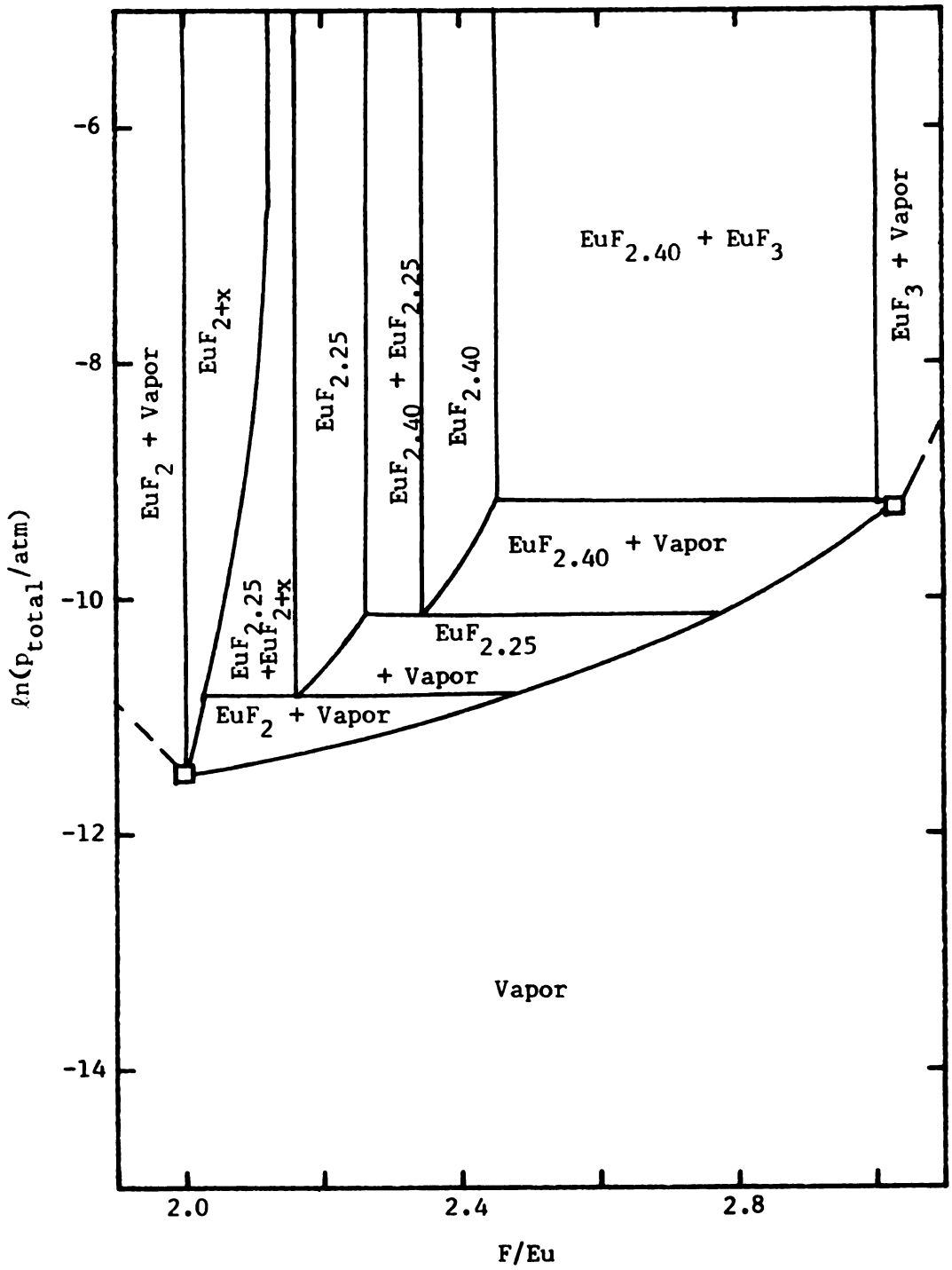

Figure 16. Qualitative Pressure-Composition Diagram for the Eu-F System (T = 1500 K)

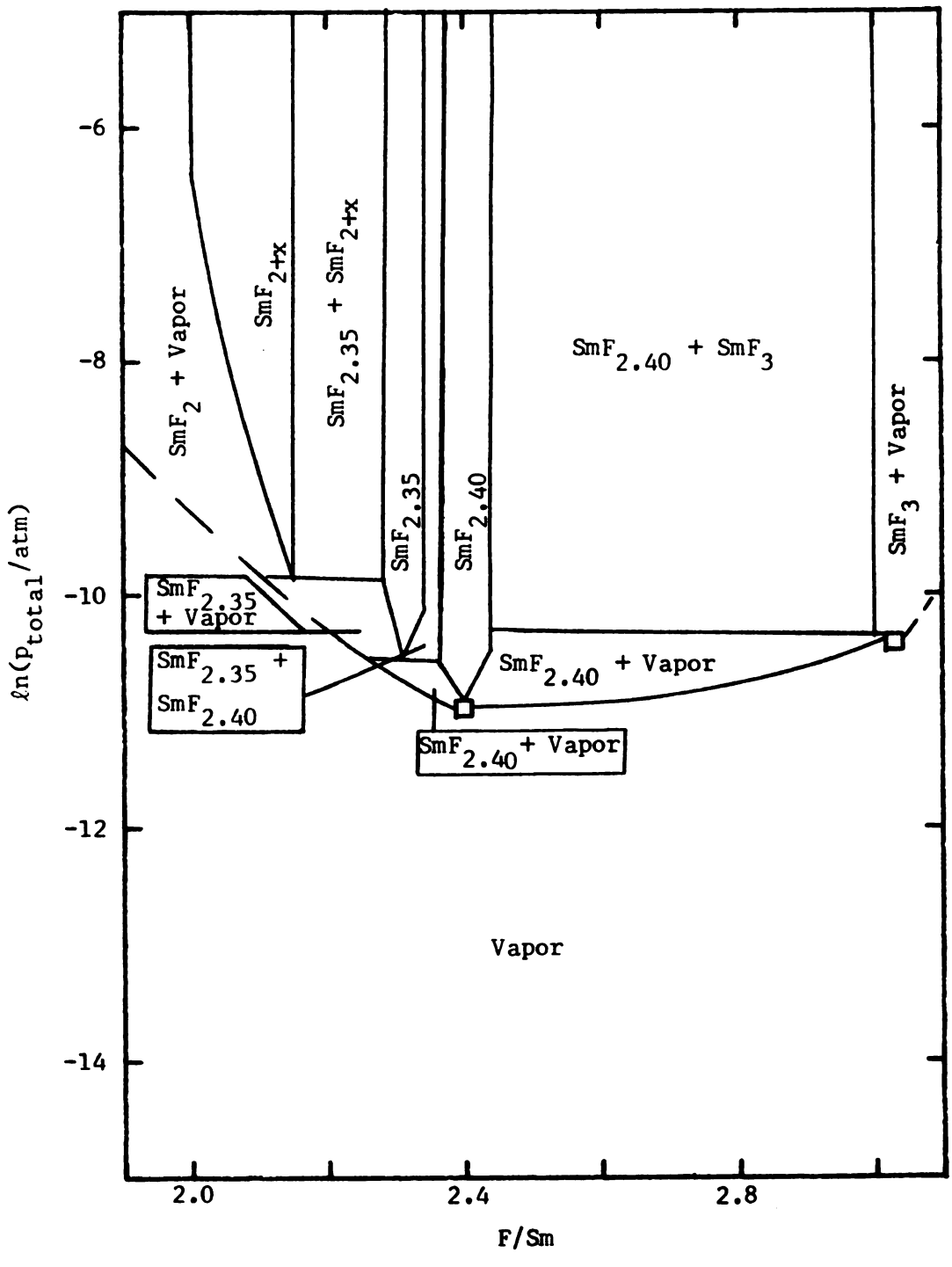

Figure 17. Qualitative Pressure-Composition Diagram for the Sm-F System (T = 1500 K)

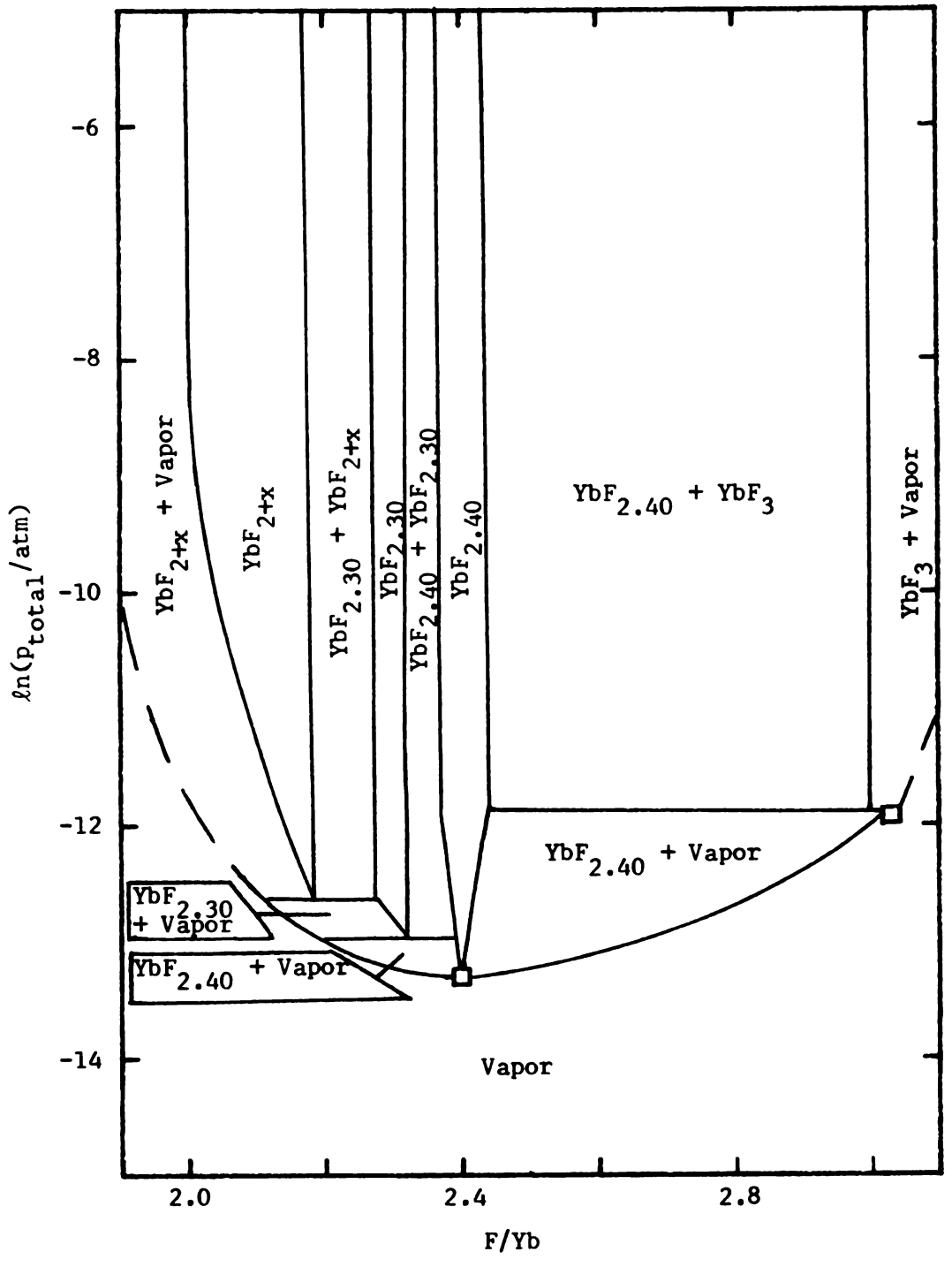

Figure 18. Qualitative Pressure-Composition Diagram for the Yb-F System (T = 1500 K)

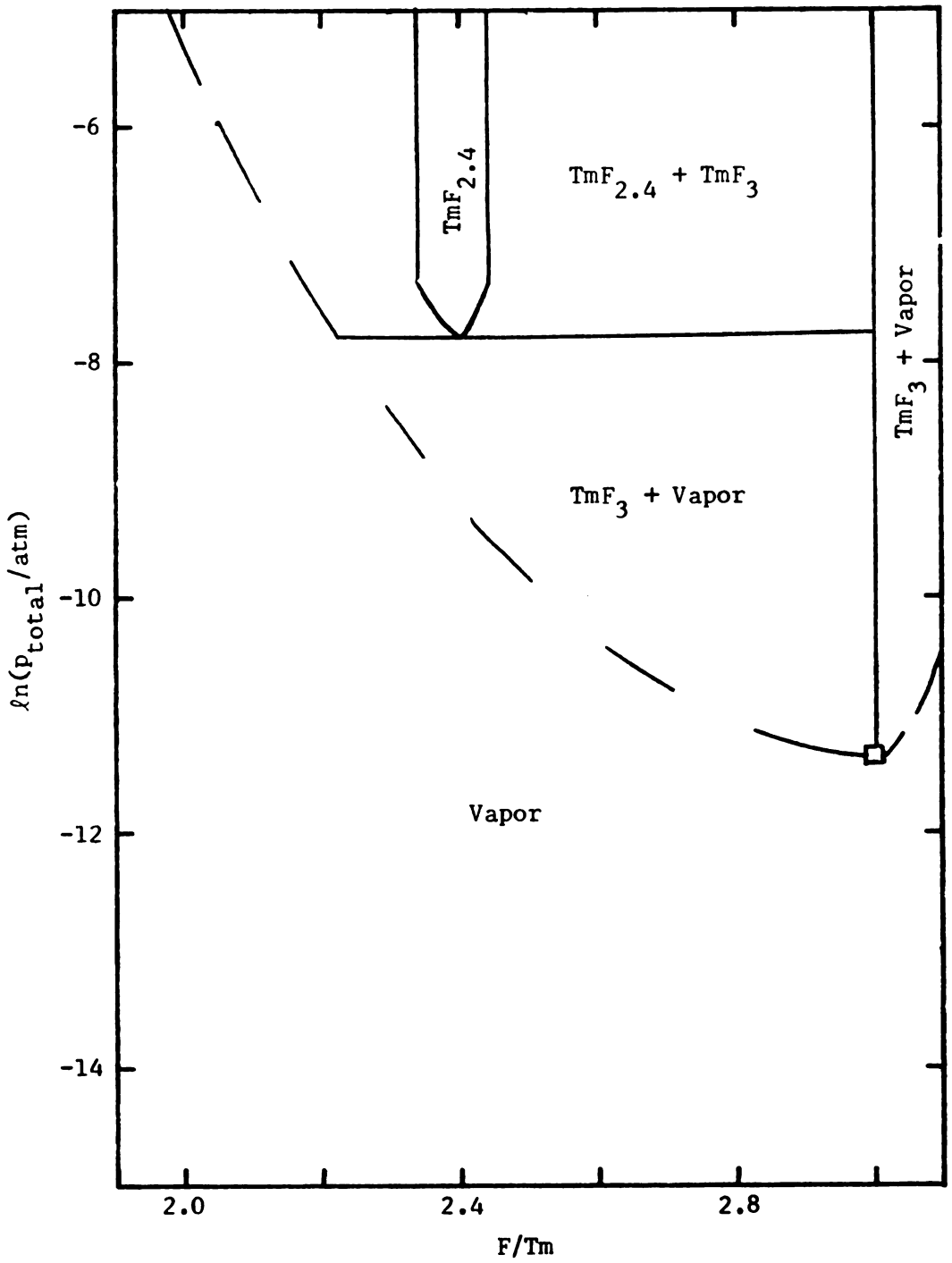

Figure 19. Qualitative Pressure-Composition Diagram for the Tm-F System (T = 1500 K)

of $TmF_3(\ell)$, illustrated in Figure 19, is congruent. The intermediate fluoride undergoes an incongruent vaporization reaction to a metal rich vapor and the solid trifluoride. A definite trend in the stability of the divalent state with respect to the trivalent state is illustrated by Figures 16 to 19. The stable, congruently vaporizing compound changes from $LnF_2(s)$ through $LnF_{2.40}(s)$ to $LnF_3(s)$ as the lanthanide element is varied from europium to samarium and ytterbium and finally thulium. Examination of the enthalpies at 298 K for reaction (6-2) helps to clarify the observed trend.

$$3\ LnF_2(s) = 2\ LnF_3(s) + Ln(g) \qquad (6\text{-}2)$$

Reaction (6-2) defines the relative stabilities of the di- and trivalent lanthanide fluorides, and the enthalpy for (6-2) is determined by the enthalpies of formation of the di- and trifluorides and the lanthanide metal gas. The chemistry of Eu and to a lesser extent Yb is influenced by the stability of the divalent state. Gschneidner[148,149] has explained this stability in terms of the ground states of the lanthanide metal and its vapor. If a thermodynamic (Born-Haber) cycle for the enthalpy of formation, ΔH_f°, of a compound, LnF_m, is depicted as follows:

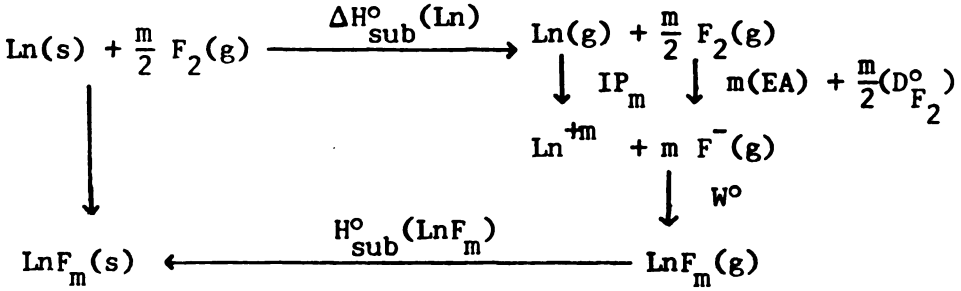

then

$$\Delta H_f^\circ = IP_m + \tfrac{m}{2}(D^\circ_{F_2}) + m\ EA + W^\circ - \Delta H^\circ_{sub}(LnF_m) + \Delta H^\circ_{sub}(Ln). \qquad (6\text{-}3)$$

The ionization potentials for the divalent lanthanides (IP_{+2}) follow

a smooth trend increasing from La to Gd (16.61 - 18.26 V) and again from Tb to Lu (17.41 - 19.22 V).[72,150] A similar trend opposite in sign would be expected for W^{o} due to the decreasing size of the ions (lanthanide contraction). The enthalpies for reaction (6-4)

$$Ln(g) + F_2(g) = LnF_2(g) \qquad (6\text{-}4)$$

would be expected to vary only slightly across the lanthanide series, and the enthalpies of sublimation, $\Delta H^{o}_{sub}(LnF_2)$, that have been measured have been found to be similar (cf. Chapter 5 and Section 6.2.). A large difference has been found[151] for the enthalpies of sublimation for the metals, $\Delta H^{o}_{f}(Ln,g)$. The variations observed have been explained by the electronic ground state of the metal and its gas.[149,151,154] The least positive $\Delta H^{o}_{f}(Ln,g)$ values are found for Yb, Eu, Sm and Tm, in that order. These elements would have more negative enthalpies of formation for their difluorides, $\Delta H^{o}_{f}(LnF_2,g)$, because of their small $\Delta H^{o}_{f}(Ln,g)$. A more complicated trend is found in the ionization energies for reaction (6-5). The

$$Ln^{+2} = Ln^{+3} + e^{-} \qquad (6\text{-}5)$$

energies of reaction (6-5) show the expected increases from La to Sm with a large increase at Eu and a decrease at Lu. This erratic behavior results in a more positive enthalpy of formation, especially for Eu^{+3} and Yb^{+3}, and somewhat more positive for Sm^{+3} and Tm^{+3}.[148,149,152] Another similar explanation of the relative stabilities of the di- and trivalent lanthanides has been reported.[153] The aqueous reduction potentials indicate the trivalent Sm, Yb and Eu aqueous ions have increasingly more positive enthalpies of formation, in that order, as determined by reduction of the trivalent to the divalent ions. The enthalpy of formation of $EuF_3(s)$ and

Eu(g) are more positive than those of YbF_3(s) and Yb(g).[23,148,149,151] Also, the enthalpy of formation of EuF_2(s) is more negative than that of YbF_2(s).[23] From these relationships the enthalpy for reaction (6-2) is more positive for Eu than for Yb. For Sm, $\Delta H_f^\circ(SmF_2,s) \approx \Delta H_f^\circ(YbF_2,s)$, $\Delta H_f^\circ(Sm,g) > \Delta H_f^\circ(Yb,g)$ and $\Delta H_f^\circ(SmF_3,s) < \Delta H_f^\circ(YbF_3,s)$; thus, ΔH_{298}° for (6-2) would be expected to be of a magnitude similar to that observed for Yb as was found in this investigation. For Tm, $\Delta H_f^\circ(TmF_2,s) \approx \Delta H_f^\circ(SmF_2,s)$, $\Delta H_f^\circ(Tm,g) > \Delta H_f^\circ(Sm,g)$ and $\Delta H_f^\circ(TmF_3,s) \approx \Delta H_f^\circ(SmF_3,s)$. No straightfoward prediction can be made about the vaporization of TmF_2(s) from the above considerations. The residue from an attempted preparation of TmF_2(s) did undergo an incongruent vaporization to give a Tm-enriched vapor and a reside enriched with TmF_3(s). None of the other lanthanide(III) fluorides has been reduced by a tantalum bomb preparation similar to the one used in this investigation (cf. Section 4.2.3.)[11] and they are expected to vaporize congruently since in these systems no reduced phase is thermodynamically stable.

Although the observed vaporization behavior of the lanthanide fluorides can be rationalized, this behavior could not have been predicted without an exact knowledge of the free energies of all the compounds involved. The dissimilarity observed for the Tm-F system when compared with the Sm- and Yb-F systems can be used cautiously to predict the behavior of the Tm-Cl system. The dichlorides, $SmCl_2$, $EuCl_2$ and $YbCl_2$, are known to sublime congruently[49,50,57] while their trichlorides decompose to yield Cl_2(g) and the dichlorides.[51] The relatively less stable divalent character of Tm might cause $TmCl_2$(s) to decompose to an intermediate chloride. If $TmCl_2$(s)

does undergo congruent sublimation one of the remaining, more trivalent lanthanide(II) chlorides might exhibit the behavior observed for the Sm- and Yb-F systems. The same tentative predictions can be made concerning the Ln-Br systems. In the Eu-Br system, $EuBr_2(s)$ is known to sublime congruently[54] and $EuBr_3(s)$ decomposes to give $EuBr_2(s)$ and $Br_2(g)$.[52] None of the other Ln-Br systems has been investigated thermodynamically. However, $YbBr_2(s)$ and $SmBr_2(s)$ will undoubtedly sublime congruently, but $TmBr_2(s)$ might decompose.

6.4. Conclusions and Suggestions for Future Investigations

This dissertaion has defined the complex and unexpected vaporization reactions for the Sm-, Tm- and Yb-F systems. Thermodynamic values have been reported for the observed reactions and values have been derived for the hypothetical congruent sublimation reactions of $SmF_2(s)$, $YbF_2(s)$, $SmF_3(s)$ and $YbF_3(s)$.

During the investigation for this dissertation, several fluorides of unknown structures were encountered. The determination of the room temperature and high temperature single crystal structures of these phases presents a challenging and possibly rewarding investigation due to their very complex superstructure and thermodynamic stability. Calorimetric measurements of the enthalpies of formation and heat capacities of the reduced fluorides [$SmF_2(s)$ and $YbF_2(s)$ or $SmF_{2.40}(s)$ and $YbF_{2.40}(s)$] would allow for a more accurate treatment of the thermodynamic data.

The complex reactions observed in the Sm- and Yb-F systems are possibly characteristic of the reactions of other reduced lanthanide halides which exhibit nonstoichiometric regions. Very few of the reduced lanthanide halides have been investigated by thermodynamic

methods. This dissertation can serve as a starting point for anyone who cares to brave the unknown vaporization reactions of other lanthanide halides. If thermodynamic investigations of other lanthanide halide systems (e.g. Tm-Cl or Tm-Br systems) are undertaken, a more complete analysis of the high temperature chemistry of these refractory halides could be attempted.

REFERENCES

REFERENCES

1. M. D. Taylor, Chem. Rev., 62, 503 (1962).

2. M. D. Taylor and C. P. Carter, J. Inorg. Nucl. Chem., 24, 387 (1962).

3. K. E. Johnson and J. R. Mackenzie, ibid., 32, 43 (1970).

4. D. Brown, " Halides of the Lanthanides and Actinides", John Wiley and Sons, Ltd., London, 1968.

5. A. V. Hariharan, Ph. D. Thesis, Michigan State University, East Lansing, Mi., 1972.

6. L. F. Drudig and J. D. Corbett, J. Amer. Chem. Soc., 83, 2462 (1971).

7. F. H. Spedding and D. C. Henderson, J. Chem. Phys., 54, 2476 (1971).

8. J. R. McCreary and R. J. Thorn, High Temp. Sci., 5, 97 (1973).

9. L. B. Asprey, F. H. Ellinger and E. Staritzky, "Rare Earth Research II", pg. 11, (K. S. Vorres, ed.), Gordon and Breach, New York, N. Y., 1964.

10. K. Lee, H. Muir and E. Catalano, J. Phys. Chem. Solids, 26, 523 (1965).

11. E. Catalano, R. G. Bedford, V. G. Silveria and H. H. Wickman, ibid., 30, 1613 (1969).

12. A. D. Kirshenbaum and J. A. Cahill, J. Inorg. Nucl. Chem., 14, 148 (1960).

13. J. J. Stezowski and H. A. Eick, Inorg. Chem., 9, 1102 (1970).

14. R. G. Bedford and E. Catalano, Proc. Eighth Rare Earth Research Conf. (T. A. Henrie and R. E. Lindstrom, ed.), pg.388, Reno, Nev., 1970.

15. T. Petzel and O. Greis, Z. anorg. allg. Chem., 396, 95 (1973).

16. B. Tanguy, J. Portier, M. Vlasse and M. Pouchard, Bull. Soc. Chim. France, 1972, 946.

17. T. Petzel and O. Greis, Z. anorg. allg. Chem., 403, 1 (1974).

18. F. H. Spedding, B. J. Beaudry, D. C. Henderson and J. Moorman, J. Chem. Phys.,60, 1578 (1974).

19. W. Klemm and W. Doll, Z. anorg. allg. Chem., 241, 233 (1939).

20. W. Doll and W. Klemm, ibid., 241, 239 (1939).

21. W. Klemm and H. Sneff, ibid., 241, 259 (1939).

22. H. Baernighausen, H. P. Beck and H. W. Grueniger, Proc. Ninth Rare Earth Research Conf. (P. E. Fields, ed.), Blacksburg, Va., 1971.

23. L. Brewer, L. A. Bromely, P. W. Gilles and N. L. Lofgren, "Chemistry and Metallurgy of Miscellaneous Materials: Thermodynamics", Paper 6 (L. L. Quill, ed.), McGraw-Hill Publications, New York, N. Y., 1950.

24. L. Brewer, ibid., Paper 7.

25. C. E. Holley, Jr., E. J. Huber, Jr. and F. B. Baker, "Progress in the Science and Technology of the Rare Earths", (L. Eyring, ed.), Vol. 3, pg. 343, Pergamon Press, Long Island City, N. Y., 1964.

26. D. A. Johnson, J. Chem. Soc. (A), 1969, 2578.

27. R. C. Feber, U. S. Atomic Energy Commission Report, LA-3764, Los Alamos, N. M., 1965.

28. G. I. Novikov and O. G. Polyachenok, Russ. Chem. Rev., 33, 342 (1964).

29. T. V. Charlu, A. K. Chaudhuri and J. L. Margrave, High Temp. Sci., 2, 1 (1970).

30. E. G. King and A. L. Christensen, U. S. Bur. Mines Bulletin, 5510 (1959).

31. E. F. Westrum, Jr. and A. F. Beale, Jr., J. Phys. Chem., 65, 353 (1961).

32. E. Rudzitis, H. M. Feder and W. N. Hubbard, J. Phys. Chem., 69, 2305 (1965).

33. A. S. Dworkin and M. A. Bredig, J. Phys. Chem., 67, 697 (1963).

34. A. S. Dworkin and M. A. Bredig, ibid., 67, 2499 (1963).

35. A. S. Dworkin and M. A. Bredig, High Temp. Sci., 3, 81, (1971).

36. C. T. Stubblefield, J. L. Rutledge and R. Phillips, J. Phys. Chem., 69, 991 (1965).

37. L. R. Morss and H. O. Haug, J. Chem. Thermodynamics, 5, 513 (1973).

38. G. R. Machlan, C. T. Stubblefield and L. Eyring, J. Amer. Chem. Soc., 77, 2975 (1955).

39. R. W. Mar and A. W. Searcy, J. Phys. Chem., 71, 888 (1967).

40. M. Lim and A. W. Searcy, ibid., 70, 1762 (1966).

41. H. B. Skinner and A. W. Searcy, ibid., 72, 3375 (1968).

42. H. B. Skinner and A. W. Searcy, ibid., 75, 108 (1971).

43. J. A. Roberts, Jr. and A. W Searcy, High Temp. Sci., 4, 411 (1972).

44. K. F. Zmbov and J. L. Margrave, Advan. Chem. Ser., 72, 267 (1968).

45. J. R. McCreary and R. J. Thorn, High Temp. Sci., 5, 365 (1973).

46. J. R. McCreary, Midwest High Temperature Conf., Northwestern University, Evanston, Ill., 1973.

47. T. Petzel and O. Greis, Z. anorg. allg. Chem., 388, 137 (1972).

48. E. R. Harrison, J. Appl. Chem., 2, 601 (1952).

49. J. L. Moriarty, J. Chem. Eng. Data, 8, 422 (1963).

50. O. G. Polyachenok and G. I. Novikov, Russ. J. Inorg. Chem., 8, 1378 (1963).

51. O. G. Polyachenok and G. I. Novikov, ibid., 9, 429 (1964).

52. J. M. Haschke, J. Chem. Thermodynamics, 5, 283 (1973).

53. A. V. Hariharan and H. A. Eick, High Temp. Sci., 4, 91 (1972).

54. J. M. Haschke and H. A. Eick, J. Phys. Chem., 74, 1806 (1970).

55. A. V. Hariharan and H. A. Eick, High Temp. Sci., 4, 379 (1972).

56. J. W. Hastie, P. Ficalora and J. L. Margrave, J. Less-Common Metals, 14, 83 (1968).

57. A. V. Hariharan, N. A. Fishel and H. A. Eick, High Temp. Sci., 4, 405 (1972).

58. W. H. Skelton and J. W. Patterson, J. Less-Common Metals, 31, 47 (1973).

59. E. W. Kaiser, W. E. Falconer and W. Klemperer, J. Chem. Phys., 56, 5392 (1972).

60. R. D. Wesley and C. W. DeKock, ibid., 55, 3866 (1971).

61. R. H. Hauge, J. W. Hastie and J. L. Margrave, J. Less-Common Metals, 23, 359 (1971).

62. M. Lesiecki, J. W. Nibler and C. W. DeKock, J. Chem. Phys., 57, 1352 (1972).

63. R. D. Wesley and C. W. DeKock, J. Phys. Chem., 77, 466 (1973).

64. J. W. Hastie, R. H. Hauge and J. L. Margrave, High Temp. Sci., 3, 56 (1971).

65. C. W. DeKock, R. D. Wesley and D. D. Radtke, High Temp. Sci., 4, 41 (1972).

66. P. A. Akishin, N. G. Rambidi and V. P. Spiridinov, "The Characterization of High-Temperature Vapors" (J. L. Margrave, ed.), pg. 300, John Wiley and Sons, Inc., New York, N. Y., 1967.

67. L. Brewer and G. M. Rosenblatt, Chem. Rev., 61, 257 (1961).

68. L. Brewer, G. R. Somayajulu and E. Brackett, Chem. Rev., 63, 111 (1963).

69. W. T. Carnall, P. R. Fields and K. Rajnak, J. Chem. Phys., 49, 4424 (1968).

70. W. T. Carnall, P. R. Fields and K. Rajnak, ibid., 49, 4450 (1968).

71. W. T. Carnall, P. R. Fields and B. G. Wybourne, ibid., 42, 3797 (1965).

72. J. Sugar and J. Reader, J. Opt. Soc. Am., 55, 1286 (1965).

73. A. Reisman, "Phase Equilibria", Academic Press, New York, N. Y., 1970.

74. J. E. Ricci, "The Phase Rule and Heterogeneous Equilibrium", Dover Publications, Inc., New York, N. Y., 1966.

75. P. W. Gilles, "The Characterization of High-Temperature Vapors", op. cit., pg. 19.

76. J. L. Margrave, "Physicochemical Measurements at High Temperatures", (J. O'M. Bockris, J. L. White and J. D. Mackenzie, eds.), Chapter 10, Butterworths Scientific Publications, London, England, 1959.

77. K. D. Carlson, "The Characterization of High-Temperature Vapors", op. cit., pg. 115.

78. H. Hertz, Ann. Physik., 17, 177 (1882).

79. M. Knudsen, ibid., 29, 179 (1909).

80. G. N. Lewis and M. Randall, "Thermodynamics", revised by K. S. Pitzer and L. Brewer, McGraw-Hill Publications, New York, N. Y., 1961.

81. J. W. Ward,R. N. R. Mulford and M. Kahn, J. Chem. Phys., 47, 1710 (1967).

82. J. W. Ward, R. N. R. Mulford and R. L. Bivins, ibid., 47, 1718 (1967).

83. R. P. Iczkowski, J. L. Margrave and S. M. Robinson, J. Phys Chem., 67, 229 (1963).

84. R. D. Freeman and J. G. Edwards, "The Characterization of High-Temperature Vapors", op. cit.,pg. 508.

85. P. Clausing, Ann. Physik., 12, 961 (1932).

86. P. Clausing, Z. Physik., 66, 471 (1930).

87. T. E. Dunham and J. P. Hirth, J. Chem. Phys., 37, 784 (1962).

88. W. L. Winterbottom and J. P. Hirth, ibid., 37, 784 (1962).

89. J. W. Ward, ibid., 47, 4030 (1967).

90. K. D. Carlson, P. W. Gilles and R. J. Thorn, ibid., 38, 2064 (1963).

91. J. W. Ward and M. V. Fraser, ibid., 49, 3743 (1968).

92. K. C. Wang and P. G. Wahlbeck, ibid., 53, 2896 (1970).

93. S. J. Wey and P. G. Wahlbeck, ibid., 57, 2932 (1972).

94. F. D. Richardson and C. B. Alcock, "Physicochemical Measurements at High Temperatures", op. cit., Chapter 6.

95. E. Storms, High Temp. Sci., 1, 456 (1969).

96. D. E. Work and H. A. Eick, J. Phys. Chem., 74, 3130 (1970).

97. K. Motzfeldt, ibid., 59, 139 (1955).

98. R. C. Paule and J. L. Margrave, "The Characterization of High-Temperature Vapors", op. cit., pg. 130.

99. D. E. Work, Ph. D. Thesis, Michigan State University, East Lansing, Mi., 1972.

100. G. M. Pound, J. Phys. Chem. Ref. Data, 1, 135 (1972).

101. M. Knudsen, Ann. Physik., 28, 999 (1909).

102. R. J. Ackermann, P. W. Gilles and R. J. Thorn, J. Chem. Phys., 25, 1089 (1956).

103. P. G. Wahlbeck and T. E. Phipps, ibid., 49, 1603 (1968).

104. K. C. Wang and P. G. Wahlbeck, ibid., 49, 1617 (1968).

105. D. A. Schulz and A. W. Searcy, J. Phys. Chem., 67, 103 (1963).

106. J. L. Margrave, "Physicochemical Measurements at High Temperatures", op. cit., Chapter 2.

107. T. B. Douglas, J. Res. N. B. S., 73A, 451 (1969).

108. R. T. Grimely, "The Characterization of High-Temperature Vapors", op. cit., pg. 195.

109. F. E. Stafford, High Temp. High Pres., 3, 213 (1971).

110. D. C. Damoth, "Advances in Analytical Chemistry and Instrumentation" (C. N. Reilley, ed.), Vol. 4, pg. 371, John Wiley and Sons, Inc., New York, N. Y., 1965.

111. R. W. Kiser, J. G. Dillard and D. L. Dugger, Advan. Chem. Ser., 72, 153 (1968).

112. G. W. Otvos and D. P. Stevenson, J. Amer. Chem. Soc., 78, 546 (1956).

113. J. B. Mann, J. Chem. Phys., 46, 1646 (1967).

114. J. E. Collin, "Mass Spectrometry" (R. I. Reed, ed.), pg. 183, Academic Press, New York, N. Y., 1965.

115. R. Jenkins and J. L. DeVries, "Practical X-Ray Spectrometry", Springer-Verlag, Inc., New York, N. Y., 1967.

116. L. S. Birks, "X-Ray Spectrochemical Analysis", Second Edition, Interscience Publishers, New York, N. Y., 1969.

117. H. Neff, Arch. Eisenheuttenw., 34, 903 (1963).

118. R. J. Ackermann and E. G. Rauh, J. Chem. Thermodynamics, 3, 445 (1971).

119. P. A. Rock, "Chemical Thermodynamics", Chapter 7, Collier-Macmillan Ltd., 1969.

120. W. S. Horton, J. Res. N. B. S., 70A, 533 (1966).

121. D. Cubicciotti, J. Chem. Phys., 70, 2410 (1966).

122. R. J. Thorn, High Temp. Sci., 3, 197 (1971).

123. O. Kubaschewski and E. Ll. Evans, "Metallurgical Thermochemistry", Pergamon Press, New York, N. Y., 1958.

124. D. R. Stull and H. Prophet, "The Characterization of High-Temperature Vapors", op. cit., pg. 359.

125. W. M. Latimer, J. Amer. Chem. Soc., 73, 1480 (1951).

126. F. Gronvold and E. F. Westrum, Jr., Inorg. Chem., 1, 36 (1962).

127. E. F. Westrum, Jr., Advan. Chem. Ser., 71, 25 (1967).

128. T. L. Hill, "An Introduction to Statistical Thermodynamics", Addison-Wesley Publishing Co., Inc., Reading, Mass., 1960.

129. L. G. Parratt, "Probability and Experimental Errors in Science", John Wiley and Sons, Inc., New York, N. Y., 1961.

130. I. M. Kolthoff and E. B. Sandell, "Textbook of Quantitative Inorganic Analysis", Third Edition, The Macmillan Co., New York, N. Y., 1952.

131. J. J. Stezowski, Ph. D. Thesis, Michigan State University, East Lansing, Mi., 1968.

132. J. H. Fang and F. D. Bloss, "X-Ray Diffraction Tables", Southern Illinois University Press, Carbondale, Ill., 1966.

133. R. L. Seiver, Ph. D. Thesis, Michigan State University, East Lansing, Mi., 1971.

134. J. M. Haschke and H. A. Eick, J. Amer. Chem. Soc., 92, 4550 (1970).

135. J. D. H. Donnay, Ed., "Crystal Data Determinative Tables", Second Edition, Amer. Cryst. Assoc., Washington, D. C., 1963.

136. P. A. Pilato, Ph. D. Thesis, Michigan State University, East Lansing, Mi., 1963.

137. R. A. Kent, Ph. D. Thesis, Michigan State University, East Lansing, Mi., 1963.

138. J. M. Haschke, Ph. D. Thesis, Michigan State University, East Lansing, Mi., 1969.

139. K. Niihara and S. Yajima, Bull. Chem. Soc. Jap., 44, 643 (1971).

140. K. F. Zmbov and J. L. Margrave, J. Phys. Chem., 70, 3014 (1966).

141. A. C. Parr and F. A. Elder, J. Chem. Phys., 49, 2665 (1968).

142. S. L. Bacon, M. S. Thesis, Michigan State University, East Lansing, Mi., 1971.

143. G. D. Blue, J. W. Green, R. G. Bautista and J. L. Margrave, J. Phys. Chem., 67, 877 (1963).

144. "JANAF Thermochemical Tables" (D. R. Stull, ed.), Dow Chemical Co., Midland, Mi., 1965.

145. C. E. Wicks and F. E. Block "Thermodynamic Properties of 65 Elements-Their Oxides, Halides, Carbides and Nitrides", Bureau of Mines Bulletin 605, U. S. Government Printing Office, Washington, D. C., 1963.

146. R. Hultgren, R. L. Orr, P. D. Anderson and K. K. Kelley, "Selected Values of the Thermodynamic Properties of Metals and Alloys", John Wiley and Sons, Inc., New York, N. Y., 1963.

147. A. S. Dworkin and M. A. Bredig, J. Phys. Chem., 75, 2340 (1971).

148. K. A. Gschneidner, Jr., J. Less-Common Metals, 17, 13 (1969).

149. K. A. Gschneidner, Jr., "Analysis and Applications of Rare Earth Materials", (O. B. Michelsen, ed.) pgs. 1, 9, Foto-Trykh, Oslo, Norway, 1973.

150. G. R. Hertel, J. Chem. Phys., 48, 2053 (1968).

151. C. E. Habermann and A. H. Daane, J. Chem. Phys., 41, 2818 (1964).

152. J. Sugar and J. Reader, J. Chem. Phys., 59, 2083 (1973).

153. D. A. Johnson, J. Chem. Soc. (A), 1969, 1528.

154. D. A. Johnson, ibid., 1969, 1525.

155. J. D. Corbett, Rev. Chim. Miner., 10, 239 (1973).

APPENDICES

APPENDIX 1

X-RAY POWDER DIFFRACTION DATA FOR THE REDUCED LANTHANIDE FLUORIDES

Appendix 1.1. X-Ray Powder Diffraction Data for Cubic[1] $YbF_{2.01}$

I	d-spacing	h k ℓ	I	d-spacing	h k ℓ
10	0.3237 nm	1 1 1	5	0.1400 nm	4 0 0
7	0.2807	2 0 0	6	0.1285	3 3 1
8	0.1980	2 2 0	5	0.1252	4 2 0
8	0.1688	3 1 1	6	0.1143	4 2 2
6	0.1617	2 2 2			

[1] a = 0.5600(1) nm

Appendix 1.2. X-Ray Powder Diffraction Data for Cubic[1] $YbF_{2.19}$

I	d-spacing	h k ℓ	I	d-spacing	h k ℓ
10	0.3225 nm	1 1 1	5	0.1396 nm	4 0 0
7	0.2797	2 0 0	6	0.1281	3 3 1
8	0.1973	2 2 0	5	0.1249	4 2 0
8	0.1683	3 1 1	6	0.1141	4 2 2
6	0.1612	2 2 2			

[1] a = 0.5585(1) nm

Appendix 1.3. X-Ray Powder Diffraction Data for Pseudo-Tetragonal[1,2] $YbF_{2.29}$

I	d-spacing	h k ℓ	I	d-spacing	h k ℓ
2	0.4958 nm		3	0.2072 nm	
2	0.4701		3	0.2042	
10	0.3196	1 0 1	3	0.1989	
2	0.3124		8	0.1968	1 1 2
2	0.3103		2	0.1852	
2	0.3030		2	0.1724	
6	0.2787	0 0 2	2	0.1709	
7	0.2772	1 1 0	7	0.1682	1 0 3
2	0.2356		8	0.1675	2 1 1
3	0.2313		6	0.1607	2 0 2
2	0.2230		3	0.1566	
3	0.2111		4	0.1397	0 0 4

[1] a = 0.3925(2); C = 0.5587(2) nm

[2] Superstructure reflections are not indexed

Appendix 1.4. X-Ray Powder Diffraction Data for Pseudo-Hexagonal[1,2] $YbF_{2.41}$

I	d-spacing	h k ℓ	I	d-spacing	h k ℓ
2	0.4503 nm		2	0.1791 nm	
2	0.3361	1 0 1	5	0.1693	1 0 10
2	0.3298		8	0.1679	1 1 6
7	0.3262	0 0 6	5	0.1675	2 0 2
10	0.3215	1 0 2	3	0.1626	
3	0.3123		5	0.1610	0 0 12
2	0.3006		4	0.1607	2 0 4
2	0.2960		2	0.1575	
8	0.2790	1 0 4	2	0.1498	
3	0.2415		2	0.1474	
2	0.2236		5	0.1393	2 0 8
2	0.2223		3	0.1288	1 0 14
2	0.2208		6	0.1278	2 0 10
2	0.2195		4	0.1272	2 1 2
2	0.2158	0 0 9	3	0.1252	
3	0.2077		5	0.1246	1 1 12
2	0.2043		3	0.1241	2 1 4
3	0.2019		2	0.1148	
7	0.1984	1 0 8	6	0.1139	1 0 16
3	0.1909		4	0.1136	1 2 8
2	0.1881				

[1] a = 0.3926(4); c = 1.940(2) nm

[2] Superstructure reflections are not indexed

Appendix 1.5. X-Ray Powder Diffraction Data for Cubic[1] $SmF_{2.00}$

I	d-spacing	h k ℓ	I	d-spacing	h k ℓ
10	0.3398 nm	1 1 1	4	0.1467 nm	4 0 0
6	0.2940	2 0 0	4	0.1347	3 3 1
8	0.2077	2 2 0	4	0.1313	4 2 0
7	0.1771	3 1 1	4	0.1199	4 2 2
5	0.1693	2 2 2			

[1] a = 0.5872(1) nm

Appendix 1.6. X-Ray Powder Diffraction Data for Pseudo-Hexagonal[1] $SmF_{2.44}$

I	d-spacing	h k ℓ	I	d-spacing	h k ℓ
6	0.3372 nm	0 0 6	6	0.1745 nm	2 0 2
10	0.3344	0 1 2	3	0.1684	0 0 12
9	0.2900	1 0 4	4	0.1669	2 0 4
7	0.2056	0 1 8	3	0.1449	2 0 8
7	0.2043	1 1 0	3	0.1335	0 1 14
4	0.1766	1 0 10	3	0.1326	2 1 2

[1] a = 0.4086(1); c = 2.0189(7) nm

Appendix 1.7. X-Ray Powder Diffraction Data for a Reduced Thulium Fluoride[1]

I	d-spacing	h k ℓ	I	d-spacing	h k ℓ
2	0.3747 nm	(0 1 1)[2]	4	0.1920 nm	(1 3 1)[2]
3	0.3641	(1 0 1)[2]	3	0.1890	(3 0 1)[2]
3	0.3428	(0 2 0)[2]	3	0.1837	(2 3 0)[2]
10	0.3241	1 0 2	3	0.1818	(3 1 1)[2]
4	0.3211	(1 1 1)[2]	3	0.1940	(2 1 2)[2]
4	0.3157	(1 1 1)[3]	2	0.1704	(0 4 0)[2]
4	0.2856	(2 1 0)[2]	8	0.1684	2 0 2
8	0.2804	0 0 6	4	0.1652	(3 2 1)[2]
4	0.2757	(2 0 0)[3]	3	0.1613	2 0 4
3	0.2692	(- - -)[4]	2	0.1541	(1 4 1)[2]
4	0.2485	(1 2 1)[2]	3	0.1397	2 0 8
3	0.2214	(0 0 2)[2]	4	0.1283	2 1 2
2	0.2155	0 0 9	2	0.1264	(- - -)[4]
2	0.2072	(- - -)[4]	4	0.1250	2 1 4
3	0.2047	(2 2 1)[2]	4	0.1141	1 0 16
8	0.1977	1 0 8			

[1] Pseudo-hexagonal: a = 0.3953(1); c = 1.937(1) nm

[2] Reflections for TmF_3, references 4, 17 and 18

[3] Reflections for $Tm_4O_3F_6$, reference 139

[4] Superstructure reflections are not indexed

APPENDIX 2

KNUDSEN EFFUSION DATA IN CHRONOLOGICAL ORDER

Appendix 2.1. Data for Yb(g) from YbF_{2+x} ($0.00 \leq x < 0.40$) Confined in Mo

T	- ℓn p
1293 K	12.753
1323	12.128
1352	11.779
1304	13.000

Appendix 2.2. Data for the Rate of Deposition of Yb(g) *vs.* Time (T = 1457 K)

Rate	Time
1.89 nm/min	354 min
1.46	373
1.31	393
1.23	421
1.09	447

Appendix 2.3. Data from $YbF_{2.40}$ Effusion Experiments

Exp	T (K)	- ℓn K	Σ' (cal $mol^{-1}K^{-1}$)	ΔH°_{298}(3rd law) (kcal mol^{-1})
1	1466	13.987	23.20	108.91
	1523	12.736	20.39	108.92
a = 7.90 x 10^{-3} cm^2	1575	11.736	18.13	109.04
	1548	12.385	19.56	109.43
Mo cell	1592	11.572	17.71	109.54
2	1580	11.461	17.32	108.76
	1666	10.186	14.29	109.67
a = 1.14 x	1728	9.544	12.61	110.81
10^{-3} cm^2	1701	9.431	12.57	109.03
	1668	10.456	14.82	110.62
Mo cell	1633	10.599	15.30	109.09
	1601	11.023	16.33	108.62
	1572	11.544	17.53	108.52
	1640	10.349	14.76	108.70
	1685	9.666	13.14	108.99
3	1618	11.120	16.67	109.31
	1531	12.471	19.82	108.23
a = 7.59 x	1626	10.898	16.19	109.09
10^{-3} cm^2	1571	11.912	18.50	108.97
	1601	12.682	20.30	108.21
Mo cell	1673	10.157	14.48	109.35
	1556	12.073	18.90	108.57
	1587	11.575	17.74	108.93
	1653	10.451	15.17	109.17
4	1532	13.088	21.04	110.55
	1585	11.963	18.52	110.37
a = 5.01 x	1504	13.631	22.28	110.35
10^{-3} cm^2	1608	11.576	17.63	110.56
graphite cell	1609	11.445	17.36	110.20
5	1569	12.250	19.18	108.97
	1606	11.695	17.88	109.47
a = 1.12 x	1660	10.776	15.58	109.66
10^{-3} cm^2	1688	10.281	14.64	109.57
	1710	9.911	13.76	109.51
Mo cell	1720	9.888	13.65	109.95
	1687	10.459	15.00	110.11
	1641	11.129	16.57	109.73
	1617	11.542	17.52	109.64
	1583	12.035	18.68	109.18

Appendix 2.3. (cont'd.)

Exp	T (K)	- ℓn K	Σ' (cal $mol^{-1}K^{-1}$)	ΔH°_{298}(3rd Law) (kcal mol^{-1})
6	1566	12.452	19.57	109.41
	1608	11.769	18.02	109.83
a = 1.12 x	1676	10.694	15.53	110.29
10^{-3} cm^2	1696	10.241	14.51	109.89
	1740	9.669	13.09	110.26
Mo cell	1724	9.882	13.62	110.14
	1669	10.789	15.76	110.22
	1655	10.976	16.20	110.02
	1633	11.367	17.09	110.01
	1606	11.697	17.88	109.48
7	1652	10.687	15.64	108.89
	1669	10.497	15.19	109.23
a = 1.12 x	1728	9.722	13.27	109.82
10^{-3} cm^2	1742	9.587	12.91	110.09
	1677	10.605	15.35	110.05
Mo cell	1648	11.252	16.78	110.52
	1585	12.107	18.81	109.50
	1616	11.631	17.70	109.88
	1646	11.117	16.52	109.06
8	1599	12.013	18.55	110.07
	1549	12.843	20.46	109.62
a = 7.28 x	1509	13.746	22.48	109.80
10^{-3} cm^2	1517	13.651	22.24	110.06
	1545	13.033	20.86	109.95
Mo cell	1499	14.046	23.13	110.06
	1487	14.366	23.83	110.23
	1469	14.723	24.65	110.07
	1531	13.573	22.01	110.68
	1566	12.664	20.02	110.08
9	1566	12.464	19.62	109.46
	1594	11.931	18.41	109.48
a = 7.28 x	1614	11.601	17.65	109.63
10^{-3} cm^2	1640	11.125	16.57	109.64
Mo cell	1577	12.248	19.13	109.46

Appendix 2.3. (cont'd.)

Exp	T (K)	- ℓn K	Σ' (cal $mol^{-1}K^{-1}$)	ΔH°_{298}(3rd law) (kcal mol^{-1})
10	1564	12.579	19.86	109.70
	1530	13.160	21.60	109.97
a = 7.28 x	1464	14.892	25.01	110.21
10^{-3} cm^2	1517	13.437	21.82	109.41
	1496	14.072	23.20	109.93
Mo cell	1538	13.222	21.28	110.05
	1579	12.349	19.32	109.91
	1488	14.257	23.61	109.97
	1452	15.155	25.60	110.21
	1575	12.518	19.68	110.19

Appendix 2.4. Data from YbF_3 Effusion Experiments

Exp	T (K)	- ℓn p	- ℓn K	Σ' (cal $mol^{-1}K^{-1}$)	ΔH°_{298}(3rd law) (kcal mol^{-1})
11	1487	12.168	12.067	18.56	107.18
	1539	11.057	10.977	15.46	106.87
a = 8.33 x	1620	9.586	9.536	12.36	106.73
10^{-3} cm^2	1604	9.932	9.874	13.17	106.97
	1573	10.443	10.375	14.43	106.88
Mo cell	1546	10.922	10.845	15.60	106.86
	1519	11.496	11.407	16.82	106.84
	1480	12.280	12.176	18.84	107.09
	1539	11.085	11.004	15.98	106.95
	1568	10.561	10.491	14.70	106.97
12	1435	13.357	13.230	21.37	107.46
	1451	13.007	12.888	20.53	107.45
a = 8.33 x	1480	12.319	12.214	18.92	107.21
10^{-3} cm^2	1509	11.732	11.639	17.51	107.18
	1569	10.639	10.567	14.85	107.26
Mo cell	1529	11.372	11.286	16.63	107.25
	1495	12.060	11.960	18.28	107.33
	1461	12.799	12.684	20.03	107.46
	1429	13.491	13.362	21.67	107.44
	1406	13.977	13.840	22.76	107.25
13	1419	13.676	13.543	22.09	107.29
	1369	15.125	14.963	25.24	107.82
a = 8.33 x	1362	15.185	15.022	25.45	107.55
10^{-3} cm^2	1350	15.420	15.253	25.95	107.28
	1342	15.650	15.478	26.45	107.32
Mo cell	1416	13.743	13.609	22.24	107.28
	1380	14.574	14.424	24.10	107.11
	1405	14.049	13.909	22.91	107.38
	1359	15.208	15.044	25.47	107.35
	1387	14.472	14.323	23.85	107.31
14	1511	11.615	11.524	17.26	106.95
	1616	9.678	9.625	12.58	106.81
a = 1.11 x	1621	9.569	9.519	12.32	106.73
10^{-3} cm^2	1662	8.929	8.891	10.74	106.80
	1701	8.391	8.364	9.39	107.00
Mo cell	1726	7.956	7.938	8.35	106.78
	1763	7.423	7.416	7.04	106.76
	1713	8.214	8.191	8.95	107.01
	1683	8.649	8.617	10.03	106.95
	1632	9.413	9.365	11.93	106.80

Appendix 2.4. (cont'd.)

Exp	T (K)	- ℓn p	- ℓn K	Σ' (cal $mol^{-1}K^{-1}$)	ΔH°_{298}(3rd law) (kcal mol^{-1})
15	1543	10.844	10.768	15.47	106.45
	1647	8.998	8.960	11.00	106.26
a = 1.11 x	1707	8.082	8.062	8.74	106.28
10^{-3} cm^2	1743	7.532	7.522	7.40	106.17
	1786	6.869	6.873	5.79	105.93
Mo cell	1794	6.787	6.793	5.57	106.01
	1738	7.649	7.638	7.66	106.33
	1699	8.279	8.254	9.19	106.53
	1668	8.721	8.688	10.29	106.43
	1610	9.699	9.646	12.67	106.56
16	1584	10.408	[1]	[1]	[1]
	1640	9.372			
a = 1.10 x	1694	8.682			
10^{-3} cm^2	1704	8.406			
	1676	8.945			
graphite	1620	9.796			
cell	1548	11.088			
	1611	9.925			
	1699	8.514			
	1660	9.135			

[1] To retain consistency and reproducibility the pressure-temperature data from the graphite cell were only compared to the pressure-temperature data from the Mo cells and not used to derive thermodynamic values

Appendix 2.5. Data for Sm(g) from SmF_{2+x} ($0.00 \leq x < 0.40$) Confined in Mo

T	- ℓn p
1113 K	11.161
1219	11.188
1325	11.290
1397	10.983
1451	11.086

Appendix 2.6. Data for the Rate of Deposition of Sm(g) vs. Time (T = 1232 K)

Rate	Time
8.62 nm/min	138 min
7.71	150
6.22	161
6.02	172
4.53	187
3.97	205
3.70	214
3.37	222
3.25	229
3.10	235
2.85	245
2.67	255
2.63	271

Appendix 2.7. Data from $SmF_{2.40}$ Effusion Experiments

Exp	T (K)	- ℓn K	Σ' (cal $mol^{-1}K^{-1}$)	ΔH°_{298}(3rd law) (kcal mol^{-1})
1	1508	11.074	19.46	103.08
	1511	11.080	19.47	103.30
a = 4.92 x 10^{-3} cm^2	1498	11.305	19.95	103.15
	1556	10.473	18.15	104.33
Mo cell	1488	11.682	20.72	103.58
	1543	10.769	18.77	104.44
2	1461	12.850	23.11	105.24
	1526	11.591	20.44	105.86
a = 4.69 x 10^{-3} cm^2	1592	10.397	17.86	106.28
	1511	11.732	20.76	105.25
	1455	12.795	23.02	104.66
Mo cell	1523	11.443	20.16	105.21
	1424	13.409	24.31	104.24
	1474	12.268	21.92	104.40
	1533	11.227	19.70	105.17
	1369	14.858	27.32	104.38
	1418	13.479	24.46	104.07
	1458	12.634	22.69	104.40
	1484	12.077	21.52	104.54
	1524	11.365	20.00	105.04
	1558	10.677	18.55	105.09
	1522	11.399	20.07	105.01
	1476	12.150	21.68	104.20
	1423	13.251	24.00	103.72
	1410	13.706	24.94	104.12
	1441	12.918	23.39	104.08
	1479	12.166	21.71	104.46
	1518	11.459	20.20	104.91
	1539	11.043	19.32	105.01
	1462	12.467	22.35	104.21
3	1630	8.487	13.89	102.36
	1557	9.684	16.58	101.98
a = 1.42 x 10^{-3} cm^2	1507	10.642	18.61	101.78
	1662	8.334	13.44	103.61
	1716	7.571	11.64	103.92
Mo cell	1570	9.672	16.52	102.74
	1506	10.763	18.85	102.08
	1596	9.452	15.96	103.56
	1675	8.390	13.50	104.51
	1556	10.390	17.98	104.09
	1601	9.628	16.29	104.37
	1635	9.097	15.08	104.65

Appendix 2.7. (cont'd.)

Exp	T (K)	- ℓn K	Σ' (cal $mol^{-1}K^{-1}$)	ΔH°_{298}(3rd law) (kcal mol^{-1})
	1682	8.393	13.47	104.94
	1724	7.809	12.07	105.12
	1758	7.358	10.98	105.26
	1791	6.800	9.87	105.26
	1789	6.884	9.85	105.15
	1766	7.230	10.66	105.30
	1731	7.822	12.05	105.55
	1705	8.274	13.10	105.75
	1659	9.025	14.83	105.76
	1608	9.785	16.57	105.31

Appendix 2.8. Data from SmF_3 Effusion Experiments

Exp	T (K)	- ℓn p	- ℓn K	Σ' (cal $mol^{-1}K^{-1}$)	ΔH°_{298}(3rd law) (kcal mol^{-1})
1	1694	7.299	7.293	7.75	102.05
	1746	6.556	6.564	5.87	101.86
a = 1.11 x	1560	9.608	9.555	13.40	102.78
10^{-3} cm^2	1638	8.227	8.202	10.05	102.43
	1684	7.563	7.551	8.35	102.46
Mo cell	1712	7.118	7.115	7.25	102.24
	1606	8.841	8.804	11.54	102.81
	1650	8.106	8.084	9.71	102.59
	1674	7.696	7.682	8.70	102.41
2	1389	13.108	12.986	20.94	101.99
	1429	11.959	11.859	18.54	101.47
a = 8.18 x	1461	11.230	11.145	16.99	101.51
10^{-3} cm^2	1495	10.484	10.413	15.39	101.49
	1452	11.441	11.352	17.43	101.54
	1417	12.290	12.184	19.23	101.64
	1404	12.816	12.699	20.31	102.18
	1449	11.601	11.509	17.76	101.79
	1380	13.306	13.180	21.37	101.88
	1353	13.964	13.824	22.75	101.83
	1423	12.302	12.196	19.24	102.01
	1466	11.258	11.172	17.02	101.86
	1397	12.882	12.764	20.47	101.94
	1359	13.911	13.772	22.63	102.05
	1412	12.572	12.460	19.80	102.07
	1453	11.542	11.451	17.63	101.89
	1488	10.778	10.702	16.00	101.86
	1439	11.826	11.729	19.12	103.06
	1485	10.838	10.761	16.12	101.90
3	1419	11.874	11.776	18.12	100.20
	1497	10.256	10.190	14.94	100.92
a = 1.16 x	1468	10.950	10.870	16.41	101.11
10^{-3} cm^2	1518	9.881	9.823	14.12	101.09
	1417	12.067	11.965	18.80	101.02
	1485	10.535	10.464	15.53	101.02
	1553	9.228	9.183	12.70	101.19
	1571	9.009	8.968	12.19	101.57
	1613	8.272	8.246	10.37	101.38
	1659	7.604	7.592	8.66	101.40
	1701	6.954	6.954	7.02	101.20
	1742	6.277	6.291	5.36	100.75
	1721	6.619	6.627	6.20	100.98

Appendix 2.8. (cont'd.)

Exp	T (K)	- ℓn p	- ℓn K	Σ' (cal $mol^{-1}K^{-1}$)	ΔH^{o}_{298}(3rd law) (kcal mol^{-1})
	1693	7.097	7.095	7.37	101.34
	1649	7.777	7.761	9.08	101.49
	1602	8.484	8.454	10.88	101.51
	1564	9.121	9.078	12.44	101.54
	1525	9.838	9.781	14.00	101.41
	1592	8.714	8.679	11.42	101.71
	1638	8.015	7.994	9.64	101.75
	1639	8.001	7.980	9.60	101.75

Appendix 2.9. Data from TmF_3 Effusion Experiments

Exp	T (K)	- ℓn p	Σ' (cal $mol^{-1}K^{-1}$)	ΔH°_{298}(3rd law) (kcal mol^{-1})
1	1444	12.346	19.43	107.28
	1418	12.955	20.85	107.43
a = 7.06 x	1474	11.841	18.12	107.61
10^{-3} cm^2	1521	10.989	15.97	107.75
	1557	10.291	14.24	107.62
Mo cell	1586	9.828	13.05	107.77
	1534	10.697	15.26	107.60
	1479	11.721	17.84	107.53
	1488	11.546	17.40	107.53
	1458	12.151	18.90	107.56
	1398	13.425	21.93	107.42
	1349	14.540	24.50	107.13
	1376	14.168	23.56	107.99
	1441	12.532	19.83	107.66
	1506	11.304	16.74	107.87
	1540	10.620	15.05	107.71
	1523	11.005	15.98	107.95
	1446	12.412	19.54	107.63
	1419	13.032	20.97	107.71
	1424	12.864	20.62	107.58
	1466	12.054	18.63	107.74
	1388	13.688	22.52	107.45
	1426	12.859	20.61	107.64
	1348	14.686	24.80	107.45
2	1474	11.440	17.32	106.44
	1537	10.527	14.90	107.25
a = 1.18 x	1586	9.705	12.80	107.38
10^{-3} cm^2	1538	10.548	14.93	107.38
	1584	9.774	12.96	107.49
Mo cell	1634	8.982	10.93	107.54
	1699	7.966	8.35	107.42
	1732	7.459	7.06	107.30
	1809	6.342	4.21	106.90
	1765	6.996	5.86	107.25
	1733	7.476	7.08	107.40
	1708	7.860	8.06	107.50
	1674	8.388	9.40	107.62
	1638	8.959	10.85	107.68
	1599	9.595	12.47	107.79
	1647	8.835	10.52	107.76
	1675	8.362	9.34	107.58
	1697	7.981	8.39	107.42

Appendix 2.9. (cont'd.)

Exp	T (K)	- ℓn p	Σ' (cal $mol^{-1}K^{-1}$)	ΔH^{o}_{298}(3rd law) (kcal mol^{-1})
	1751	7.214	6.41	107.35
	1787	6.649	5.00	107.00
	1747	7.203	6.43	107.11
	1718	7.672	7.60	107.35

APPENDIX 3

DERIVED THERMODYNAMIC FUNCTIONS FOR SELECTED LANTHANIDE FLUORIDES

Appendix 3.1. Derived Thermodynamic Functions for $YbF_3(g)$[1]

T (K)	C_p° (cal $mol^{-1}K^{-1}$)	S_T° (cal $mol^{-1}K^{-1}$)	$H_T^\circ - H_{298}^\circ$ (cal mol^{-1})	$-(G_T^\circ - H_{298}^\circ)/T$ (cal $mol^{-1}K^{-1}$)
298	17.04	81.83	(2)	81.83
500	18.64	91.09	3631	83.83
1000	19.53	104.38	13242	91.14
1200	19.63	107.95	17159	93.65
1400	19.70	110.98	21093	95.92
1600	19.74	113.61	25037	97.97
1800	19.77	115.94	28987	99.84
2000	19.79	118.02	32942	101.55

[1] For assumptions made in derivation see Section 5.5.2.

[2] $H_{298}^\circ - H_0^\circ = 4035$ cal mol^{-1}

Appendix 3.2. Derived Thermodynamic Functions for $YbF_3(s,\ell)$[1]

T (K)	C_p° (cal $mol^{-1}K^{-1}$)	S_T°[2] (cal $mol^{-1}K^{-1}$)	$H_T^\circ - H_{298}^\circ$ (cal mol^{-1})	$-(G_T^\circ - H_{298}^\circ)/T$ (cal $mol^{-1}K^{-1}$)
298	23.44	26.56	0	26.56
500	24.18	38.84	4799	29.24
1000	26.51	56.30	17463	38.84
1200	27.47	61.22	22861	42.17
1400	28.57	70.26	34404	45.68
1600	29.09	79.08	47312	49.51
1800	29.09	82.51	53130	52.99
2000	29.09	85.57	58948	56.10

[1]Derived using the enthalpy increments from Reference 18

[2]For estimation of absolute entropy see Section 5.5.2.

Appendix 3.3. Derived Thermodynamic Functions for $YbF_2(g)$[1]

T (K)	C_p° (cal $mol^{-1}K^{-1}$)	S_T° (cal $mol^{-1}K^{-1}$)	$H_T^\circ - H_{298}^\circ$ (cal mol^{-1})	$-(G_T^\circ - H_{298}^\circ)/T$ (cal $mol^{-1}K^{-1}$)
298	12.52	69.47	(2)	69.47
500	13.34	76.18	2627	70.93
1000	13.76	85.60	9435	76.17
1200	13.80	88.11	12191	77.95
1400	13.83	90.24	14955	79.56
1600	13.85	92.09	17724	81.02
1800	13.86	93.72	20495	82.34
2000	13.87	95.19	23268	83.55

[1]For assumptions made in derivation see Section 5.5.1.

[2]$H_{298}^\circ - H_0^\circ$ = 3125 cal mol^{-1}

Appendix 3.4. Derived Thermodynamic Functions for $YbF_2(s,\ell)$[1]

T (K)	C_p° (cal $mol^{-1}K^{-1}$)	S_T° (cal $mol^{-1}K^{-1}$)	$H_T^\circ - H_{298}^\circ$ (cal mol^{-1})	$-(G_T^\circ - H_{298}^\circ)/T$ (cal $mol^{-1}K^{-1}$)
298	17.34	22.50	0	22.50
500	17.98	31.62	3565	24.49
1000	19.58	44.57	12956	31.62
1200	20.22	48.20	16936	34.09
1400	20.86	51.36	21043	36.33
1600	21.50	54.19	25279	38.39
1800	23.90	61.36	37376	40.59
2000	23.90	63.88	42156	42.80

[1]For assumptions made in derivation see Section 5.5.1.

Appendix 3.5. Derived Thermodynamic Functions for $SmF_3(g)$[1]

T (K)	C_p° (cal $mol^{-1}K^{-1}$)	S_T° (cal $mol^{-1}K^{-1}$)	$H_T^\circ - H_{298}^\circ$ (cal mol^{-1})	$-(G_T^\circ - H_{298}^\circ)/T$ (cal $mol^{-1}K^{-1}$)
298	17.99	81.13	(2)	81.13
500	20.13	91.02	3878	83.26
1000	21.61	105.57	14420	91.15
1200	21.75	109.53	18759	93.90
1400	21.78	112.88	23113	96.37
1600	21.73	115.79	27465	98.62
1800	21.63	118.34	31801	100.68
2000	21.52	120.62	36116	102.56

[1]For assumptions made in derivation see Section 5.5.5.

[2]$H_{298}^\circ - H_0^\circ$ = 4202 cal mol^{-1}

Appendix 3.6. Derived Thermodynamic Functions for $SmF_3(s,\ell)$[1]

T (K)	C_p° (cal $mol^{-1}K^{-1}$)	S_T° (cal $mol^{-1}K^{-1}$)	$H_T^\circ - H_{298}^\circ$ (cal mol^{-1})	$-(G_T^\circ - H_{298}^\circ)/T$ (cal $mol^{-1}K^{-1}$)
298	25.68	27.09[2]	0	27.09
500	25.68	40.37	5163	30.04
1000	27.18	59.59	19156	40.43
1200	30.12	64.75	24822	44.06
1400	35.98	69.81	31401	47.38
1600	35.60	82.93	51656	50.65
1800	35.60	87.13	58776	54.47
2000	35.60	90.88	65896	57.93

[1]Derived using the enthalpy increments from Reference 18

[2]For estimation of absolute entropy see Section 5.5.5.

Appendix 3.7. Derived Thermodynamic Functions for $SmF_2(g)$[1]

T (K)	C_p° (cal $mol^{-1}K^{-1}$)	S_T° (cal $mol^{-1}K^{-1}$)	$H_T^\circ - H_{298}^\circ$ (cal mol^{-1})	$-(G_T^\circ - H_{298}^\circ)/T$ (cal $mol^{-1}K^{-1}$)
298	15.07	72.59	(2)	72.59
500	15.83	80.60	3134	74.33
1000	16.27	91.76	11195	80.57
1200	16.24	94.72	14447	82.69
1400	16.12	97.22	17684	84.59
1600	15.96	99.36	20893	86.30
1800	15.78	101.23	24068	87.86
2000	15.60	102.89	27205	89.28

[1] For assumptions made in derivation see Section 5.5.4.

[2] $H_{298}^\circ - H_0^\circ$ = 3558 cal mol^{-1}

Appendix 3.8. Derived Thermodynamic Functions for $SmF_2(s,\ell)$[1]

T (K)	C_p° (cal $mol^{-1}K^{-1}$)	S_T° (cal $mol^{-1}K^{-1}$)	$H_T^\circ - H_{298}^\circ$ (cal mol^{-1})	$-(G_T^\circ - H_{298}^\circ)/T$ (cal $mol^{-1}K^{-1}$)
298	14.63	27.10	0	27.10
500	15.91	34.97	3082	28.80
1000	19.09	46.97	11834	35.14
1200	20.37	50.57	15780	37.41
1400	21.64	53.80	19980	39.53
1600	22.91	56.77	24436	41.50
1800	23.90	63.99	36653	43.63
2000	23.90	66.51	41433	45.79

[1] For assumptions made in derivation see Section 5.5.4.

Appendix 3.9. Derived Thermodynamic Functions for $TmF_3(g)$[1]

T (K)	C_p° (cal $mol^{-1}K^{-1}$)	S_T° (cal $mol^{-1}K^{-1}$)	$H_T^\circ - H_{298}^\circ$ (cal mol^{-1})	$-(G_T^\circ - H_{298}^\circ)/T$ (cal $mol^{-1}K^{-1}$)
298	17.05	82.51	(2)	82.51
500	18.65	91.78	3633	84.51
1000	19.57	105.08	13251	91.83
1200	19.72	108.66	17180	94.34
1400	19.87	111.71	21139	96.61
1600	20.02	114.37	25128	98.67
1800	20.18	116.74	29148	100.55
2000	20.34	118.88	33200	102.28

[1]For assumptions made in derivation see Section 5.5.7.

[2]$H_{298}^\circ - H_0^\circ$ = 4024 cal mol^{-1}

Appendix 3.10. Derived Thermodynamic Functions for $TmF_3(s,\ell)$[1]

T (K)	C_p° (cal $mol^{-1}K^{-1}$)	S_T° (cal $mol^{-1}K^{-1}$)	$H_T^\circ - H_{298}^\circ$ (cal mol^{-1})	$-(G_T^\circ - H_{298}^\circ)/T$ (cal $mol^{-1}K^{-1}$)
298	22.47	27.62[2]	0	27.62
500	24.40	39.79	4771	30.25
1000	26.25	57.34	17482	39.86
1200	26.81	62.17	22788	43.19
1400	23.39	71.60	35159	46.49
1600	33.54	80.68	48460	50.09
1800	33.54	84.63	55168	53.98
2000	33.54	88.16	61876	57.22

[1]Derived using the enthalpy increments from Reference 18

[2]For estimation of absolute entropy see Section 5.5.7.

APPENDIX 4

MASS SPECTROMETRY DATA

Appendix 4.1. Ion Intensity of Yb^+ from $YbF_{2+x}(s)$ Confined in Mo vs. Time

(T = 1338 K)		(T = 1396 K)	
$I^+(174)$[1,2]	Time	$I^+(174)$	Time
68	10 min	193	109 min
58	72	85	169
16	197	63	201
13	221	56	239

[1]Ionization energy = 45 ± 5 V

[2]An ion intensity of 100 = 2/3 x 10^{-12} amp

[3]Measured from time of appearance of Yb^+ peak from $YbF_{2.0}$

Appendix 4.2. Ionization Efficiency Curve Data for Yb^+ from YbF_{2+x} Confined in Mo (T = 1335 K)

$I(Yb^+)^{1,2,3}$	Volts	$I(Yb^+)$	Volts	$I(Yb^+)$	Volts
238	40.35	5	9.46	194	17.67
235	34.87	9	10.15	161	16.28
234	30.75	64	11.40	127	13.81
235	25.45	114	12.78	96	12.37
219	20.43	145	13.25	52	11.34
205	17.36	152	14.15	34	10.71
139	14.93	203	20.27	21	10.41
105	12.42	180	18.67	187	20.02
38	10.76				

[1] I = sum of ion currents for masses 170, 171, 172, 173, 174 and 176

[2] Ion current of 100 = $2/3 \times 10^{-12}$ amp

[3] Time = 30 to 90 min after time of appearance of Yb^+ peak from $YbF_{2.0}$

Appendix 4.3. Intensity of Yb^+ and Intensity Fractions of Yb^+, YbF^+ and YbF_2^+ from YbF_{2+x} ($0.0 \leq x \leq 0.4$) Confined in Mo vs. Time (T = 1653 K)

Yb^+ $I^+(174)$[1,2]	Yb^+ $IF^+(174)$[3]	YbF^+ $IF^+(193)$	YbF_2^+ $IF^+(212)$	Time[4]
178	0.763	0.183	0.053	636 min
118	0.645	0.258	0.097	770
68	0.625	0.244	0.131	808
38	0.535	0.307	0.158	921
30	0.532	0.298	0.170	1044
23	0.461	0.359	0.180	1109
35	0.455	0.295	0.250	1222
28	0.377	0.347	0.275	1354
30	0.316	0.294	0.389	1432
18	0.291	0.328	0.381	1452
15	0.299	0.320	0.380	1512
11	0.307	0.356	0.337	1647
10	0.244	0.337	0.420	1787
9	0.255	0.289	0.456	1959
12	0.228	0.317	0.455	2129
12	0.174	0.315	0.511	2169
18	0.238	0.317	0.446	2200
9	0.222	0.292	0.486	2300
14	0.202	0.341	0.457	2343
11	0.187	0.319	0.494	2550
9	0.220	0.275	0.505	2680

[1] Ionizing energy = 45 ± 5 V

[2] 100 = 2/3 x 10^{-12} amp

[3] $I^+(174)$/total Yb-containing ion current

[4] Measured from time of appearance of Yb^+ peak from $YbF_{2.0}$

Appendix 4.4. Ionization Efficiency Curve Data for Yb^+, YbF^+ and YbF_2^+ from YbF_{2+x} ($0.0 \leq x < 0.4$) Confined in Mo (T = 1667 K)

Yb^+		YbF^+		YbF_2^+	
$I^+(174)$[1,2]	Volts	$I^+(193)$	Volts	$I^+(212)$	Volts
106	29.59	44	29.72	29.2	42.95
96	24.95	35	25.92	23.9	30.95
91	22.00	38	22.64	16.8	25.92
103	19.94	39	20.68	13.3	23.62
79	17.70	23	19.00	12.4	20.96
68	15.70	19	17.22	8.7	19.28
57	13.53	13	15.10	8.0	17.55
48	12.42	12.5	13.12	7.6	15.41
35	11.23	10	12.05	2.9	13.26
8.7	9.85	8.7	11.08	5.9	14.53
3.5	9.29	2.7	10.17	8.9	16.35
9	10.31	12	13.57	9.7	18.21
18	10.88	15	15.50	10.6	18.28
31	11.65	20	16.05	14.2	20.69
55	12.61	24	18.55	13.3	22.64
57	14.60	41	28.92	24.8	29.17
84	18.29	44	45.00	31.9	43.72
135	43.45				

[1] $100 = 1/3 \times 10^{-12}$ amp

[2] Time = 800 to 975 min after time of appearance of Yb^+ peak

Appendix 4.5. Ionization Efficiency Curve Data for Yb^+, YbF^+ and YbF_2^+ from $YbF_{2.40}$ Confined in Mo (T = 1735 K)

Yb^+ $I^+(174)$[1,2]	YbF^+ $I^+(193)$	YbF_2^+ $I^+(212)$	Volts
29.71	43.25	77.86	43.45
22.00	33.00	60.00	37.70
22.00	33.00	51.00	34.67
23.00	30.50	49.00	32.39
20.20	33.00	52.60	29.94
14.79	27.43	39.93	26.63
9.00	22.00	29.00	23.32
7.50	19.50	29.80	21.01
9.50	20.00	26.50	18.78
5.67	11.00	12.53	16.23
9.00	9.67	7.25	15.32
6.00	6.67	5.67	14.38
3.17	5.67	3.67	13.33
5.38	4.88	3.00	12.24
1.75	0.50	0.50	11.33

[1] $100 = 1/3 \times 10^{-12}$ amp

[2] Time = 2527 to 2687 min after time of appearance of Yb^+ peak from $YbF_{2.00}$

Appendix 4.6. Ionization Efficiency Curve Data for Yb^+, YbF^+ and YbF_2^+ from $YbF_{3.0}(\ell)$ Confined in Mo (T = 1673 K)

$I(Yb^+)^{1,2}$	Volts	$I(YbF^+)^3$	Volts	$I(YbF_2^+)^4$	Volts
55.7	44.62	26.40	44.15	329.5	45.70
50.3	39.32	26.50	37.74	282.0	37.56
40.0	37.01	26.60	30.63	228.0	30.15
37.3	35.56	19.70	28.95	162.1	25.96
34.8	34.10	16.50	27.37	95.3	21.45
27.3	32.73	15.00	25.70	79.0	19.55
27.3	32.73	8.70	23.93	42.2	17.51
22.0	31.54	5.40	21.95	17.3	15.45
15.5	29.53	9.35	20.45	21.4	15.71
10.2	28.68	1.01	19.67	34.3	17.00
		4.00	18.90	54.5	18.62
		3.61	21.10	98.0	20.32
		5.98	22.72	107.7	22.14
		11.30	24.67	129.7	23.64
		13.80	26.80	154.7	25.50
		17.20	28.23	192.3	29.52
		20.80	29.75	277.3	36.57
		23.30	34.33	117.0	22.96
		25.60	44.07	89.3	21.43
		3.20	18.22	60.7	19.66
				47.3	18.03
				27.2	16.45
				11.7	15.32
				10.0	14.40

[1] 100 = 1/3 x 10^{-12} amp

[2] I = ion currents for masses 172 + 174 + 176

[3] I = ion currents for masses 191 + 193 + 195

[4] I = ion currents for masses 210 + 212 + 214

APPENDIX 5

UNTREATED DATA FROM KNUDSEN EFFUSION EXPERIMENTS IN CHRONOLOGICAL ORDER

Appendix 5.1. Target Collection Data for Yb(g) from YbF_{2+x} ($0.00 \leq x < 0.40$) Confined in Mo

T(obs)	TT[1]	Exposure Time	Counts/30 sec Before Exposure	Counts/30 sec After Exposure
			16891[2]	16617[2] 24794[3]
1273 K	-7 K	45.00 min	13864	26441
1302	-7	16.00	13959	22082
1330	-7	10.00	13615	20671
1284	-7	47.00	13874[2] 16654[2]	29594[2] 15920[3] 24449[3]

$a = 7.90 \times 10^{-3}$ cm^2, C = 10.21 cm, R = 0.826 cm [see equations (3-5) and (3-6)]; D (Wien's Law) = -1.646×10^{-5}

[1] TT = T(IPTS - 1948) - T(obs)

[2] Standard Blank Yb(l)

[3] Standard Yb(l)

Appendix 5.2. Target Collection Data for $YbF_{2.40}$ Effusion Experiments

T(obs)	TT[1]	Exposure Time	Counts/30 sec Before Exposure	Counts/30 sec After Exposure
		Experiment 1		
			16654^{2}	15920^{2}
				24449^{3}
1437 K	-6 K	110.00 min	13963	29818
1501	-15	31.00	14156	28394
1550	-15	12.00	13993	28772
1525	-15	20.00	13837	26753
1565	-14	10.00	14197_{2}	28626_{2}
			16640^{2}	15766^{2}
				24464^{3}
a = 7.90×10^{-3} cm^2, C = 10.21 cm, R = 0.826 cm [see equations (3-5) and (3-6]; D (Wien's Law) = -1.646×10^{-5}				
		Experiment 2		
			15081^{2}	17398^{2}
				26149^{3}
1554	-14	87.00	13255	37396
1636	-14	28.00	16033	43377
1696	-16	5.00	16245	26923
1670	-15	10.00	13769	34719
1637	-14	15.00	16302_{2}	28901_{2}
			15100^{2}	17072^{2}
				26346^{3}
1603	-13	33.00	13753	35182
1574	-14	50.00	13020	34315
1547	-15	80.00	13611	34147
1610	-13	34.00	13609	41108
1654	-14	14.00	12765_{2}	35061_{2}
			15087^{2}	17082^{2}
				26157^{3}
a = 1.14×10^{-3} cm^2, C = 10.25 cm, R = 0.826 cm [see equations (3-5) and (3-6)]; D (Wien's Law) = -1.646×10^{-5}				
		Experiment 3		
			16510^{2}	17573^{2}
				26312^{3}
1589	-13	13.00	13762	43448
1508	-15	70.00	13585	55812
1597	-13	11.00	12888	44116
1546	-15	30.00	13086	44540
1574	-14	17.00	13552_{2}	45414_{2}
			16398^{2}	17440^{2}
				26229^{3}

Appendix 5.2. (cont'd.)

T(obs)	TT[1]	Exposure Time	Counts/30 sec Before Exposure	Counts/30 sec After Exposure
1498 K	-15 K	75.00 min	13482	50100
1642	-14	4.00	14341	37838
1532	-15	44.00	13816	52563
1561	-14	23.00	13496	49443
1622	-13	7.00	14012[2]	44213[2]
			16740[2]	17484[3]
				26055[3]

a = 7.57×10^{-3} cm^2, C = 10.37 cm, R = 0.833 cm [see equations (3-5) and (3-6)]; D (Wien's Law) = -1.646×10^{-5}

Experiment 4

			15580[2]	16461[2]
				24926[3]
1483	8	45.31	15817	23261
1534	7	27.01	15595	28392
1455	9	85.21	15581	23767
1558	5	17.00	15792	27725
1559	5	15.24	15551[2]	27749[2]
			15587[2]	16464[3]
				25199[3]

a = 5.01×10^{-3} cm^2, C = 9.89 cm, R = 0.833 cm [see equations (3-5) and (3-6)]; D (Wien's Law) = -1.800×10^{-5}

Appendix 5.2. (cont'd.)

T(obs)	TT[1]	Exposure Time	Counts/60 sec Before Exposure	Counts/60 sec After Exposure
		Experiment 5		
			9157_4	8770_4
				13202_5
1550 K	-15 K	120.00 min	8054	12395
1584	-13	60.00	8576	12172
1634	-12	25.00	7875	11584
1662	-13	15.00	7988	11544
1685	-15	12.00	7924_4	12067_4
			9283_4	8474_5
				13376_5
1694	-15	10.26	8032	12092
1661	-13	15.00	8277	11535
1616	-12	35.00	8576	12502
1594	-13	55.00	8287	12352
1564	-15	95.00	7846_4	12142_4
			8805_4	8838_5
				13237_5

a = 1.12×10^{-3} cm^2, C = 10.50 cm, R = 0.833 cm [see equations (3-5) and (3-6)]; D (Wien's Law) = -1.391×10^{-5}

		Experiment 6		
			8654_4	8745_4
				13225
1547	-15	130.00	8129	12826
1586	-13	65.00	7735	12326
1650	-13	20.00	8258	12337
1671	-14	13.00	8043	12190
1713	-14	5.00	8142_4	10975_4
			8659_4	8793_5
				13233_5
1698	-15	10.00	8473	12886
1643	-12	22.00	8442	12372
1629	-12	28.00	8224	12327
1608	-12	45.00	7845	12277
1584	-13	65.00	7852_4	12437_4
			8894_4	8770_5
				13202_5

a = 1.12×10^{-3} cm^2, C = 10.50 cm, R = 0.833 cm [see equations (3-5) and (3-6)]; D (Wien's Law) = -1.391×10^{-5}

Appendix 5.2. (cont'd.)

T(obs)	TT[1]	Exposure Time	Counts/60 sec Before Exposure	Counts/60 sec After Exposure
		Experiment 7		
			8045_4	8060_5^4
				12316
1626 K	-11 K	35.00 min	7858	14305
1643	-12	25.00	7470	12912
1674	-14	15.00	7362	12109
1702	-15	10.00	7384	11927
1715	-14	7.00	7521_4	11116_5^4
			8407_4	8260_5^4
				11572
1651	-13	22.00	7559	11735
1622	-11	37.00	7869	11544
1565	-15	110.00	7750	12376
1593	-12	65.00	7324	11814
1620	-11	35.00	7668_4	11654_5^4
			8475_4	8307_5^4
				12400

a = 1.12×10^{-3} cm^2, C = 10.51 cm, R = 0.833 cm [see equations (3-5) and (3-6)]; D (Wien's Law) = -1.391×10^{-5}

		Experiment 8		
			8894_4	8635_5^4
				12889
1578	-14	5.00	8292	9621
1531	-14	34.50	8080	12648
1489	-11	70.00	8257	12022
1498	-12	65.00	8299	12137
1527	-14	40.00	8393_4	12768_5^4
			8932_4	8676_5^4
				12941
1479	-11	100.00	8495	12602
1467	-10	121.00	8372	12014
1449	-10	220.11	8175	12955
1512	-13	65.00	7899	12300
1547	-15	33.10	8054_4	13653_5^4
			8865_4	8674_5^4
				13201

a = 7.28×10^{-3} cm^2, C = 10.61 cm, R = 0.833 cm [see equations (3-5) and (3-6)]; D (Wien's Law) = -1.391×10^{-5}

Appendix 5.2. (cont'd.)

T(obs)	TT[1]	Exposure Time	Counts/60 sec Before Exposure	Counts/60 sec After Exposure
		Experiment 9		
			8992^{4}	8119^{4}
				12660^{5}
1547 K	-15 K	30.00 min	8106	13045
1573	-14	16.00	8515	12868
1591	-13	12.00	8241	12826
1615	-12	8.00	7909	12887
1558	-15	26.00	8420_{4}	13816_{4}
			9028^{4}	8294^{4}
				12660^{5}
a = 7.28 x 10^{-3} cm^2, C = 10.61 cm, R = 0.833 cm [see equations (3-5) and (3-6)]; D (Wien's Law) = -1.391 x 10^{-5}				
		Experiment 10		
			8256^{4}	8018^{4}
				12334^{5}
1545	-14	31.00	7548	12966
1511	-13	60.00	7380	12257
1444	-10	279.40	7686	12742
1498	-12	70.00	7369	12319
1476	-11	122.00	7687_{4}	12714_{4}
			8289^{4}	8299^{4}
				12386^{5}
1519	-14	50.00	7755	12442
1560	-15	22.00	7814	12719
1468	-10	151.00	7612	12792
1433	-10	360.00	7382	12511
1556	-15	22.00	7437_{4}	11682_{4}
			8232^{4}	8319^{4}
				12329^{5}
a = 7.28 x 10^{-3} cm^2, C = 10.61 cm, R = 0.833 cm [see equations (3-5) and (3-6)]; D (Wien's Law) = -1.391 x 10^{-5}				

[1] TT = T(IPTS - 1948) - T(obs)

[2] Standard Blank Yb(1)

[3] Standard Yb(1)

[4] Standard Blank Yb(2)

[5] Standard Yb(2)

Appendix 5.3. Target Collection Data for $YbF_{3.00}$ Effusion Experiments

T(obs)	TT[1]	Exposure Time	Counts/30 sec Before Exposure	Counts/30 sec After Exposure
		Experiment 11		
			14102_2	14159_2 22786_3
1434 K	15 K	46.00 min	11617	25183
1484	14	14.00	11256	23476
1561	13	4.01	12023	26764
1546	13	6.00	12157	27722
1516	14	11.00	12433_2 13980_2	29594_2 13719_2 22283_3
1490	14	14.00	12835	26551
1463	15	30.00	12578	29436
1427	15	50.00	12150	25251
1483	14	14.00	11217	23202
1511	14	11.00	11140_2 13987_2	26989_2 14202_2 22573_3
		Experiment 12		
			14421_2	15512_2 24038_3
1382	16	101.00	13215	23732
1398	16	70.00	13558	23876
1427	15	43.00	13905	26241
1455	15	26.00	13783	27007
1512	14	6.00	13892_2 14409_2	23063_2 15067_2 24067_3
1473	15	15.00	14320	25345
1441	15	25.00	14266	23723
1408	16	61.00	14155	25165
1377	16	90.00	13805	22225
1355	16	150.00	13535_2 14477_2	19617_2 15419_2 24105_3

a = 8.33×10^{-3} cm^2, C = 12.32 cm, R = 0.833 cm [see equations (3-5) and (3-6)]; D (Wien's Law) = -1.800×10^{-5}

a = 8.33×10^{-3} cm^2, C = 12.30 cm, R = 0.833 cm [see equations (3-5) and (3-6)]; D (Wien's Law) = -1.800×10^{-5}

Appendix 5.3. (cont'd.)

T(obs)	TT[1]	Exposure Time	Counts/30 sec Before Exposure	Counts/30 sec After Exposure
		Experiment 13		
			14477[2]	14987[2] 23545[3]
1367 K	16 K	120.00 min	13731	22390
1319	17	260.00	14050	18708
1313	17	260.00	12720	17075
1301	17	260.00	12893	16390
1293	17	400.00	13263, 14806[2]	17461, 15073[2] 23643[3]
1365	16	60.00	13923	18003
1331	16	240.00	13635	20665
1354	16	125.00	13593	19739
1309	17	301.00	13382	18126
1338	16	120.00	14143, 14862[2]	18064, 14962[2] 23665[3]

a = 8.33 x 10^{-3} cm^2, C = 12.30 cm, R = 0.833 cm [see equations (3-5) and (3-6)]; D (Wien's Law) = -1.800 x 10^{-5}

		Experiment 14		
			14033[2]	14716[2] 23271[3]
1456	15	140.00	12616	22788
1557	13	30.00	10778	25105
1562	13	30.00	10924	26883
1601	13	15.00	10620	25651
1636	14	10.00	10905, 13865[2]	27880, 14475[2] 23390[3]
1660	14	5.30	11881	26119
1695	14	3.00	12621	26252
1648	14	6.00	11943	24461
1620	13	11.00	10717	25342
1572	13	26.00	11810, 13458[2]	28070, 14672[2] 23087[3]

a = 1.11 x 10^{-3} cm^2, C = 12.37 cm, R = 0.833 cm [see equations (3-5) and (3-6)]; D (Wien's Law) = -1.800 x 10^{-5}

Appendix 5.3. (con'td.)

T(obs)	TT[1]	Exposure Time	Counts/30 sec Before Exposure	Counts/30 sec After Exposure
		Experiment 15		
			14394[2]	10891[2] 18692[3]
1487 K	14 K	110.00 min	12351	23735
1587	13	16.00	11409	21435
1642	14	7.00	12458	23185
1676	14	5.00	12380	26161
1716	14	2.50	12550[2] 14434[2]	25562[2] 10938[2] 18610[3]
1723	15	2.50	12808	27038
1671	14	5.00	12502	24341
1634	14	8.00	12348	22184
1607	13	16.00	11363	25199
1551	13	36.00	11335[2] 14273[2]	22882[2] 11039[2] 18553[3]

$a = 1.11 \times 10^{-3}$ cm^2, C = 12.26 cm, R = 0.833 cm [see equations (3-5) and (3-5)]; D (Wien's Law) = -1.800×10^{-5}

Appendix 5.3. (cont'd.)

T(obs)	TT[1]	Exposure Time	Counts/30 sec Before Exposure	Counts/30 sec After Exposure
		Experiment 16		
			15767[2]	15882[2] 24750[3]
1555 K	-15 K	60.00 min	14981	29181
1606	-13	24.32	14755	30668
1658	-14	10.00	14333	27169
1667	-14	8.46	13470	28216
1641	-14	10.00	14713 15949[2]	24633 16008[2] 24844[3]
1588	-14	20.00	14673	23373
1521	-15	75.00	15383	24609
1580	-14	30.00	14311	25852
1663	-14	15.00	13818	26353
1625	-13	12.00	15392 15638[2]	33786 16028[2] 24852[3]

a = 1.10 x 10^{-3} cm^2, C = 12.30 cm, R = 0.833 cm [see equations (3-5) and (3-6)]; D (Wien's Law) = -1.800 x 10^{-5}

[1]TT = T(IPTS - 1948) - T(obs)

[2]Standard Blank Yb(1)

[3]Standard Yb(1)

Appendix 5.4. Target Collection Data for Sm(g) from SmF_{2+x} ($0.00 \leq x < 0.40$) Confined in Mo

T(obs)	TT[1]	Exposure Time	Counts/30 sec Before Exposure	Counts/30 sec After Exposure
			4147[2]	4128[2] 15874[3]
1094 K	-1 K	27.00 min	4077	14951
1201	-6	26.00	4170	13921
1304	-7	28.00	4175	13289
1372	-7	21.00	4113	13180
1426	-6	33.00	4087 4045[2]	16692 4115[2] 15882[3]

a = 4.92×10^{-3} cm^2, C = 10.00 cm, R = 0.795 cm [see equations (3-5) and (3-6)]; D (Wien's Law) = -1.646×10^{-5}

[1] TT = T(IPTS - 1948) - T(obs)

[2] Standard Blank Sm(1)

[3] Standard Sm(1)

Appendix 5.5. Target Collection Data for $SmF_{2.40}$ Effusion Experiment 1

T(obs)	TT[1]	Exposure Time	Counts/30 sec Before Exposure	Counts/30 sec After Exposure
			4045[2]	4115[2] 15882[3]
1474 K	-3 K	20.00 min	4155	18717
1477	-3	61.85	4199	48805
1475	-13	20.00	4276	15840
1532	-15	8.00	4269	14673
1465	-13	37.00	4109	18796
1520	-15	12.00	4241 4131[2]	15837 4056[2] 15837[3]

a = 4.92 x 10^{-3} cm^2, C = 10.00 cm, R = 0.795 cm [see equations (3-5) and (3-6)]; D (Wien's Law) = -1.646 x 10^{-5}

[1] TT = T(IPTS - 1948) - T(obs)

[2] Standard Blank Sm(1)

[3] Standard Sm(1)

Appendix 5.6. Target Collection and Deposition Data for $SmF_{2.40}$ Effusion Experiments

T(obs)	TT[1]	Exposure Time	Counts/30 sec Before Exposure	Counts/30 sec After Exposure	Deposit[2]
			Experiment 2		
			4079^{3}	4215^{3} 15781^{4}	
1428^{5}K	-7 K	61.00 min	4224	12221	18.9 nm
1488^{5}	-2	20.00	4207	13416	23.4
1398	-7	50.00	4178	8205	9.9
1445	-6	25.00	4010	10438	15.3
1497	-2	10.00	4124_{3} 4176^{3}	11625_{3} 4203^{3} 15945^{4}	16.9
1534	-15	10.00	4212	16569	29.1
1487	-2	10.00	4081	10298	14.3
1447	-6	31.00	4167	13148	21.2
1450	-6	30.00	4157	12905	20.2
1516	-15	10.00	4176_{3} 4124^{3}	13107_{3} 4193^{3} 15733^{4}	20.3

$a = 4.69 \times 10^{-3}$ cm^2, C = 9.02 cm, R = 0.795 cm [see equations (3-5) and (3-6)]; D (Wien's Law) = -1.646×10^{-5}

Appendix 5.6. (cont'd.)

T(obs)	TT[1]	Exposure Time	Counts/30 sec Before Exposure	Counts/30 sec After Exposure	Deposit[2]
			Experiment 3		
			4231[3]	4171[3] 15839[4]	
1214[6,7] K	25 K	13.00 min	3992	23923	43.8 nm
1546[6]	17	3.00	4130	15486	23.4
1516	16	10.00	4106	13360	20.3
1586	18	4.00	4067	14814	22.9
1551	17	7.00	4036[3] 4134[3]	13249[3] 4224[3] 15902[4]	20.0
1631	18	2.00	4110	13460	20.1
1663	17	2.00	4235	19792	31.4
1695	15	1.00	4271	15377	24.6
1694	15	1.00	4182	15304	25.0
1639	17	3.00	3985[3] 4147[3]	17464[3] 4190[3] 15629[4]	29.9

a = 1.42 x 10^{-3} cm^2, C = 10.42 cm, R = 0.795 cm [see equations (3-5) and (3-6)]; D (Wien's Law) = 2.630 x 10^{-5}

[1] TT = T(IPTS - 1948) - T(obs); TT for experiment 3 = T(IPTS - 1948) - T(obs) + 31 K

[2] Thickness as determined by quartz crystal

[3] Standard Blank Sm(l)

[4] Standard Sm(l)

[5] a = 4.92 x 10^{-3} cm^2, C = 10.00 cm

[6] C = 8.56 cm

[7] Sm(g)

Appendix 5.7. Rate Data for $SmF_{2.40}$ Effusion Experiments

T(obs)	TT[1]	Rate[2]	T(obs)	TT[1]	Rate[2]
		Experiment 2[3]			
1433 K	-6 K	0.292 nm/min	1488 K	14 K	0.880 nm/min
1504	-15	1.01	1428	-7	0.310
1565	-14	3.256	1488	-2	1.17
a = 4.92 x 10^{-3} cm^2, C = 10.00 cm					
1398	-7	0.198	1487	-2	1.43
1445	-6	0.610	1447	-6	0.685
1497	-2	1.69	1397	-7	0.232
1346	-7	0.0475	1385	-7	0.148
1393	-7	0.185	1415	-7	0.321
1430	-6	0.425	1450	-6	0.674
1454	-5	0.735	1484	-3	1.35
1489	-2	1.48	1516	-15	2.03
1534	-15	2.91	1434	-6	0.500

a = 4.69 c 10^{-3} cm^2, C = 9.02 cm, R = 0.795 cm [see equations (3-5) and (3-6)]; D (Wien's Law) = -1.646 x 10^{-5}

Appendix 5.7. (cont'd.)

T(obs)	TT[1]	Rate[2]	T(obs)	TT[1]	Rate[2]
		Experiment 3[4]			
1546 K	17 K	7.800 nm/min	1624 K	18 K	19.0 nm/min
1479	17	2.41	1491	17	2.43
1430	20	0.940	1429	20	8.33
1575	17	9.00			
C = 8.56 cm					
1516	16	2.03	1695	15	24.6
1586	18	5.73	1694	15	25.0
1478	17	0.805	1673	16	17.8
1520	16	1.70	1639	17	9.95
1551	17	2.86	1614	18	6.38
1593	18	5.70	1573	17	3.05
1631	18	10.1	1527	16	1.45
1663	17	15.7			

a = 1.42×10^{-3} cm^2, C = 10.42 cm, R = 0.795 cm [see equations (3-5) and (3-6)]; D (Wien's Law) = -2.630×10^{-5}

[1]TT = T(IPTS - 1948) - T(obs); TT for experiment 3 = T(IPTS - 1948) - T(obs) + 31 K

[2]Rate of deposition as determined by quartz crystal

[3]Pressures calculated by use of ($2.4_6 \pm 0.0_8$) nm/μg Sm

[4]Pressures calculated by use of ($2.2_5 \pm 0.0_7$) nm/μg Sm

Appendix 5.8. Target Collection Data for $SmF_{3.00}$ Effusion Experment 1

T(obs)	TT[1]	Exposure Time	Counts/30 sec Before Exposure	Counts/30 sec After Exposure
			3564[2]	3980[2] 43066[3]
1619[4]K	--	20.00 min	3537	43066
1663	-14 K	12.00	3589	43731
1714	-17	5.00	3538	38284
1536	-15	120.00	3529	45172
1608	-13	30.00	3622[2] 3514[2]	44130[2] 4113[2] 43320[3]
1653	-14	15.00	3464	42285
1680	-15	10.00	3495	43527
1578	-14	75.00	3534	58642
1619	-13	20.00	3577	34073
1643	-14	15.00	3529[2] 3527[2]	37658[2] 4081[2] 43283[3]

a = 1.11×10^{-3} cm^2, C = 9.99 cm, R = 0.795 cm [see equations (3-5) and (3-6)]; D (Wien's Law) = -1.646×10^{-5}

[1] TT = T(IPTS - 1948) - T(obs)

[2] Standard Blank Sm(2)

[3] Standard Sm(2)

[4] Temperature varied 60°; target was not used.

Appendix 5.9. Target Collection and Deposition Data for $SmF_{3.00}$ Effusion Experiments

T(obs)	TT[1]	Exposure Time	Counts/30 sec Before Exposure	Counts/30 sec After Exposure	Deposit[2]
			Experiment 2		
			4124^{3}	4204^{3} 15553^{4}	
$1433^{5,6}$K	-6 K	21.00 min	3960	15144	29.2 nm
$1464^{5,7}_{5}$	-5	6.00	3852	11479	18.4
1425^{5}	-7	13.00	4102	10857	16.5
1422_{8}	-7	17.00	4031	12033	20.0
1417^{8}	-7	35.00	3999_{3} 4045^{3}	14605_{3} 4127^{3} 15765^{4}	27.9
1373	-7	52.00	4091	10533	17.2
1336	-7	86.00	4158	7997	10.3
1426	-7	15.00	4113	11164	18.6
1413	-7	21.00	4149	11299	19.7
1455	-5	6.00	4004_{3} 4111^{3}	9574_{3} 4222^{3} 15617^{4}	----

$a = 8.18 \times 10^{-3}$ cm^2, C = 10.06 cm, R = 0.795 cm [see equations (3-5) and (3-6)]; D (Wien's Law) = -1.646×10^{-5}

Appendix 5.9. (cont'd.)

T(obs)	TT[1]	Exposure Time	Counts/30 sec Before Exposure	Counts/30 sec After Exposure	Deposit[2]
			Experiment 3		
			4173[3]	4181[3] 15585[4]	
1455 K	-5 K	28.00 min	4213	9085	12.0 nm
1585	-14	6.00	4221	13899	23.7
1669	-15	2.00	4107	16302	28.8
1710	-17	2.00	4082	27259	56.0
1662	-15	2.00	4183[3] 4136[3]	14641[3] 4112[4] 15674[4]	25.0
1618	-13	3.00	4166	12189	20.0
1575	-14	7.00	4034	13324	22.6
1540	-15	10.00	4094	11469	17.1
1608	-13	4.00	4174	12704	20.3
1609	-13	4.00	4264[3] 4156[3]	12979[3] 4084[4] 15666[4]	20.6

$a = 1.16 \times 10^{-3}$ cm^2, C = 8.93 cm, R = 0.795 cm [see equations (3-5) and (3-6)]; D (Wien's Law) = -1.646×10^{-5}

[1] TT = T(IPTS - 1948) - T(obs)

[2] Thickness as determined by quartz crystal

[3] Standard Blank Sm(1)

[4] Standard Sm(1)

[5] C = 9.02 cm

[6] $a = 7.28 \times 10^{-3}$ cm^2

[7] $a = 7.73 \times 10^{-3}$ cm^2

[8] Temperature varied 40°; target was not used.

Appendix 5.10. Rate Data for $SmF_{3.00}$ Effusion Experiments

T(obs)	TT[1]	Rate[2]	T(obs)	TT[1]	Rate[2]
		Experiment 2[3]			
1365 K	-7 K	0.218 nm/min	1433 K	-6 K	1.39 nm/min
1403	-7	0.679			
$a = 7.28 \times 10^{-3}$ cm^2, C = 9.02 cm					
1464	-5	3.08			
$a = 7.73 \times 10^{-3}$ cm^2, C = 9.02 cm					
1425	-7	1.27	1392	-7	0.549
$a = 8.18 \times 10^{-3}$ cm^2, C = 9.02 cm					
1379	-7	0.353	1373	-7	0.331
1422	-7	1.17	136	-7	0.120
1356	-7	0.218	1387	-7	0.449
1331	-7	0.114	1426	-7	1.24
1397	-7	0.586	1457	-5	2.63
1437	-6	1.64	1413	-7	0.938
1455	-5	2.48			

$a = 8.18 \times 10^{-3}$ cm^2, C = 10.06 cm, R = 0.795 cm [see equations (3-5) and (3-6)]; D (Wien's Law) = -1.646×10^{-5}

Appendix 5.10. (cont'd.)

T(obs)	TT[1]	Rate[2]	T(obs)	TT[1]	Rate[2]
		Experiment 3[4]			
1394 K	-7 K	0.115 nm/min	1710 K	-17 K	28.0 nm/min
1465	-4	0.565	1689	-16	20.0
1439	-6	0.285	1662	-15	12.5
1484	-3	0.816	1618	-13	6.42
1392	-7	0.0949	1575	-14	3.21
1455	-5	0.429	1540	-15	1.72
1529	-15	1.55	1503	-15	0.850
1546	-15	1.92	1565	-14	2.56
1585	-14	3.96	1608	-13	5.08
1628	-14	7.61	1609	-13	5.51
1669	-15	14.4			

$a = 1.16 \times 10^{-3}$ cm^2, C = 8.93 cm, R = 0.795 cm [see equations (3-5) and (3-6)]; D (Wien's Law) = -1.646×10^{-5}

[1] TT = T(IPTS - 1948) - T(obs)

[2] Rate of deposition as determined by quartz crystal

[3] Pressures for first six data points calculated by use of $(2.5_7 \pm 0.1_7)$ nm/μg Sm; for the remainder, $(2.7_8 \pm 0.0_6)$ nm/μg Sm

[4] Pressures calculated by use of $(2.4_5 \pm 0.0_4)$ nm/μg Sm

Appendix 5.11. Target Collection and Deposition Data for $TmF_{3.00}$ Effusion Experiments

T(obs)	TT[1]	Exposure Time	Counts/30 sec Before Exposure	Counts/30 sec After Exposure	Deposit[2]
			Experiment 1		
			14715_3	14494_3 37879_4	
1486 K	-3 K	10.00 min	13083	31101	24.0 nm
1533	-15	5.00	15391	33817	23.7
1560	-14	3.00	15691	33347	22.5
1511	-15	6.00	13638	28499	19.2
1430	-7	20.00	15641_3 14882_3	27496_3 14507_3 38764_4	15.4
1473	-4	11.00	13263	29053	19.4
1517	-15	6.00	12802	29698	20.6
1488	-2	9.00	13313	30192	21.2
1399	-7	44.00	13408	27031	16.7
1437	-6	21.00	12660_3 14806_3	26854_3 14467_3 38594_4	17.8

$a = 7.06 \times 10^{-3}$ cm^2, C = 9.03 cm, R = 0.833 cm [see equations (3-5) and (3-6)]; D (Wien's Law) = -1.646×10^{-5}

Appendix 5.11. (cont'd.)

T(obs)	TT[1]	Exposure Time	Counts/30 sec Before Exposure	Counts/30 sec After Exposure	Deposit[2]
			Experiment 2		
			14806[3]	14647[3] 38175[4]	
1514 K	-15 K	29.00 min	14940	27644	17.5 nm
1558	-14	20.00	14791	34716	25.2
1700	-16	2.00	14119	33975	24.4
1733	-18	2.00	14078	45843	38.7
1676	-15	3.00	14598[3] 14840[3]	35050[3] 14594[4] 37446[4]	24.7
1643	-14	5.00	14194	34079	24.5
1617	-13	7.00	14929	32774	22.1
1719	-17	2.00	15311	41270	31.0
1754	-19	1.00	14821	37303	27.0
1686	-16	2.00	15130[3] 14754[3]	31510[3] 14584[4] 38134[4]	19.8

$a = 1.18 \times 10^{-3}$ cm^2, C = 8.96 cm, R = 0.833 cm [see equations (3-5) and (3-6)]; D (Wien's Law) = -1.646×10^{-5}

[1] TT = T(IPTS - 1948) - T(obs)

[2] Thickness as determined by quartz crystal

[3] Standard Blank Tm

[4] Standard Tm

Appendix 5.12. Rate Data for $TmF_{3.00}$ Effusion Experiments

T(obs)	TT[1]	Rate[2]	T(obs)	TT[1]	Rate[2]
		Experiment 1[3]			
1417 K	-7 K	0.634 nm/min	1353 K	-7 K	0.105 nm/min
1393	-7	0.348	1414	-7	0.527
1445	-6	1.04	1473	-4	1.76
1486	-3	2.40	1517	-15	3.45
1533	-15	4.77	1488	-2	2.36
1560	-14	7.50	1419	-7	0.593
1511	-15	3.20	1394	-7	0.322
1449	-6	1.17	1399	-7	0.380
1457	-5	1.39	1437	-6	0.843
1430	-7	0.767	1364	-7	0.169
1374	-7	0.219	1400	-7	0.382
1327	-7	0.0731	1326	-7	0.0632

$a = 7.06 \times 10^{-3}$ cm^2, C = 9.03 cm, R = 0.833 cm [see equations (3-5) and (3-6)]; D (Wien's Law) = -1.646×10^{-5}

Appendix 5.12. (cont'd.)

T(obs)	TT[1]	Rate	T(obs)	TT[1]	Rate[2]
		Experiment 2^4			
1451 K	-12 K	0.247 nm/min	1676 K	-15 K	8.23 nm/min
1514	-15	0.603	1643	-14	4.90
1560	-14	1.35	1608	-13	2.80
1515	-15	0.590	1572	-14	1.50
1558	-14	1.26	1617	-13	3.16
1604	-13	2.74	1644	-14	5.03
1667	-15	7.42	1666	-15	7.31
1700	-16	12.2	1719	-17	15.5
1775	-19	36.5	1754	-19	27.0
1733	-18	19.2	1701	-16	12.0
1715	-17	15.7	1686	-16	9.90

$a = 1.18 \times 10^{-3}$ cm^2, C = 8.96 cm, R = 0.833 cm [see equations (3-5) and (3-6)]; D (Wien's Law) = -1.646×10^{-5}

[1] TT = T(IPTS - 1948) -T(obs)

[2] Rate of deposition as determined by quartz crystal

[3] Pressures calculated by use of $(3.1_1 \pm 0.0_7)$ nm/μg Tm

[4] Pressures calculated by use of $(2.9_2 \pm 0.0_5)$ nm/μg Tm

Appendix 5.13. X-Ray Fluorescence Analysis of Standards

Sample	Counts/μg/min Standard	Blank	Counts/min Standard	Blank of Standard
Yb(1)	3828 ± 366	28508 ± 290	45574 ± 127	25074 ± 221
Yb(2)	1327 ± 151	11928 ± 148	19376 ± 172	10411 ± 163
Sm(1)	2066 ± 258	8262 ± 92	31428 ± 144	8482 ± 92
Sm(2)	2066 ± 258	7128 ± 107	85186 ± 270	7074 ± 46
Tm	5410 ± 364	33620 ± 438	85568 ± 528	34958 ± 645